Modified B_{12} Derivatives as Biomimetic Model and Novel Inhibitors of B_{12}-dependent Enzymes

---

Dissertation

zur

Erlangung der naturwissenschaftlichen Doktorwürde (Dr. sc. nat.)

vorgelegt der

Mathematisch-naturwissenschaftlichen Fakultät

der

Universität Zürich

von

Marjorie Sonnay

aus

Oron, Vaud

Promotionskomitee

Prof. Dr. Roger Alberto (Vorsitz)
PD Dr. Felix Zelder (Leitung)
Prof. Dr. Roland Sigel
Prof. Dr. Thomas Ward

Zürich 2016

Abstract

Vitamin B_{12}. The simplicity of the designation is misleading. We are indeed before an extremely complex subject, at the converging point of biology and chemistry. It groups variety of topics, from the importance of B_{12} for life (mammals, microorganisms, etc.) to an elegant molecular structure allowing, among others, for extremely specific analytical detection. The present work reports of two different aspects of B_{12}.

The first project aimed at gaining insights into the activation of B_{12} cofactors, more specifically about the role of the base-off/histidine-on binding configuration and the H-bonded catalytic triad observed in certain B_{12}-dependent enzymes. For this purpose, we propose the first intramolecular biomimetic model of the His-on configuration.

In this model, the cofactor-bound histidine is imitated by an imidazole moiety, covalently linked to the corrin ring through a peptide backbone and coordinating to the lower side of the cobalt center. The resulting intramolecular complex is an excellent structural model of the histidine-coordinated B_{12} cofactor, as proven by 2D-NMR and QM/MM calculations. The effect of the axially-bound imidazole deprotonation on the model properties was thoroughly investigated using a variety of analytical methods. These investigations allowed for depicting a clear picture: increasing the σ-donor character of the lower axial ligand from an imidazole to an imidazolate moiety influences in a similar way the absorbance properties, the redox properties and the trans-influence exercised on the upper-coordinated cyanide ligand. Worth mentioning is the drastic shift in the reduction potential to a lower value upon deprotonation of the imidazole ligand, which indicates a stabilization of the Co(III) species when bound to an imidazolate.

Immobilization of the B_{12} derivative on C18 silica material was as well utilized to obtain an unprecedented model of the histidine H-bonding observed at the active site of B_{12}-dependent enzymes. With this strategy, hydrogen bonding between the B_{12}-imidazole derivative and an exogenous carboxylate was proven using DRUV-vis. This supramolecular system hence represents the first modeling of the regulatory ligand triad observed in B_{12} His-on protein complexes.

Hence, interesting insights were gained with this model, which allow for a better understanding of the His-on configuration observed in B_{12}-dependent enzymes. Partial deprotonation of the coordinated His-residue indeed offers B_{12}-dependent proteins an elegant tool for fine-tuning the cofactor's electron donating properties on demand, thus allowing for an important control over the coenzyme's reactivity.

The second part reports of another face of B_{12}: the construction of antivitamin B_{12} as *E. coli* antibacterial. This concept takes advantage of B_{12} crucial role in cell replication. *E. coli* has no ability to synthesize B_{12} *de novo*, however it can append the dimethylbenzimidazole backbone to the short-loop B_{12} derivative cobinamide. Our antivitamin B_{12} is designed to closely resemble cobinamide by exchanging only the backbone terminal group (from OH for cobinamide to NH_2 for the antivitamin). Comparison of the two compounds properties indeed proved that the absorbance and the redox potential are identical and this minor modification is only detectable by ^{1}H-NMR. Furthermore, preliminary results of the bacterial test showed that this antivitamin exhibits a remarkable antibacterial activity. It is thought that this minor modification prevents the enzymatic reactions required for backbone attachment, thus impeding the cell replication process in the bacterium.

Zusammenfassung

Vitamin B_{12}. Die schiere Einfachheit dieser Bezeichnung ist irreführend. Wir bewegen uns hier auf einem äusserst komplexen Gebiet, welches sich über die Chemie hinaus bis weit in die Biologie hinein erstreckt; von der essentiellen Rolle von B_{12} für das Leben (Säugetiere, Mikroorganismen, etc.) bis zu einer einzigartig eleganten chemischen Struktur, welche - unter vielem weiterem - Anwendungen im Bereich der äusserst spezifischen Analytik ermöglicht. Die vorliegende Arbeit präsentiert zwei verschiedene Aspekte von B_{12}.

Das erste Projekt richtet das Augenmerk auf die Aktivierung von B_{12} Co-Faktoren - genauer: auf die Rolle der sogenannten base-off/histidine-on Bindungskonfiguration, sowie die Wasserstoff-verbrückte katalytische Triade, wie sie in manchen B_{12}-abhängigen Enzymen beobachtet werden kann. Zu diesem Zweck präsentieren wir das erste biomimetische Modell mit intramolekularer His-on Konfiguration.

In besagtem Modell wird die Funktion des Co-Faktor-gebundenen Histidins übernommen von einem Imidazolrest, welcher über ein Peptidrückgrat kovalent mit dem Corrinring verbunden, sowie von der unteren Seite her an das Kobaltzentrum koordiniert ist. 2D-NMR und QM/MM Berechnungen bestätigten, dass der resultierende intramolekulare Komplex ein exzellentes Strukturmodell des Histidin-koordinierten B_{12}-Co-Faktors ist. Der Einfluss der Deprotonierung des axial gebundenen Imidazolrestes auf die Modelleigenschaften wurde mit einer Reihe verschiedener Methoden sorgfältigst untersucht. Diese Untersuchungen führten zu einer anschaulichen Darstellung des anwachsenden Donor-Charakters des unteren axialen Liganden vom Imidazol zum Imidazolat. Diese Eigenschaft beeinflusst das Absorptionsspektrum, das Redoxverhalten und den Transeffekt auf den oberen axialan Cyanidliganden. Besonders erwähnenswert ist die markante Erniedrigung des Reduktionspotentials bei der Deprotonierung des Imidazols, was auf eine Stabilisierung der Co(III) Spezies im Falle eines koordinierten Imidazolats hinweist.

Des weiteren wurde das B_{12}-Derivat auf C18-Kieselgel immobilisiert, um ein weiteres und ebenso neuartiges Modell der Histidine-Wasserstoffbrücke zu erhalten, welche im aktiven Zentrum B_{12}-abängiger Enzyme beobachtet wird. In genanntem Modell konnte die Wasserstoffbrücke zwischen dem Imidazol-Derivat und dem exogenen Carboxylat mittels

DRUV-Vis nachgewiesen werden. Somit verkörpert dieses supramolekulare System das erste Modell der regulatorischen Ligandentriade, wie sie in B_{12}-His-on Proteinkomplexen beobachtet wird. Das Modell erlaubte interessante Einsichten, welche zu einem besseren Verständnis der His-on Konfiguration in B_{12}-abhängigen Enzymen beitragen. Teilweise Deprotonierung des koordinierten Histidinrests ermöglicht B_{12}-abhängigen Proteinen einen eleganten Weg zur bedarfsabhängigen Feineinstellung der Elektronendonoreigenschaften des Co-Faktors, sodass die Reaktivität des Co-Enyzms kontrolliert werden kann.

Das zweite Projekt beschäftigt sich mit einer anderen Facette von B_{12}: Der Synthese eines Antivitamins zur antibakteriellen Behandlung von *E. coli*. Dieses Konzept macht sich die essentielle Rolle von B_{12} in der Zellreplikation zunutze. *E. coli* verfügt nicht über die Möglichkeit, B_{12} *de novo* zu synthetisieren, kann aber den Dimethylbenzimidazolrest an das verkürzt vorhandene Rückgrat des B_{12}-Derivats Cobinamid binden. Unser Antivitamin ist so angelegt, dass es dem Cobinamid sehr ähnlich sieht. Der einzige Unterschied besteht in der ausgetauschten funktionellen Gruppe am Ende des verkürzten Rückgrates (Cobinamid-OH versus Antivitamin-NH_2). Ein Vergleich dieser beiden Derivate zeigte identisches Absorptions- und Redoxverhalten und offenbarte, dass die Modifikation nur durch Proton-NMR detektierbar ist. Des weiteren weisen vorläufige Auswertungen von Bakterientests auf eine bemerkenswerte antibakterielle Aktivität hin. Es wird angenommen, dass die geringfügige Modifikation ausreicht, um ein enzymatisches Anhängen des vollständigen Rückgrates zu verhindern und somit den Zellteilungsprozess zu behindern.

Abbreviation List

AdoCbl	Adenosylcobalamin
ACN	Acetonitrile
b	Broad
B_{12}	Vitamin B_{12}
Boc	tert-Butyl carbamate
CV	Cyclic Voltammetry
Cbl	Cobalamin
Cbi	Cobinamide
d	Doublet
dd	Doublet of Doublet
DCM	Dichloromethane
DFT	Density Functional Theory
DIPEA	N,N-Diisopropylethylamine
DMAP	4-Dimethylaminopyridine
DRUV-vis	Diffuse Reflectance Ultraviolet-visible Spectroscopy
Dmbz	Dimethylbenzimidazole
DMF	Dimethylformamide
E. Coli	*Escherichia coli*
EDC	1-Ethyl-3-(3-dimethylaminopropyl)carbodiimide
ESI	Electron Spray Ionisation
EA	Ethyl Acetate
FH4	Tetrahydrofolate
FTIR	Fourier-Transform Infrared Spectroscopy
HCl	Hydrochloric acid
HOBt	Hydroxybenzotriazole
HPLC	High Performance Liquid Chromatography
IR	Infrared Spectroscopy
m	Multiplet
MeCbl	Methylcobalamin
MeOH	Methanol
MetH	Methionine Synthase

MMCM	Methylmalonyl Coenzyme A Mutase
N^5-CH_3-FH4	5-Methyl-tetraydrofolate
NEt_3	Triethylamine
NH_3	Ammonia
QM/MM	Quantum Mechanics/Molecular Mechanics
Rf	Retention Factor
ROESY	Rotating Frame Overhauser Effect Spectroscopy
Rt	Retention Time
RT	Room Temperature
s	Singlet
SPE	Solid Phase Extraction
T	Temperature
TEMPO	2,2,6,6-Tetramethylpiperidine 1-oxyl
TBTU	2-(1H-Benzotriazole-1-yl)-1,1,3,3-tetramethyluronium tetrafluoroborate
TFA	Trifluoroacetic Acid
TLC	Thin Layer Chromatography
UPLC	Ultra Performance Liquid Chromatography

Table of Content

1. Introduction

1.1. B_{12} Structure and Properties

Nearly 70 years ago, vitamin B_{12} (B_{12}) was isolated for the first time from liver extract, and was recognized as the "antipernicious anemia factor".[1-2] This journey, which began 90 years ago, is marked by several crucial milestones, including the determination of the crystal structure of B_{12} [3-4] as well as the long and complex total synthesis of the vitamin.[5] Moreover, some of these remarkable breakthroughs were rewarded by Nobel prices. However, despite the colossal amount of work accomplished around this molecule, some secrets of vitamin B_{12} are still nowadays not fully understood. The thorough investigations endured by B_{12} since its discovery are due to two major motives: (i) the elegant and complicated structure of this molecule, and (ii) its crucial role in biological processes, where it acts as cofactor for several different enzymes.[6]

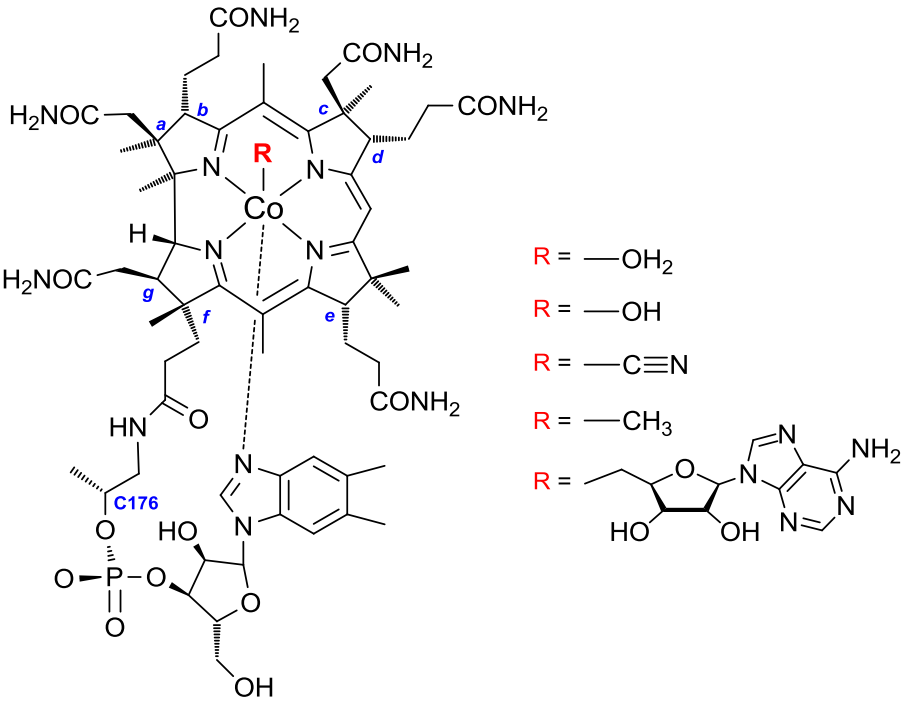

Figure 1 - General structure of cobalamins with distinct upper ligands: R = OH_2 aquaCbl, R = OH hydroxoCbl, R = CN cyanoCbl or vitamin B_{12}, R = CH_3 MeCbl, R = 5'-deoxyadenosyl AdoCbl (charges are omitted).

Vitamin B_{12} and all cobalamins derivatives (Cbl) (Figure 1) are composed of a cobalt center, which is coordinated in the equatorial plane by a tetradentate corrin macrocycle

bearing seven amide side chains (*a* – *g*), while in the axial position up to two ligands can be coordinated to the metal center. At the upper position (β-), the possibilities of ligand are varied, and include NC-, H_2O-, HO- which form inorganic B_{12} complexes, and Me- or adenosyl- which constitute organometallic B_{12} cofactors. The most common axial ligand at the lower position (α-) is the 5,6-dimethylbenzimidazole unit (Dmbz), which is intramolecularly bound to the corrin ring through the *f*-side chain. This specific side chain differs from the other amide chains: it is composed of a 1-aminopropanol unit, a phosphodiester, a ribose unit and is terminated by the coordinating Dmbz base. Protonation of the latter leads to decoordination, which results in the "base-off" derivative (Scheme 1). Several factors can affect the base-on/base-off equilibrium, the most important being the nature of the upper β ligand.[7] Indeed, exchange from a NC- to a H_2O- moiety engender an important stabilization of the base-on configuration, as demonstrated by the respective $pK_{base\text{-}off}$ of 0.1 and -2.1.[8] Furthermore, modulations in the backbone itself affect as well the $pK_{base\text{-}off}$. Since this specific equilibrium is fundamental for good functioning of B_{12}-dependent enzymatic reactions, several investigations were performed on backbone-modified B_{12} derivatives.[9]

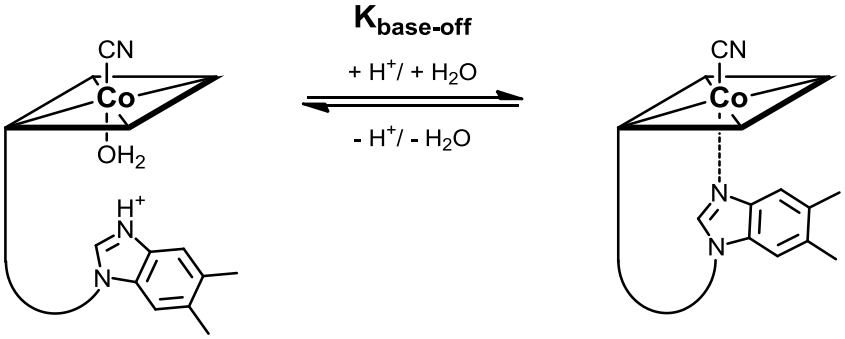

Scheme 1 - Base-on / base-off equilibrium of vitamin B_{12} (charges are omitted).

Hence, Kräutler and coworkers presented a compound with a modified aminoproanol unit, a study inspired by Eschenmoser.[10-11] The aim was to determine the influence of the presence of the (R)-methyl group situated on the C176 (Figure 1). Investigation on methylnorcobamin, a B_{12} derivative lacking the C176 methyl group, revealed a weaker coordination of the Dmbz base compared to natural B_{12}.[10] This phenomenon was first hypothesized by Eschenmoser and Kreppelt, who proposed a thorough structural analysis

of the B_{12} natural backbone. It revealed the presence of a supplementary gauche effect due to the (R)-methyl group when B_{12} is in the base-off configuration, thus favoring the base-on (Figure 2).[11-12] Hence, the absence of C176-methyl renders the base-off form of methylnorbocamin less unfavored. This effect thus demonstrates the important influence of a distant modification of the backbone on the properties of the cobalt center.

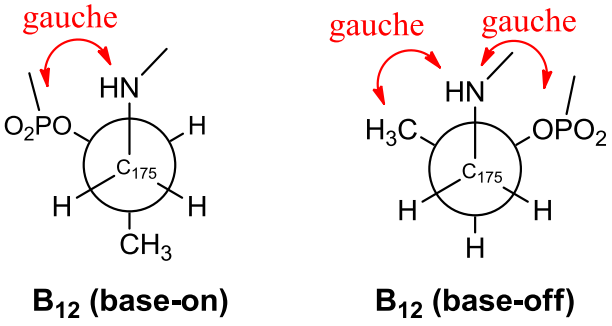

Figure 2 - Gauche effect in the base-on and base-off form of vitamin B_{12}.

Toraya et al. presented as well multiple backbone modified B_{12} derivatives, where the ribose moiety is replaced by olygomethylene chains of different lengths.[13] For those compounds, the $pK_{base\text{-}off}$ were measured on the β-CN derivative, while the AdoCbl cofactor derivative was used for biological investigations. They demonstrated that no link was observed between the strength of base-coordination to the cobalt center and the enzymatic efficiency. Furthermore, despite these modifications the AdoCbl derivatives were still binding to the enzyme, while some showed as well a reduced catalytic activity.[13-14]

Finally, our group proposed to replace the natural backbone of B_{12} by peptides of similar length. Physico-chemical properties were influenced by the peptide structure, and proved the (R)-methyl at C176 as well as the presence of a (L)-proline to stabilize the base-on form of the compound towards decoordination as well as reduction.[15] Furthermore, the Ado-peptide B_{12} exhibited inhibitory potential towards bacteria, as proven during biological studies.[9]

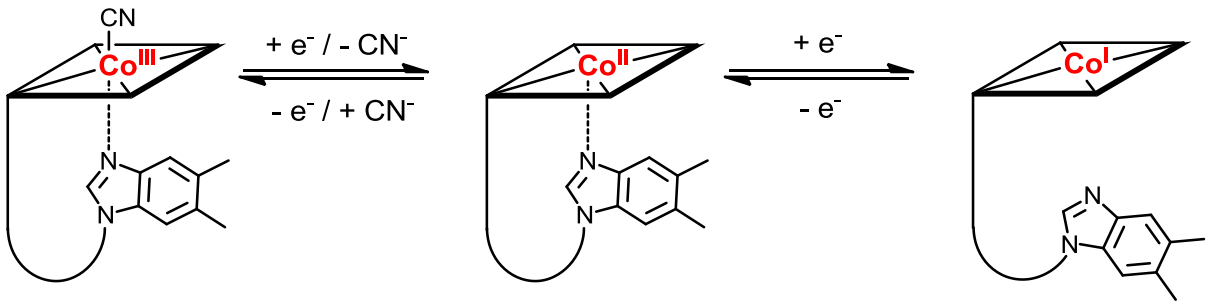

Scheme 2 – Reaction between the Co(III), Co(II) and Co(I) forms of cyanocobalamin (charges are omitted).

Vitamin B_{12} is the only vitamin bearing a metal center, which allows for formation of organometallic complexes and thus renders accessible a broad panel of enzymatic reactions.[16] The cobalt center in cobalamins can be found in three different oxidation states, each exhibiting a different coordination geometry: the Co(III)-octahedral complexes (d^6 electrons), the Co(II)-square pyramidal complexes (d^7 electrons) and the Co(I)-square planar complexes (d^8 electrons) (Scheme 2). While the backbone of the latter is dissociated, the Co(III) and Co(II) complexes exists in the base-on or base-off configuration, depending on the pH as well as on the $pK_{base\text{-}off}$ values. Modification of either the α- or β- axial ligand thus influences the pH specific configuration of Co(III) and Co(II) complexes by shifting the equilibrium represented by the $K_{base\text{-}off}$ value. Furthermore, such modulations affect as well the respective redox properties of the Cbl derivatives. For example, the one-electron reduction of both organometallic cofactor (MeCbl and AdoCbl) is estimated to be around -1.6 V[a] and -1.5 V[a], respectively, a value highly negative and out of the reach of biological reductants.[17] This phenomenon originates from the important σ-donating character of the Me and Ado group, which stabilizes the Co(III) state towards reduction.

Modifications of axial ligands are as well strongly influencing the respective absorbance spectra of cobalamins.[18] B_{12} derivatives indeed exhibit an intense and beautiful color, with high extinction coefficients. The resulting absorption spectrum exhibits three major bands between 650 and 300 nm, namely the α-, β- and γ-band. These major bands result mainly from π-π* transitions within the corrin ring,[19] and are influenced by the nature of the axial

[a] Potentials are referenced to saturated calomel electrode (SCE), at 0.242 V compared with normal hydrogen electrode (NHE).

ligand through the *cis*-effect exercised on the corrin ring.[20] The extinction coefficient of the γ-band represents as well a useful tool for detecting a change in the axial ligand, since it will increase as the difference in the donor strength will decrease.[21] The corrin ring thus allows for precise detection of the nature of the axial ligand in cobalamin derivatives.

1.2. B_{12} in Biological Systems

The tremendous interest engendered by B_{12} is originating from its role as coenzyme in numerous critical biological reactions in the biosphere, from mammals to simple organisms as bacteria.[22] For humans, lack of vitamin B_{12} is incompatible with life. However, this micronutrient is exclusively synthesized by certain microorganisms, and B_{12} uptake is only possible through nutrition.[23] Due to the complexity of the molecule, the uptake and cell delivery follows an elaborate process. Cell delivery of the vitamin is mediated by three proteins: intrinsic factor (IF), haptocorrin (HC) and transcobalamin II (TCII).[24-25] Combination of these proteins ensures for delivery of the intact B_{12} in the base-on form exclusively, due to their high binding constant and selectivity.[26-28] B_{12} is then metabolized within the cell, to form the two cofactors AdoCbl and MeCbl,[23] required by the two B_{12}-dependent enzymes present in humans: methylmalonyl CoA mutase (MMCM) and methionine synthase (MetH).[6]

1.2.1. AdoCbl-dependent enzymes - Methylmalonyl Mutase (MMCM)

AdoCbl or coenzyme B_{12} acts as cofactor in microorganisms and in humans for various intramolecular rearrangement reactions. Differences arise from the nature of the migrating group,[29] however the generally accepted reaction scheme is similar for all processes: the cofactor undergoes homolytic cleavage, hence forming a Co(II) species and the corresponding Ado• radical (Figure 3).[6, 29-30]

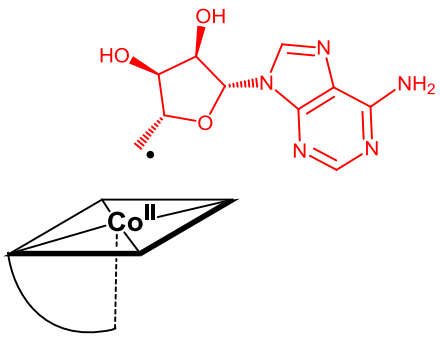

Figure 3 - Products of AdoCbl homolytic fission (charges are omitted).

In the case of the human enzyme methylmalonyl mutase, the catalyzed reaction is the 1,2-rearrangement of methylmalonyl-CoA to succinyl-CoA (Scheme 3).[31] After homolysis of

the Co-C bond, the Ado• radical abstracts the migrating hydrogen from methylmalonyl CoA. The substrate radical then undergoes intramolecular rearrangement to form the succinyl radical, which abstracts one hydrogen from adenosyl. The newly-formed Ado• radical then react with the Co(II) species to form again the coenzyme B_{12}.[32-34] MMCM plays an important role in the degradation of fatty acids, amino acids and cholesterol into succinyl-CoA, a useful metabolite used in the Krebs cycle.[35-36]

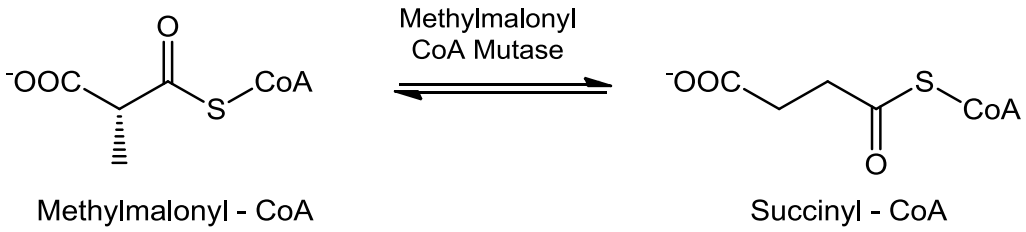

Scheme 3 - Formation of succinyl - CoA from methylmalonyl – CoA, catalyzed by the enzyme MMCM.

Interestingly, the mode of coenzyme binding differs between the various AdoCbl-dependent enzymes. The cofactor can adopt two configurations: the common base-on form, or the so-called "base-off/histidine-on" form.[37-40] In the latter, the Dmbz backbone is replaced by a histidine residue (His) of the enzyme, which coordinates to the cobalt center. This specific binding was first reported by Brennan et al., who solved the crystal structure of the MetH of *E. coli*, bound to the cofactor MeCbl.[41] This specific system is described in details in Chapter 1.3.

1.2.2.MeCbl-dependent enzymes - Methionine Synthase (MetH)

The cofactor MeCbl takes part in numerous methyl transfer reactions in all living organisms (except plants).[42] In this domain, the best-studied example is the one of Methionine Synthase (MetH). Together with MMCM, these enzymes are the only B_{12}-dependent enzymes in humans. MetH catalyzes the transfer of a methyl group from 5-methyl-tetraydrofolate (N^5-CH_3-FH4) to homocysteine to form tetrahydrofolate (FH4) and methionine (Scheme 4). During this process, the Co(I) supernucleophile undergoes oxidative addition with N^5-CH_3-FH4 to form FH4 and the cofactor MeCbl. In a following step, homocysteine nucleophilically attacks the axially bound methyl group to from

methionine and the reduced Co(I) species.[43-46] Cleavage of the Co-C bond thus follows a heterolytic process, resulting in Co(I) and the methyl cation.[47]

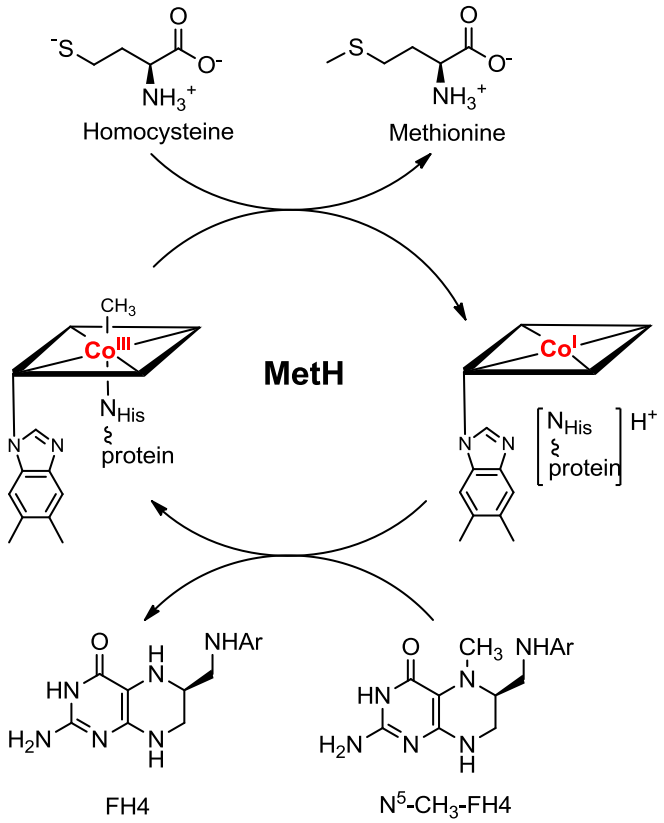

Scheme 4 - MetH catalytic cycle (charges are omitted).[48]

The relevance of this enzymatic catalysis is double for the human body: first, the production of methionine, an essential amino acid, allows for a limited uptake of this compound from the diet.[49] Secondly, FH4 is of great importance for DNA replication. Indeed, FH4 is further converted to 5,10-methylene-FH4 through a B_{12}-independent process. The latter is then involved in the production of thymidine monophosphate, one of the four nucleobase of DNA.[50] Hence, an impaired MetH system impacts DNA replication and cell division,[51] as seen in patients suffering from fatal pernicious anemia where it results in failure of blood cell production.[52]

Unlike AdoCbl, the MeCbl-dependent methyltransferases bind the B_{12} cofactor uniquely in the base-off/His-on configuration.[43] Furthermore, solving the first crystal structure of the cofactor-bound MetH revealed that the Co-bound histidine is part of a hydrogen-bounded amino acid triad, together with an aspartic acid (Asp) and a serine (Ser) (Scheme 5).[41] However, the role of this triad for catalysis in MetH is somehow controversial since

investigations were carried out by mutation of the ligand triad.[53] Interestingly, the effect on the catalysis were significant (k_{cat} value: 0 % for mutation of His and 5.6 % for mutation of Asp, compared to wild-type enzyme, 27 s^{-1}), with the exception of the mutation of the Ser residue (k_{cat}: 68 %, compared to wild-type enzyme, 27 s^{-1}).[53] Such a study thus implies that the histidine Co-coordination as well as hydrogen-binding to Asp is of great importance for the catalysis, while the role of the Ser residue appears to be less relevant. Hence, even if the ligand triad for B_{12}-dependent enzymes catalysis is essential, its exact role still remains unknown nowadays. Some insights were brought by Brunold and coworkers, who discovered that a decrease in the lower ligand basicity modulates the electronic structure of the Co(II)cofactor state (see chapter 1.4).[54]

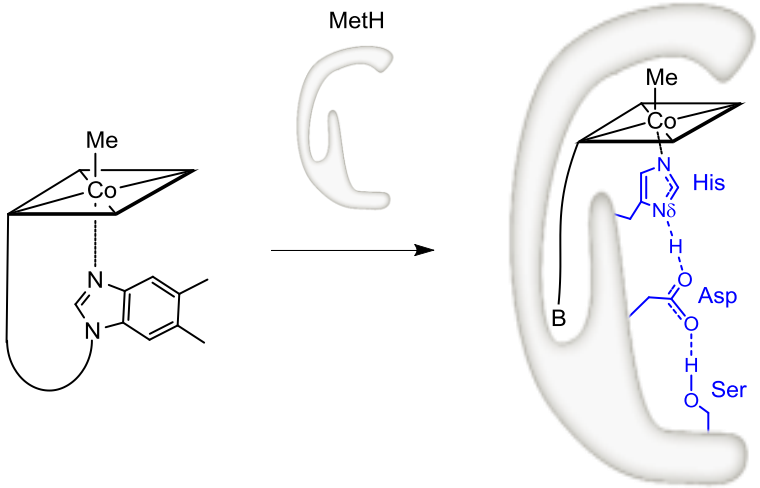

Scheme 5 – Base-off/His-on configuration of MeCbl in MetH (B: Dmbz base).

1.3. Charge relay systems – In MetH and in Nature

The ligand triad encountered in MetH is composed of three different amino acids (histidine: His, aspartic acid: Asp, serine: Ser), bound through a hydrogen network.[41] The significance of such a system arises from the possibility to reversibly protonate the Co(III)-bound His residue (charge relay). This feature is achieved by uptake of a proton from the solvent by the Ser and its subsequent transfer to the buried His (Scheme 6). Protonation of the histidine is hypothesized to favor the cleavage of the methyl group, resulting in the Co(I) species.[41] Ludwig et al. indeed demonstrated the association of the reduction of enzyme-bound B_{12} derivative and the uptake of a proton by the catalytic triad.[55] On the contrary, partial deprotonation generates a more basic histidine ligand, which would stabilize the methylated cofactor.[41]

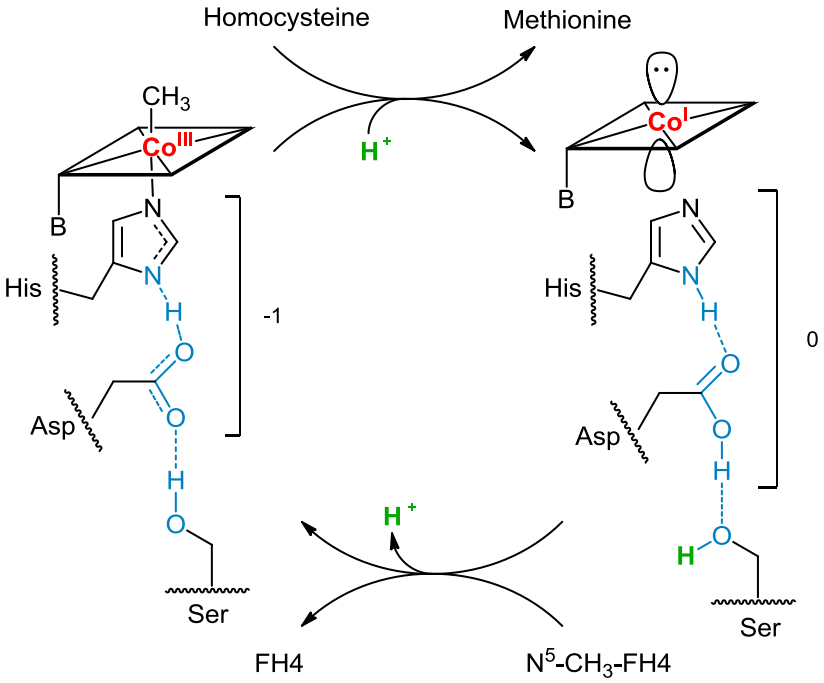

Scheme 6 - Catalytic cycle of MetH, including the charge relay system (blue) (charges are omitted).

Discovery of the first charge relay system in biological systems was achieved in 1969 by Hartley and coworkers. The enzyme of interest was α-chymotrypsin,[56] a protein not dependent on a metallocoenzyme and which performs proteolysis in the duodenum.[57] The study revealed the presence of three hydrogen bonded amino acids, in this case aspartic acid, histidine and serine. The reactivity of the serine residue towards hydrolysis of amides

and esters was revealed to originate from polarization of the systems due to the negatively charged aspartic acid, which enhances the serine nucleophilicity (Figure 4).[56, 58]

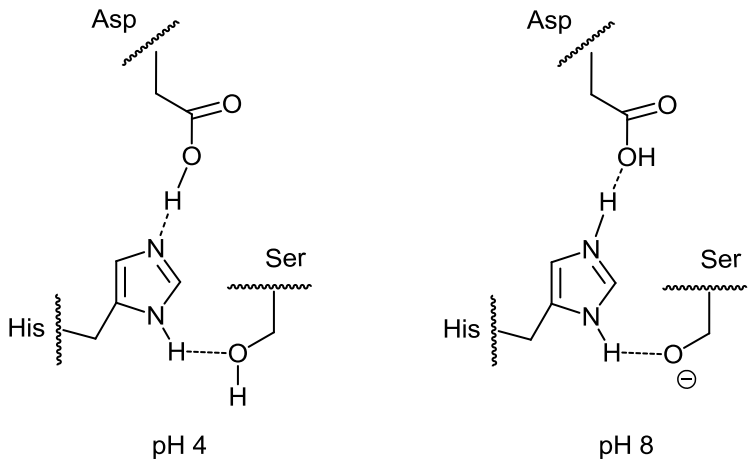

Figure 4 – Canonical forms of the α-chymotrypsin active site at pH 4 (left) and pH 8 (right)
(figure adapted from [56]).

Since then numerous similar systems were identified, revealing that the eventuality of finding charge relay system is not dependent on the enzymes function, and is indeed reported for multiple enzymes families as hydrolysases or transferases. Moreover, while the principle is always identical, modulations in the triad formation are also often encountered.[59-60]

Catalytic triads have as well been identified in heme-proteins, where the iron center of the heme cofactor binds to a histidine residue. The latter is then hydrogen-bonded to various amino acids, depending on the nature and the function of the protein.[61-63] Notorious examples of such schemes are encountered in Hemoglobins, Myoglobins and Cytochromes C where the Fe-bound histidine is hydrogen-bonded to a carbonyl of the peptide chain.[63] In particular, cytochromes *c* peroxidase presents a catalytic triad formed of iron-bound histidine and aspartic acid,[64] an organization considerably close to the one observed for MetH.

1.4. The effects of Histidine deprotonation – Study of different systems

Essential insights about the influence of histidine deprotonation in iron-heme systems were gained from detailed researches performed with various methods.[64-66] In this context, Chacko and La Mar reported the detection of imidazolate-character of the iron-axial ligand.[67] The studied models were (bis)imidazolate and cyanide-imidazolate complexes of natural porphyrin derivatives, where the imidazole group was used as ^{1}H-NMR probe. With these complexes, they observed an upfield shift of the imidazole protons upon deprotonation of this axial ligand.[67] The Fe-N(imidazole) stretching vibrations were as well explored as probe of the histidine deprotonation in cytochrome *c* peroxidase and hemoglobin by Su et al. By this method, a shift towards higher frequency was perceived when measuring a system displaying a stronger imidazolate character.[68]

The trans influence exercised by the imidazole on an upper cyanide ligand was amply investigated. Here, cyanide is of great interest due to its high affinity with the ferric-heme iron center under study.[69] IR, ^{13}C- and ^{15}N-NMR studies were performed on the upper cyanide-ligand of heme proteins and related model complexes, and revealed its interesting potential as sensitive probe for detection of hydrogen-bonding interactions with axial histidine/imidazole ligand.[70-75] Furthermore, several studies reported as well a tight connection between the influence of the imidazolate character in the complex and the reduction potential of the iron center.[64, 68, 75]

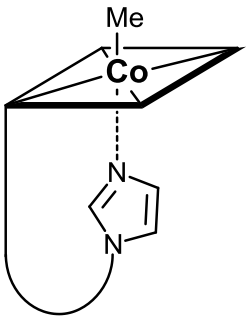

Figure 5 – *Coα*-(1*H*-Imidazolyl)-*Coβ*-methylcob(III)amide.[76]

In the case of B_{12}-dependent enzymes, several models of the base-off/His-on complex were as well proposed. Among others, Fasching et al. used guided biosynthesis to synthesize a

backbone modified B_{12} derivative as model for Co(III)-His coordination. In the latter, the backbone is terminated by an imidazole group instead of the natural Dmbz base (Figure 5). By investigating the organometallic activity of this compound, they concluded that the replacement of Dmbz by an imidazole moiety is not strongly influencing the B_{12} reactivity.[76]

Marzilli and coworkers proposed a different model, which allows the study of a coordinated imidazole and the influence of its deprotonation on the trans (upper) methyl ligand.[77] For this purpose, FT-Raman spectrometry was used on the short-loop derivative Me(N-acetylhistidine)cobinamide derivative (Scheme 7). Measurements were performed on the imidazole species at pH 10, and in 1 M NaOH solution to obtain the imidazolate species. However, deprotonation did not lead to any changes in the vibration band, thus proving that the frequencies of the Co-CH_3 stretching mode do not depend on the nature of the trans ligand.[78]

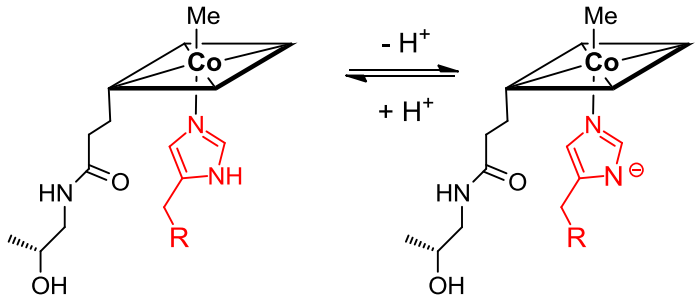

Scheme 7 - pH equilibrium of Me(N-acetylhistidine)cobinamide (charges are omitted).

Detailed spectroscopic and computational studies were performed by Brunold and coworkers on a series of different AdoCbl and MeCbl cofactor derivatives.[19, 54, 79-80] In particular, replacement of the upper and lower axial ligand (respectively methyl and Dmbz) by H_2O was assessed using magnetic circular dichroism, electronic absorption and computational calculations on (OH_2)Cbl, MeCbl and MeCbi (Figure 6). It revealed that the upper axial ligand significantly modulates the strength of the lower Co-N(Dmbz) bond, while modification on the lower ligand has negligible effect on the Co-C bond.[19] This effect was explained as followed: due to the strong σ-donor character of the upper methyl group, some electron density is transferred from the corresponding molecular orbital (MO) to the unoccupied $3d_{z^2}$, consequently rendering the interaction between the N(Dmbz) lone-pair and the Co $3d_{z^2}$ weakly σ-antibonding.[80] Exchanging the α-Dmbz ligand by H_2O eliminates

this σ-antibonding interaction, thus affecting the corresponding HOMO energy. However, this modification leaves the Co-C bond strength almost unchanged, because of the smaller σ-donating character of Dmbz and H_2O.[19, 80]

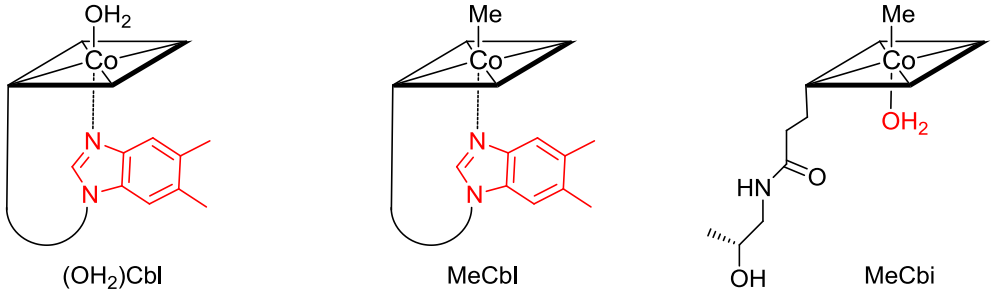

Figure 6 - Structure of (OH_2)Cbl, MeCbl and MeCbi (charges are omitted).

In a similar study, the effect of the Co-histidine coordination was investigated, and proved to have an insignificant effect on the electronic properties of the Co(III) ground state of AdoCbl.[79] However, a decrease in the basicity of the lower ligand causes a change in the electronic structure of the Co(II)-cofactor state, as proven when investigated AdoCbl derivatives with imidazole and pyridine derivatives as lower axial ligands.[54] Applying this knowledge to His-on enzymes, they proposed that stabilizing the Co(II)Cbl derivative through a modification of the lower axial ligand allows the enzyme to reduce the barrier to Co-C bond hemolysis.[54]

Our group presented a biomimetic model of the base-off/His-on coordination which followed an utterly different approach.[81] The proposed model is based on the immobilization of B_{12} derivatives on C18 silica material ($C18_{cc}$). This assembly leads to decoordination of the Dmbz base and the subsequent coordination of histidine. Indeed, in non-biological systems the strong Co-Dmbz coordination prevents ligand replacement at the lower face of the cobalt center.[82] Immobilization thus represented an elegant solution to facilitate substitution on the α-side, and allowed for the building of the first base-off/His-on biomimetic model.[81]

1.5. Antivitamins

A different aspect of vitamin B_{12} research will be presented in the current chapter. Indeed, while the previous chapters aimed at laying the foundations for a deeper knowledge of the role of a specific B_{12}-binding configuration, I wish now to introduce B_{12}-derivatives acting as antivitamin as well as the design process of such an intriguing class of compounds. I co-authored a review on this subject, which main aspects will first be shortly summarized here.[83]

This journey starts with the definition of antivitamin and their applications. Somogoyi and Trautner defined antivitamins as "molecules that diminish or abolish specific functions of vitamins".[84] Antivitamins present two different general mode of action: they either target the proteins responsible for the good functioning of vitamins (for cell delivery, biosynthesis or for enzymatic modification), or they alter the vitamin into non-functioning compounds.[83] While abolishing vitamins function might appear counterintuitive and unhealthy, antivitamins are in the contrary of great interest for the treatment of vitamin-dependent diseases. Hence, they have been largely investigated for their therapeutic effects, which resulted in the discovery of several drugs. Among these, a specific example is worth mentioning: Prontosil,[85] which inhibits the synthesis of folic acid, a necessary vitamin for bacterial growth.[83] Prontosil is a sulfonamide-based antibacterial drug (Figure 7), discovered in 1935 by G. Domagk.[86] It was the first commercially available antivitamin-based drug, but more importantly, it provided a basis for the development of numerous drugs derived from sulfonamides.[87]

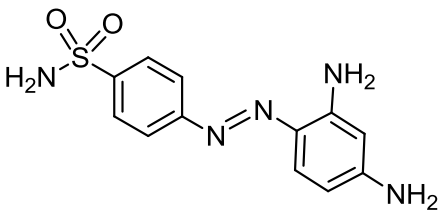

Figure 7 - Structure of Prontosil.

Several antimetabolites-based drugs appeared on the market since the discovery of Prontosil, as anticoagulant (antivitamin K)[88] or chemotherapeutic agent (antivitamin B9, or antifolate)[89] for example. However, no compound acting as antivitamin B_{12} ever reached

the market, despite intensive researches.[90] Vitamin B_{12} represents indeed an interesting target for the development of anticancer or antibacterial species due to its indirect role in the synthesis of thymidine monophosphate, a DNA building blocks. The development of antivitamin B_{12} is thus based on the importance of B_{12} for cell replication, rendering fast-proliferating cells as cancer cells high consumers of the vitamin.[91]

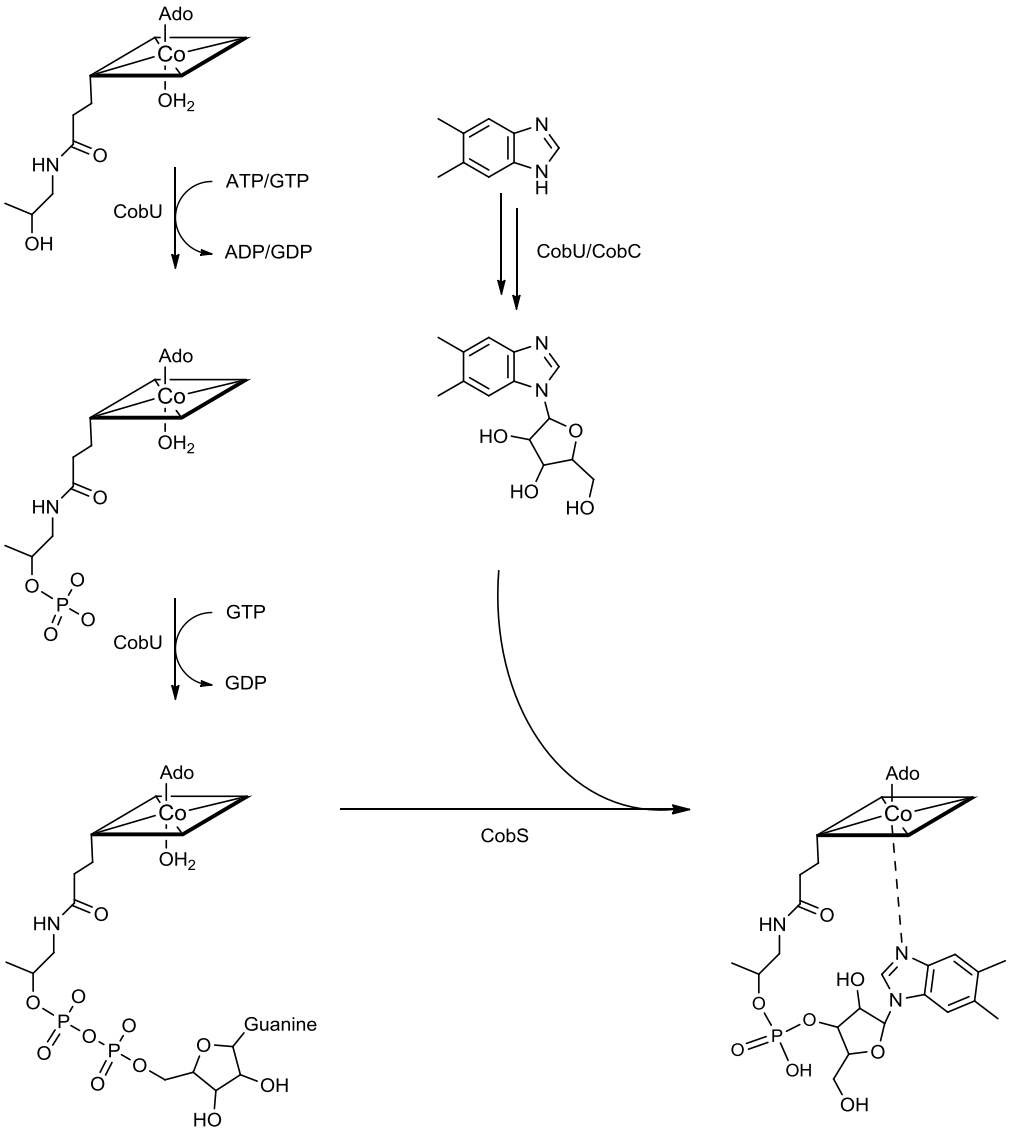

Scheme 8 – Biosynthesis of AdoCbl from AdoCbi, nucleotide loop assembly pathway (adapted from [92]) (charges are omitted).

For the design of antivitamin B_{12} acting as antibacterial, the process is somehow different due to the ability of some microorganisms to synthesize B_{12}. In this context, the case of *E. coli* is of great interest. This bacterium possesses only part of the genes encoding for the synthesis of B_{12}, thus enabling it to synthesize B_{12} uniquely when provided with the

cobinamide precursor. Three sets of genes (*cobU*, *cobT* and *cobS*) are present in *E. coli*, which expression is induced by the presence of cobinamide. The resulting enzymes (CobU, CobT and CobS) catalyze the phosphorylation of Cbi (cobinamide kinase-guanylyltransferase), the formation of the ribose-Dmbz building block (dimethylbenzimidazole phosphoribosyltransferase) and their subsequent assembly to obtain the final coenzyme B_{12} (cobalamin synthase) (Scheme 8).[92-95] Based on this knowledge, the design of an antibacterial B_{12} would thus require only a small modification to render the entire process non-functional.

However, it is important to observe that *E. coli* is not the most optimal bacterium regarding antivitamin B_{12} studies. Indeed, the particularity of *E. coli* is that it possess two methionine synthase, one B_{12}-dependent methionine (MetH) as well one B_{12}-independent (MetE).[96] The B_{12}-dependent pathway is preferably used due to (i) its greater catalytic activity,[97] as well as (ii) the repression of the corresponding *metE* gene in the presence of cobalamin.[96] However, the presence of MetE renders the study of antivitamin B_{12} extremely complex. The use of a mutated E. coli (NCIMB 8134), lacking the B_{12}-independent pathway, represents thus an interesting solution for studies of antibacterial B_{12}-derivatives.[98]

2. Objectives

This dissertation is composed of two different parts, linked by the B_{12}-framework. In part I (chapter 2.1) is presented the biomimetic model of the B_{12}-His coordination observed in B_{12}-dependent enzymes. Part II (chapter 2.2) describes the design and investigation of an antivitamin B_{12} acting as antibacterial against *E.coli*.

2.1. Part I: Biomimetic Model

Despite highly thorough investigations, the role of the Co-His coordination and its potential reversible deprotonation is still not fully understood nowadays. More importantly, while the importance of reversible protonation regarding catalytic activity became controversial after studying mutated enzymes, it revealed as well that the hydrogen bonding between His-Asp is crucial for activity.[53]

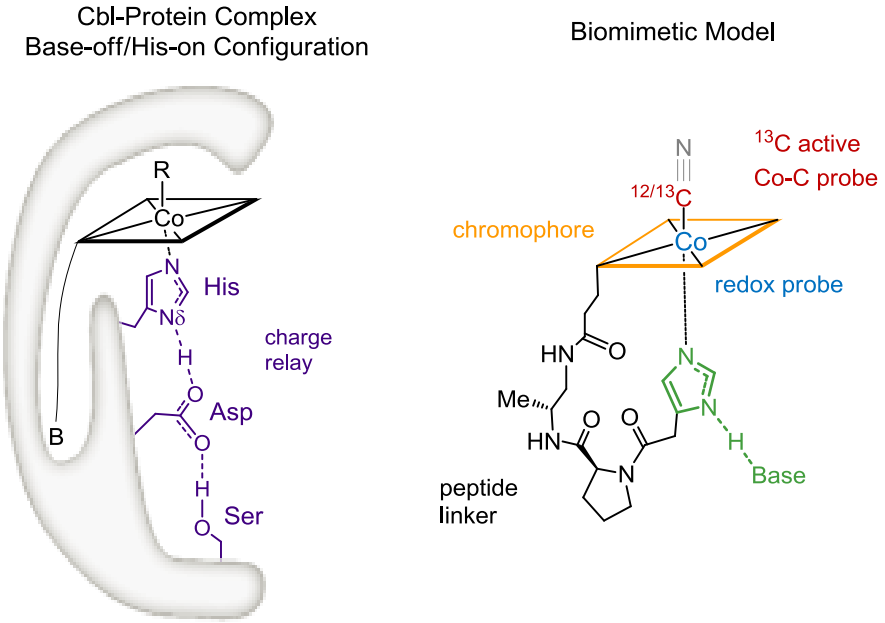

Figure 8 - Left: Cbl-protein complex in the Base-off/His-on configuration. Right: structure of the biomimetic model (charges are omitted).

I thus propose here the design and synthesis of the first intramolecular biomimetic model of the His-on configuration, as observed in several B_{12}-dependent enzymes. This model is composed of a modified backbone terminated with an imidazole moiety specifically bound to allow deprotonation. Such a system renders possible the study of the modifications engendered by deprotonation on several properties of the model. This precisely constructed

model is composed of a corrin ring chromophore, a peptide backbone, an upper cyanide ligand and a cobalt center (Figure 8). Together, they allow for investigating modifications in (i) the absorption properties of the compound, (ii) the Co-C bond strength and (iii) the cobalt redox properties.

A modeling of the histidine H-bonding interaction, as observed in ligand triad of B_{12}-dependent enzyme, is as well proposed. In this context, immobilization of the B_{12} derivative on C18 silica material allows for imitating the enzyme hydrophobic active site, hence enabling the investigation of hydrogen bonding between the B_{12}-imidazole derivative and carboxylate moieties.

2.2. Part II: Antivitamin as *E. Coli* Antibacterial

The very specific B_{12}-pathway encountered in *E. coli* renders this bacterium a target of choice for antivitamin B_{12}. First, due to its inability to synthesize B_{12} *de novo*, a B_{12} derivative could inhibit the bacteria's cell replication process. Secondly, *E. coli*'s capacity to use cobinamide as AdoCbl precursor renders the design of an antivitamin straightforward: a small modification of the cobinamide structure is indeed expected to exhibit important antibacterial activity.

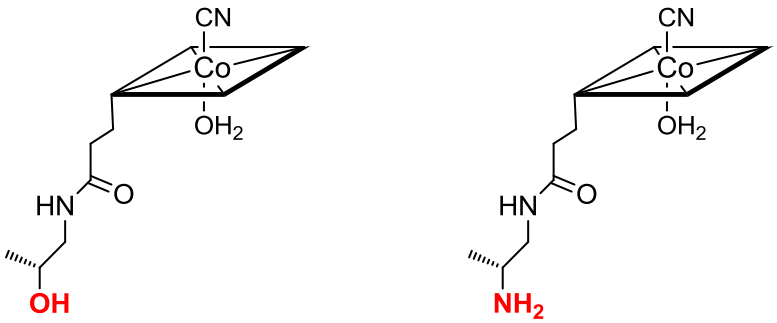

Figure 9 - Structure of cobinamide (left) and of the antivitamin B_{12} candidate (right) (charges are omitted).

For this purpose, the antibacterial B_{12} was designed to resemble cobinamide in every point, except for one difference: the short backbone is terminated by an amine instead of the hydroxyl group present in cobinamide (Figure 9). Modifying uniquely the backbone terminal moiety is expected to allow the cellular uptake of the B_{12} derivative while preventing the enzymatic reactions yielding to backbone addition.

However, *E. coli* possesses as well a second methionine synthase which is B_{12}-independent. Therefore, the use of a modified *E. coli* strain lacking this pathway is required. This study thus stands only as proof-of-concept and the antivitamin B_{12} candidate is not expected to be active in wild-type *E. coli*.

3. Results and Discussion

3.1. Biomimetic Model

This section is aimed at presenting the biomimetic model of the cofactor His-on complex found in several B_{12}-dependent enzymes. The synthesis and structural evaluation of the model are first introduced, followed by a brief study demonstrating the role of a small structural change in the backbone. The influence of imidazole deprotonation on different properties is then presented, which includes the investigation on: (i) the absorbance, (ii) the trans influence on the CN upper ligand with IR and NMR, and (iii) the reduction properties of the Co center. Following, the use of a blocked model to perform control experiments is reported. This chapter is concluded with the presentation of a supramolecular assembly, resulting from the immobilization of the model on C18 silica material. Such a system is aimed at mimicking the H-bonding interaction witnessed in the ligand triad of cofactor His-on complexes.

3.1.1. Synthesis and Structural Analysis – Evaluation of the model quality

The replacement of the natural backbone of B_{12} with a biomimetic peptide was already successfully applied for the design of backbone B_{12} derivatives.[9] Peptides are indeed of great interest primary due to the broad selection of natural and unnatural amino acids, which allows the construction of a variety of structural motifs.[9] Furthermore, it represents also a replacement of choice for phosphodiester,[99-101] as encountered in the natural backbone of B_{12}. The peptide imidazole backbone derivatives **1-H**$^+$ and **2-H**$^+$ (Figure 10), which represent the models of His-on B_{12} complexes, are composed of a diamine connector, a proline and an imidazole unit, and were synthesized using common peptide coupling techniques.[15] The fundamental difference between **1-H**$^+$ and **2-H**$^+$ is the presence, in **1-H**$^+$, of a (R)-configured methyl group at C176 on the ethylenediamine unit. However, the synthesis of both compounds **1-H**$^+$ and **2-H**$^+$ is similar.

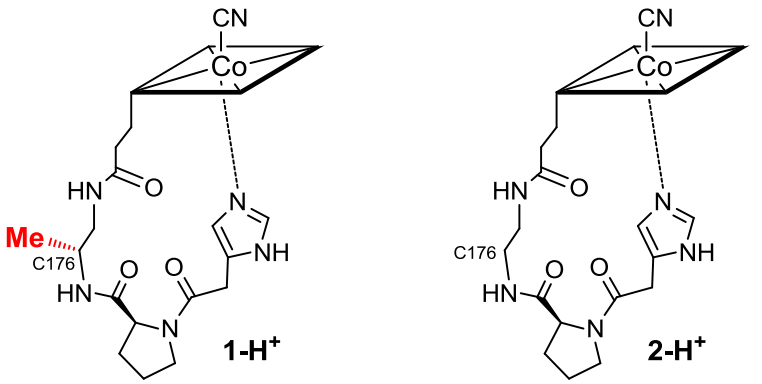

Figure 10 - Peptide imidazole backbone derivatives **1-H**$^+$ and **2-H**$^+$ (charges are omitted).

For the addition of the Boc-ethylenediamine moiety to cobyric acid (**3**) to obtain **5** (Scheme 9, A), a slight change of colour from red to dark pink was observed. Isolation of the compound for characterization was performed, although not mandatory. Indeed, after quenching of the reaction and washing of the water phase with DCM, the dried crude can be directly used for further reaction. The following deprotection of the terminal amine was achieved in acidic solution, which led to compound **6**. The addition of the imidazole containing building block (**7**) finally yielded the crude pink derivative **1-H**$^+$ (Scheme 9, C).

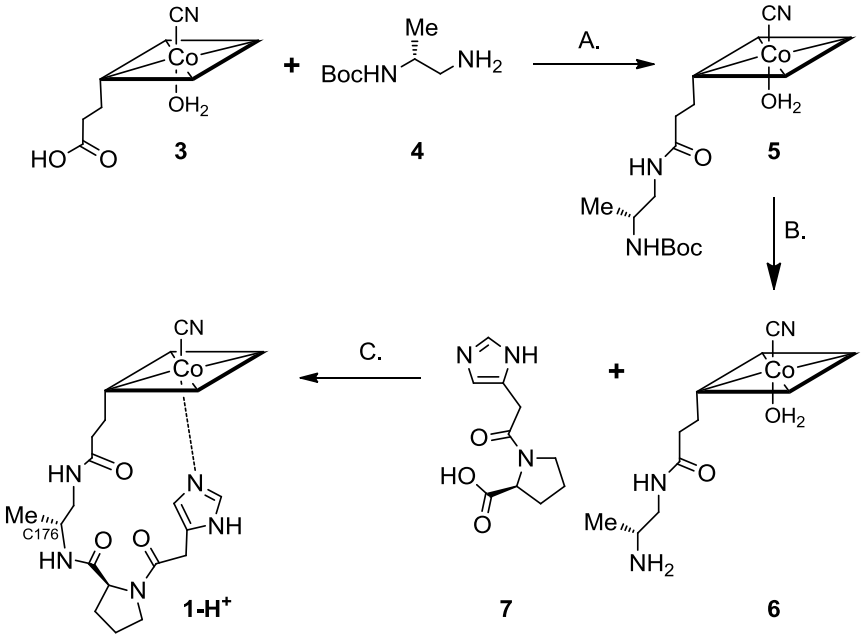

Scheme 9 - Synthesis of **1-H**$^+$ (A. NEt_3, ethylchloroformate, DMF, 0°C. B. HCl 1 M. C. DIPEA, HOBt, TBTU, DMF, 0°C) (charges are omitted).

Further purification of the crude mixture by preparative HPLC afforded two isomers: the β-aqua, α-CN and the α-aqua, β-CN Cbl derivative. In order to obtain the desired base-on

1-H$^+$, the collected purified compound was dissolved in H_2O and the purple dicyano-derivative was formed by addition of ~1.2 equivalent of KCN salt. The pH was then lowered to 3.8, and the solution was stirred for 24h without protection from air. By this process, the cobalt-bound cyanide is released as HCN, with subsequent coordination of the imidazole nitrogen. UV-vis was used to verify the completion of the reaction. Further comparison with B_{12} absorbance spectra revealed no difference (Figure 11), thus proving the base-on configuration of **1-H**$^+$. Furthermore, the high resolution mass spectrum displays a signal at m/z = 610.30054, a value consistent with $C_{59}H_{85}O_9N_{16}Co$ (calculated: m/z = 610.30032) which corresponds to $[M+H]^{2+}$.

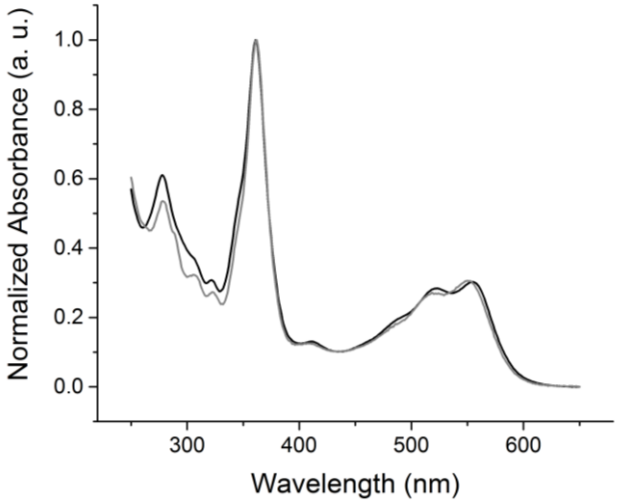

Figure 11 - Absorbance spectra of B_{12} (grey) and base-on **1-H**$^+$ (black).

The model was then evaluated on its structural concordance with the His-on B_{12} configuration in the enzyme. Through-space correlation are observed between $H_{im}2$ (blue in Figure 12) and the lower side chains 7A and 81 as well as the methyl group 51, all of which are situated at the northern face of the corrin ring. These interactions are complementary to correlations at the southern face of the molecule, between $H_{im}5$ and the corrin side chains 151, 131, as well as the 1R situated on the peptide backbone (red in Figure 12).

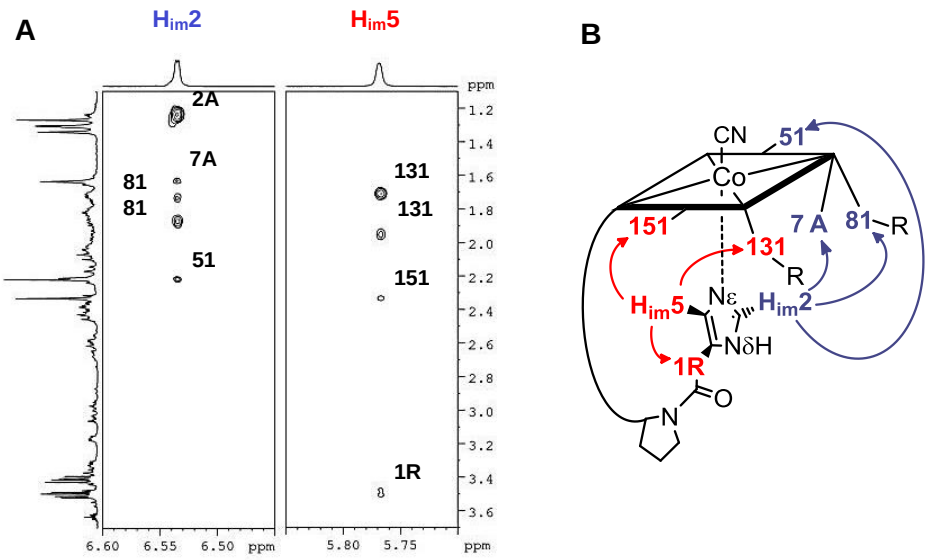

Figure 12 - **A:** 2D - ROESY coupling of **1-H**$^+$ **B:** the corresponding correlation in the structure (charges are omitted).

These data thus unambiguously indicate a coordination of the imidazole group to the cobalt center through the Nε-nitrogen. Furthermore, these measurements also allowed determining the positioning of the imidazole unit with respect to the macrocycle, and revealed that it follows the C51 – C151 axis of the corrin ring (Figure 12, **B**).

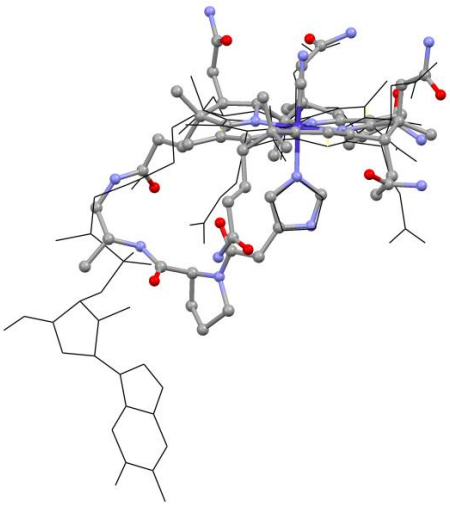

Figure 13 - Overlap of MeCbl crystal structure in MetH (wireframe, only MeCbl and His shown, PDB: 1BMT)[41] and model of **1-H**$^+$ (ball and sticks).

The specific structural behavior observed for **1-H**$^+$ is in good agreement with the structure adopted by the MeCbl cofactor in the active site of methionine synthase (MetH, PDB: 1BMT), as proven when overlapping the crystal structure of His-on MeCbl in MetH[41] and the **1-H**$^+$ model obtained by QM/MM calculations (Figure 13).

3.1.2. Methyl effect on the base-on/base-off equilibrium

The study of the compound coordination chemistry was achieved using spectrophotometric pH titration, which yielded to the determination of a $pK_{base\text{-}off}$ value of 1.7 ($R^2 = 1.0$) for compound **1-H**$^+$ (Figure 14). The same measurement performed on **2-H**$^+$ resulted in a $pK_{base\text{-}off}$ of 2.4 ($R^2 = 1.0$).

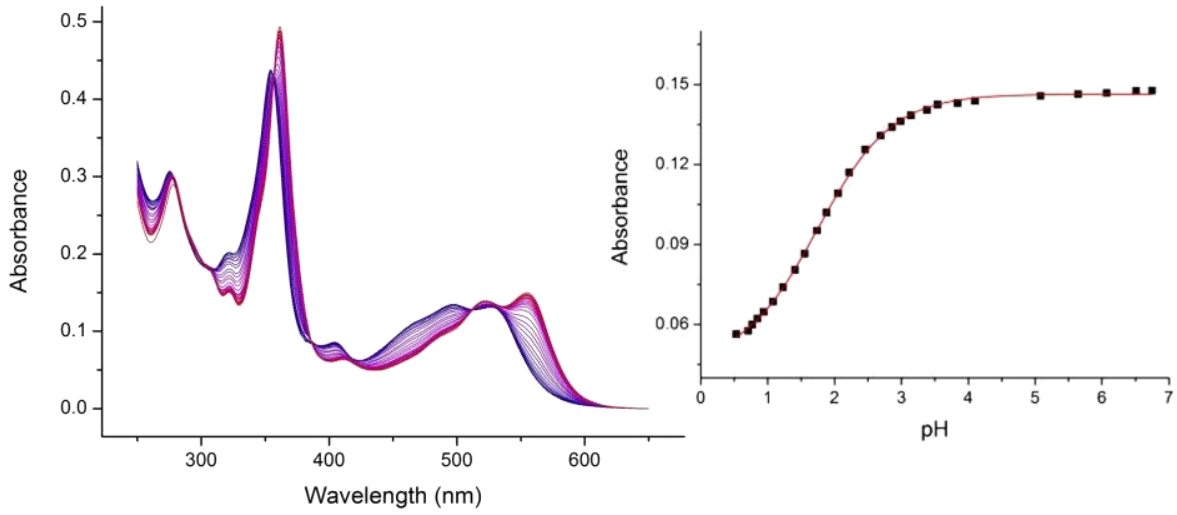

Figure 14 – Left: pH titration of **1-H**$^+$ from pH 7.0 (red) to pH 0.2 (blue). Right: corresponding pka determination plot (absorbance at 555 nm).

Those values are in agreement with previous studies performed on the stabilization role of the (R)-configured methyl group at position 176.[10] Indeed, the presence of the C176 methyl group appears to favor the base-on configuration through an impressive long distance constitutional effect.[102] As depicted in Figure 15, the presence of a methyl group on the C176 induces a supplementary `gauche` effect in the base-off configuration **1-2H**$^{2+}$, while no additional unfavorable interactions are observed between the base-on and base-off configuration of **2-H**$^+$. This behavior thus explains the lower $pK_{base\text{-}off}$ of **1-H**$^+$.

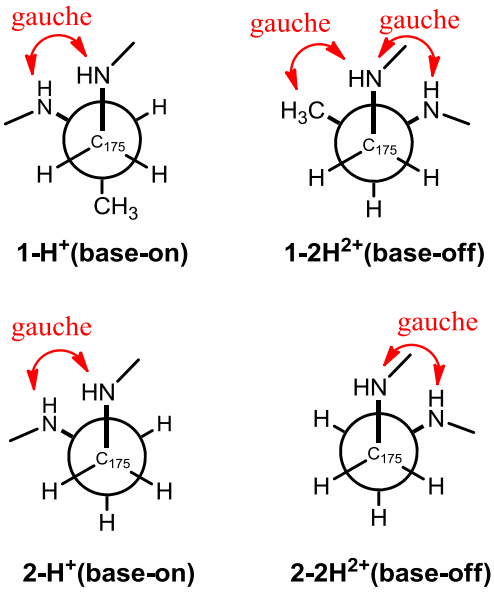

Figure 15 - Gauche effect in the base-on configuration **1-H**$^+$ and **2-H**$^+$ (right) and the respective base-off configuration **1-2H**$^+$ and **2-2H**$^+$ (left).

3.1.3. Influence of the Reversible Deprotonation:

Through hydrogen bonding, the charge relay system can reversibly and partially deprotonate the histidine residue bound to the Co-center in B_{12}-dependent enzymes.[55] While such a phenomenon is expected to influence the reactivity of the B_{12} cofactor, the extents of this effect need to be thoroughly investigated. The biomimetic models **1-H**$^+$ and **2-H**$^+$ are thus of great interest, since they allow a complete study of the effects of the Nδ-imidazole deprotonation on diverse properties (Scheme 10). Therefore, in the next chapter are presented the different methods used to study the influence of the imidazole deprotonation (UV-vis, NMR, cyclic voltammetry, 2D-IR) and their respective results.

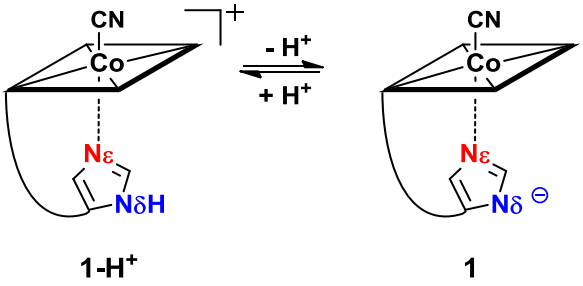

Scheme 10 - pH equilibrium between **1-H**$^+$ and **1**.

On the Chromophore – UV-Vis Spectrometry

The effect of the reversible deprotonation of the Nδ-imidazole nitrogen of **1-H**$^+$ and **2-H**$^+$ were first studied by UV-vis pH titration. For both compounds, a bathochromic shift from 554 nm to 564 nm and 522 nm to 530 nm was observed for the α and β bands respectively, when increasing the pH from 8.5 to 12.5. Additionally, the presence of two isosbestic points at 541 nm and 524 nm was established (Figure 16, left). The Nδ deprotonation of the model increases the σ-donor character of the coordinated imidazole, which thus affects the absorbance properties of the model. By studying a series of Cbls with different β-ligand, it was indeed proven that the shift of the absorbance maximum follows the nephelauxetic series ($F < O < N < Cl < CN < Br < I$). Thus, a ligand presenting more nephelauxetic effect exhibits a shift towards higher wavelength.[103]

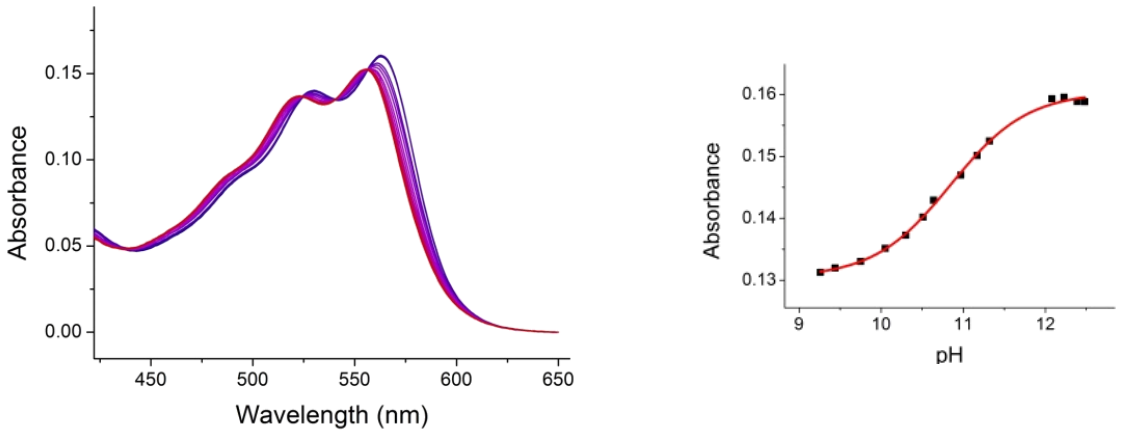

Figure 16 - Left: pH titration of **1-H**$^+$ from pH 8.5 (red) to pH 12.5 (blue); Right: corresponding pka determination plot (absorbance at 565 nm).

The pKa(Nδ) value determined for **1-H**$^+$ is equivalent to the pKa(Nδ) of **2-H**$^+$, both being equal to 10.8 ($R^2 = 1.00$ and 0.99, respectively) (Figure 16, right). The coordinated imidazole thus exhibits a more acidic pKa value compared to the free imidazole, which is situated 4 pH unit higher (14.5[104]). Indeed, the imidazole electron density will be altered due to coordination of the Nε to the lewis acidic Co-centre, a phenomenon which weakens the Nδ-H bond, thus rendering the H^+ more acidic. Furthermore, these results reveal that both compounds have an identical behavior towards imidazole protonation. It indicates that the strength of intramolecular coordination Co-Nε is equal in both systems, which results in an unchanged acidity of the Nδ proton. These results are in agreement with the previously mentioned supplementary gauche effect found in the base-off **1-2H**$^{2+}$ (Chapter 3.1.2, Figure 15 bottom). Indeed, such an effect renders the base-on configuration more favorable but does not modify the coordination strength.

On the trans-influence (Co-C bond)

The trans influence is a ground state effect which describes the influence of the axial ligands on bond lengths.[16, 77, 105-106] The trans influence engendered when modifying the lower ligand can be probed using CN as upper axial ligand. Indeed, CN represents a good probe due to its sensitivity to changes in electronic environment.

^{13}CN as ^{13}C-NMR probe

^{13}CN has been amply used as probe for trans influence, for example in cobaloximes and corrinoids derivatives.[107-108] It was as well used in the study of CN-Fe-Heme enzymes[72-74] (Chapter 1.4), which inspired as well the following study.

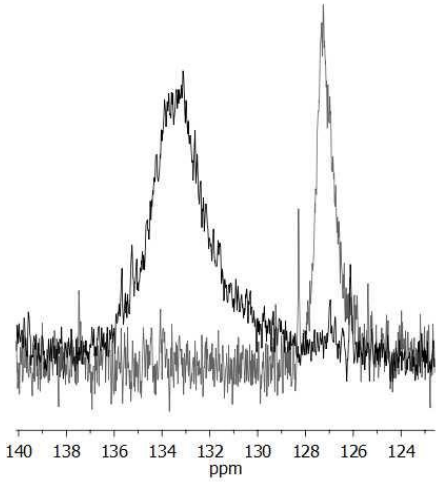

Figure 17 - ^{13}C-NMR of upper ^{13}CN ligand of **1-H**$^+$ (pH = 7.0, grey) and **1** (pH = 12.5, black).

The measurements were performed at two different pH values (pH 7 and pH 12.5). Indeed, as derived from UV-vis studies (Chapter 3.1.3, Figure 16), the biomimetic model exists at pH 7 in its fully protonated base-on form (**1-H**$^+$), whereas increase of the pH to 12.5 gives the deprotonated species **1**. In this study, the upper ligand was an isotopically labeled ^{13}CN. The ^{13}C-NMR of **1-H**$^+$ revealed a broad peak at 127 ppm, corresponding to the ^{13}CN moiety, which shifts downfield (133 ppm) when raising the pH to 12.5 to form **1** (Figure 17).

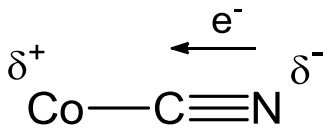

Figure 18 - Coordination of CN to the cobalt center leads to polarization towards the carbon of CN.

This behavior is in agreement with previous studies,[107-108] and is explained by the polarization of the electron density towards the cyanide carbon upon coordination of cyanide to the cobalt center (Figure 18). This effect is indeed reflected by the important upfield shift observed between free CN$^-$ (168 pm) and the coordinated CN in **1-H**$^+$

(127 ppm). Furthermore, this effect is influenced by the nature of the trans lower ligand. The coordination of a stronger σ-donor to the trans axial position (imidazolate, **1**) thus results in a decreased polarization of the cyanide π-electron density compared to **1-H**$^+$, which leads to a downfield shift of the ^{13}C-NMR resonance.[107]

On the upper axial C≡N bond - IR spectrometry

Cyanide represents as well an excellent probe for infrared spectroscopy.[70, 109-111] However, while Fourier Transform Infrared spectroscopy (FTIR) of CN is well suited for solid state investigation,[70, 77, 112-113] detection becomes complicated in solution. In the case of B_{12}, FTIR of a solid sample yielded a recognizable C≡N band (2134 cm^{-1}). However, when the same study was performed in solution, the CN band became extremely weak, with a poor signal-to-noise ratio. Hence, detection of a shift in those conditions is not possible. Since solubilizing the compound is primordial in order to modulate the solution's pH, another technique had to be found to study the C≡N vibrations.

For this purpose, a collaboration with the group of Prof. Peter Hamm (UZH) was instigated in order to measure 2D-IR of our model.[b] 2D-IR was used here as an innovative ultra-sensitive technique for the detection of low-concentrated bound cyanide in solutions.[114] Furthermore, only minimal amount of sample is needed (1 µl, 10 mM **1-H**$^+$). Measurements were performed in buffered D_2O solution, at pH 5.2 and pH 12.5 on the backbone B_{12} derivative **1-H**$^+$ and **1**.

[b] 2D IR measurements were performed by Klemens Koziol, Group of Prof. Peter Hamm, University of Zurich.

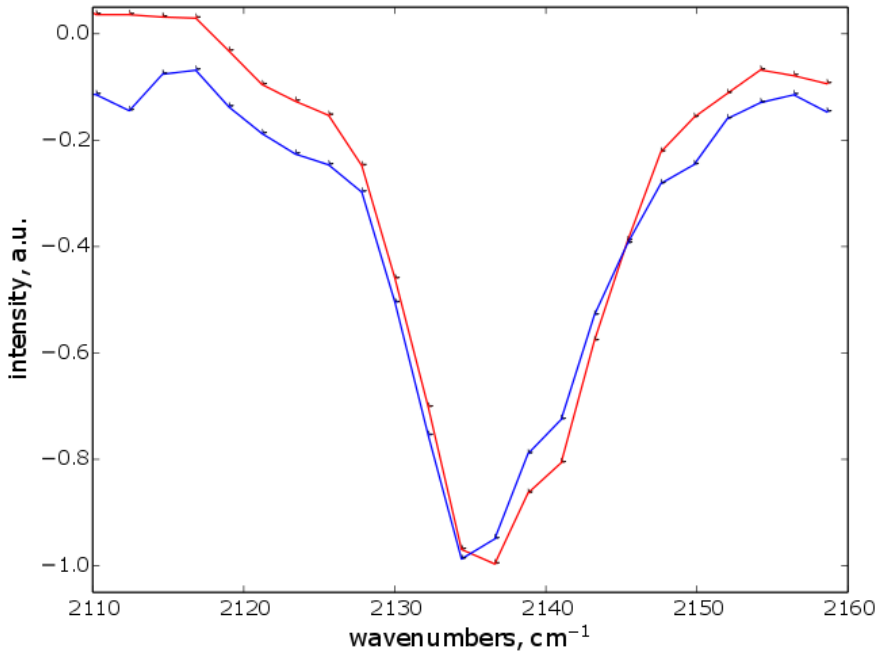

Figure 19 – Diagonal cut of 2D-IR spectra of **1-H**$^+$ (red) and **1** (blue).

Comparison between different β-bound CN vibrations in B_{12} derivatives teach us that coordination of free cyanide (2079 cm^{-1} [21]) leads to a shift towards high frequencies (B_{12}: 2132 cm^{-1} [21]). Modification of the lower ligand from benzimidazole to a stronger σ-donating ligand, like CN, leads to lengthening of the Co-CN bond. In this case the cyanide moiety resembles more the ionic free cyanide, and results in a shift of the vibration energies to a lower frequency compared to B_{12} ($(CN)_2B_{12}$: 2119 cm^{-1} [21]).[77] Following this trend suggests that the modulation of the α-ligand from an imidazole to an imidazolate group would lead as well to a shift in the IR frequency. Measurement of **1-H**$^+$ exhibited the C≡N band at 2137 ± 5 cm^{-1}. As observed in Figure 19, the CN band underwent a small shift to 2136 ± 6 cm^{-1} upon formation of **1** at pH 12.5. However, this shift is smaller than the error calculated for the Gaussian fitting of the data, and is thus not relevant.

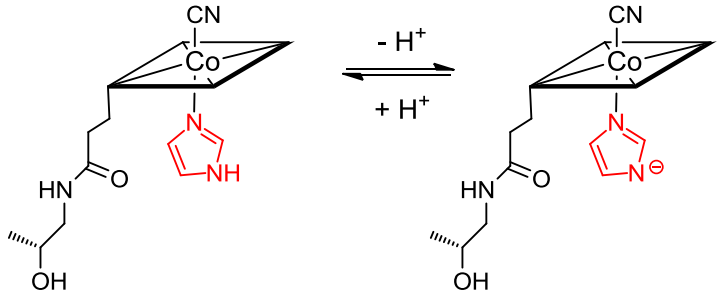

Scheme 11 - pH equilibrium of imidazole-bound cobinamide (Im-Cbi) (charges are omitted).

This assumption was supported by an additional set of experiments, using imidazole-bound cobinamide (Im-Cbi, Scheme 11) as model of the His-on B_{12} complex (Scheme 11). Samples were prepared by addition of 100 equivalents of imidazole to a β-CN Cbi solution (22 mM) in buffered D_2O buffered (pH 8.0 and 12.5). Coordination of the imidazole to the cobinamide and its subsequent deprotonation were followed by UV-vis spectroscopy. Upon coordination of the imidazole group, a bathochromic shift of the α-, β-, and γ- bands was observed ($\Delta\lambda$ = 25, 26 and 6 nm, respectively). Furthermore, deprotonation led to a similar bathochromic shift for the Im-Cbi model (9 nm, α-band, Appendix I, Figure A 1) and for the biomimetic model **1** (10 nm, α-band). This model is well-suited for investigation of CN stretching frequency, since the excess of free imidazole is not appearing in the measurement window (2110 – 2150 cm^{-1}). As for **1-H**$^+$, the CN band was observed at 2136 ± 4 cm^{-1} and exhibits a small shift of 1 cm^{-1} to 2135 ± 5 cm^{-1} upon deprotonation of the imidazole moiety at pH 12.5 (Appendix I, Figure A 2). Hence, this second model supports the results obtained with the peptide backbone derivative **1-H**$^+$, and indicates that the trans-influence on the C≡N vibrational energy is hardly detectable with this method.

On the cobalt reduction potential – Co as redox probe for cyclic voltammetry

The influence of proton release on the electrochemical properties of **1-H**$^+$ was then examined with cyclic voltammetry, using the cobalt center as redox probe. At pH 8.5, the reduction potential E_{red} of **1-H**$^+$ was equal to -920 ± 15 mV. Switching toward the fully deprotonated form **1** (pH 12.5) significantly lowered it by 180 mV, to a value of -1100 ± 0 mV (Figure 20). Performing these measurement on **2-H**$^+$ and **2** resulted in a slightly lower reduction potential, but a similar shift of 170 mV (from -930 ± 30 mV for **2-H**$^+$ to -1100 ± 20 mV for **2**).

The cathodic reduction of the Co(III) center is thus influenced by the basicity of the imidazole/imidazolate axial ligand. Indeed, the reduction of **1**, which bears a more electron-donating imidazolate moiety, is more difficult than **1-H**$^+$. The proton uptake therefore generates a less basic imidazole axial ligand and facilitates the reduction of **1-H**$^+$. Therefore, the Co(III) state is stabilized for the deprotonated compound **1** compared to

1-H$^+$. The direct correlation with the B_{12}-enzyme system indicates that replacement of the lower axial ligand by an His-coordinating residue allows a fine-tuning of the reduction potential by the protein, and confers to the cofactor's Co(III) state a stabilization towards reduction when partial deprotonation of the α-coordinating ligand occurs.

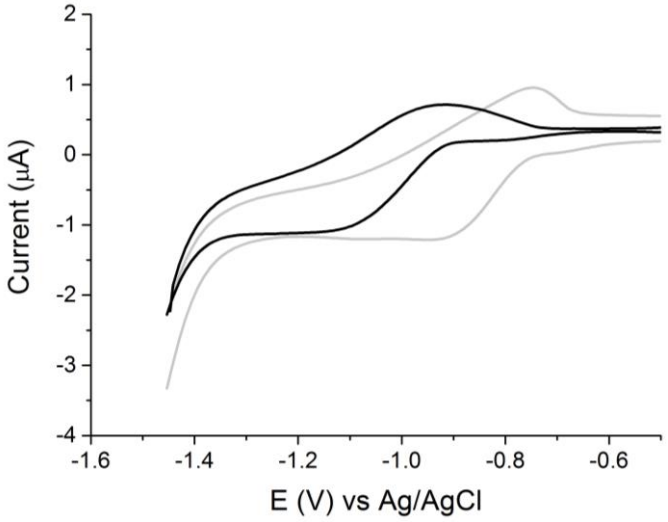

Figure 20 - Cyclic voltammogram of **1-H**$^+$ (pH = 8.5, grey) and **1** (pH = 12.5, black).

Comparison of the collected data for **1**, **1-H**$^+$ and B_{12} brings interesting insights into the effect of the lower ligand on B_{12} and B_{12} derivatives properties.[19, 54, 80, 115] Plotting of the cathodic reduction potential against the ^{13}C-NMR shift of the upper CN axial ligand of **1**, **1-H**$^+$, B_{12} as well as dicyano-cobinamide ($(CN)_2$-Cbi) and aquacyano-Cbi ((OH_2)CN-Cbi) (Figure 21) was thus carried out. These compounds all present different inter- or intra-coordinating lower ligand: -imidazolato, -imidazole, -dimethylbenzimidazole, -cyano and -aqua and give thus instructive information on the influence of lower ligand modulation. Indeed, the obtained linear correlation suggests that the relative sigma-donating capacities of the lower ligand similarly influence both the reduction potential as well as the upper CN ^{13}C shift (Figure 22).

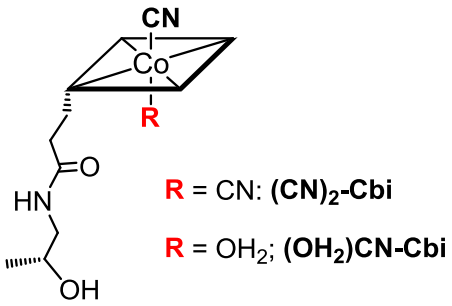

Figure 21 - Structure of (OH_2)CN-Cbi and $(CN)_2$-Cbi (charges are omitted).

This graph emphasizes as well the role of the histidine coordination to the cobalt center. Indeed, the base-on/base-off switch of vitamin B_{12} is not sufficient to reach lower reduction potentials. The base decoordination, modeled here by the aquacyano Cbi, leads to destabilization of the Co(III), as proven by the less negative reduction potential (- 796 mV). Hence, B_{12} alone cannot tune its redox properties towards a more stable Co(III) form. However, deprotonation of the lower imidazole ligand to an imidazolato moiety leads to an important stabilization of the Co(III) towards reduction (-1100 mV). Partial deprotonation of the imidazole moiety thus represents a very elegant method for B_{12}-dependent enzyme for fine tuning the cofactor properties and reactivity.

Figure 22 also depicts the position of the α-band. The latter reflects the d_{z2} contribution of the lower axial ligands to the HOMO orbital.[80, 116] Hence, the σ-donating character of the α-axial ligand is reflected by the position of the α-band: a stronger σ-donor leads to a bathochromic shift,[80] which coincides with the trends proposed in Figure 22. A linear correlation is as well observed when plotting the α-band absorbance against the E_{red}, which indicates again a similar influence of the σ-donor character of the lower axial ligand on the E_{red} and on the maximum absorbance wavelength.

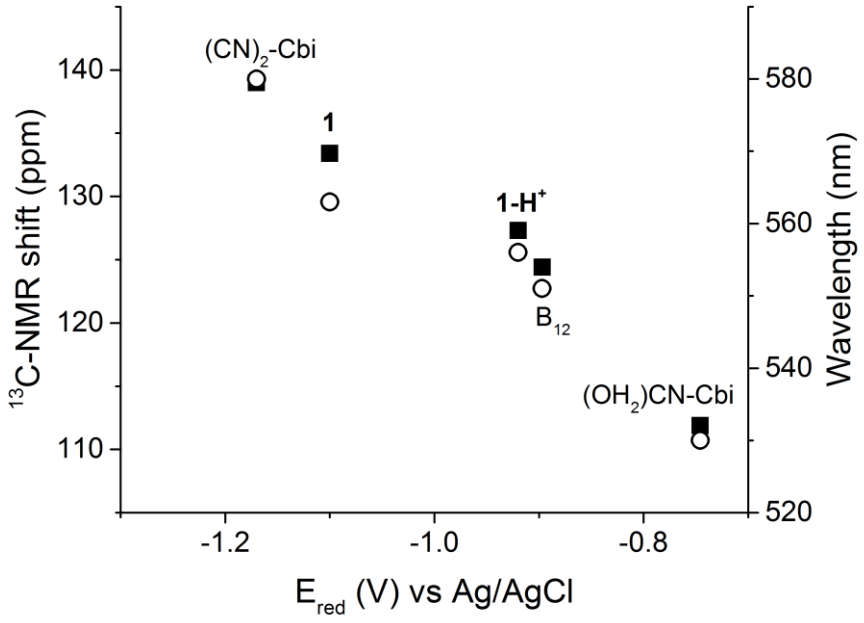

Figure 22 - Correlation between E_{red} and the ^{13}C-NMR shift of CN (left axis, ■) and the α-band wavelength (right axis, ○); B_{12} data correspond to both pH 7.0 and pH 12.5.

Detailed spectroscopic and theoretical studies were performed by Brunold and coworkers[54] as well as by Marzilli and coworkers,[78] with different but related histidine-on Cbls models, bearing an alkylated upper methyl ligand. However, no trans-influence of the lower axial ligand was observed in those models. This difference is attributed to the upper ligand nature. Indeed, apparently the less σ-donating CN group is more affected by the lower trans ligand, as opposed to the stronger σ-donating alkylated methyl group.[80]

Complementary Electrochemical study

The electrochemistry study of the biomimetic model were presented for the compound **1-H**$^+$ (**2-H**$^+$) and **1** (**2**), all derivatives bearing a cyanide group as β-axial ligand. The resulting voltammograms present both a merging of the two one-electron waves, as expected for cyanocobalamins.[117] In order to gain more insights about this process, two other derivatives were investigated: the **(OH$_2$)-2-H**$^+$ and the reduced **2-H**^+_r [118] (Figure 23).

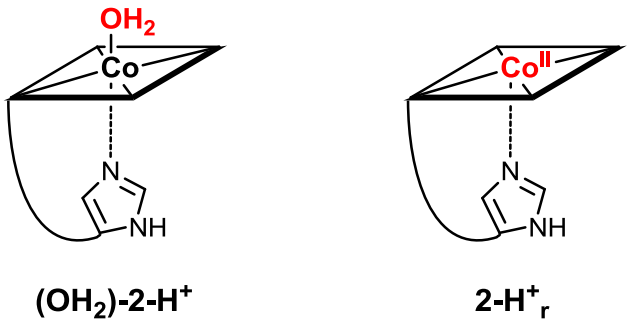

(OH$_2$)-2-H$^+$ **2-H^+_r**

Figure 23 - Structure of the aqua-derivative **(OH$_2$)-2-H$^+$** and of the reduced derivative **2-H^+_r** (charges are omitted).

The aqua derivative **(OH$_2$)-2-H$^+$** was expected to result in two one-electron waves, corresponding to the Co(III)/Co(II) and the Co(II)/Co(I) oxidoreduction couples. Measurement at pH 7.5 and 11.5 both presented two oxidation waves but only one reduction wave, situated at -580 mV at pH 7.5, with the protonated imidazole compound (Appendix I, Figure A 4, left), and at -640 mV with the imidazolate group derivative, at pH 11.5 (Appendix I, Figure A 4, right). Hence, modification of the upper ligand from CN to H_2O results in an important change in the reduction potential (-1100 to -580 mV), but still yields a shift of 60 mV upon deprotonation of the imidazole group.

For the Co(II) derivative **2-H^+_r**, a single wave is observed at -720 mV at pH 5, corresponding to the Co(II)/Co(I) reduction (Appendix I, Figure A 6, left). When raising the pH to 12, the reduction is shifted to -860 mV (Appendix I, Figure A 6, right), which corresponds to a difference of -140 mV.

In conclusion, these three different derivatives (**2-H$^+$**, **(OH$_2$)-2-H$^+$** and **2-H^+_r**) all present a shift of the reduction potential upon deprotonation of the imidazole group, however this shift is considerably varying depending on the nature of the upper ligand and on the oxidation state of the cobalt center.

3.1.4. Vitamin B_{12} as `blocked` model

Control experiments were performed with a `blocked` model, where the reversible protonation of the lower coordinating imidazole ligand is impossible. For this purpose, vitamin B_{12} itself was studied at different pH by CV (Figure 24, A), UV-vis (Figure 24, B) and ^{13}C NMR (Figure 24, C). Indeed, B_{12} (Figure 1) contains a lower 5,6-dimethylbenzimidazole ligand for which reversible protonation of the imidazole nitrogen is impossible since one nitrogen is involved in Co-coordination, while the second one is part of the glycosidic bond. In effect, the results exhibited no significant shifts upon pH changes (Figure 24), thus proving that all results obtained with **1-H**$^+$ and **1** indeed originated from the reversible deprotonation of the imidazole ligand.

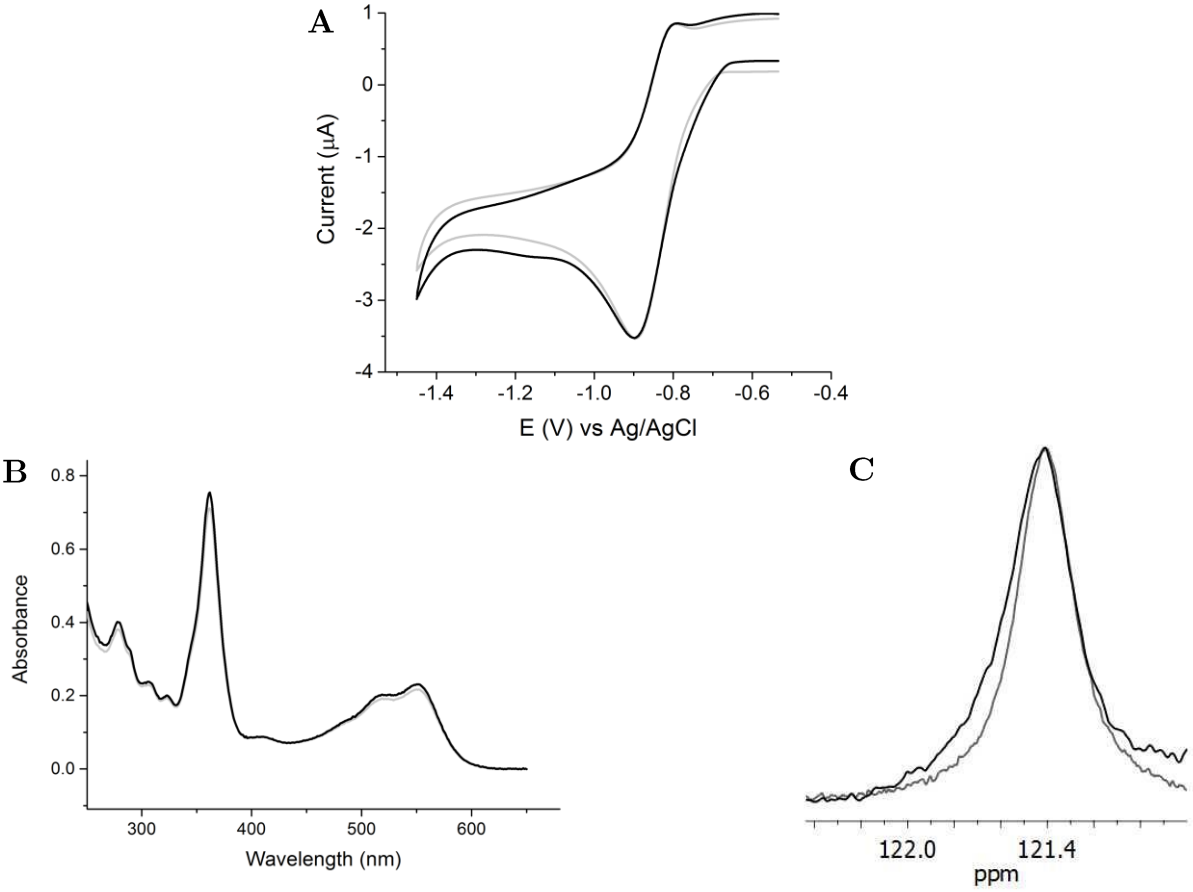

Figure 24- **A**: CV of B_{12} at pH 7.0 (grey) and pH 12.5 (black). **B**: Absorbance spectra of B_{12} at pH 7.0 (grey) and pH 12.5 (black). **C**: ^{13}C-NMR resonance of upper ^{13}CN ligand in B_{12} at pH 7.0 (grey) and pH 12.5 (black).

Table 1 recapitulates the data obtained for the peptide backbone derivatives **1-H**$^+$ and **1**, as well as the data of B_{12} at pH 7.0 and pH 12.5 and of the two cobinamide derivatives aquaCNCbi and $(CN)_2$Cbi.

Table 1

Entry	**Compound**	**E_{red} (mV)**	**CN ^{13}C-NMR shift (ppm)**	**λ of α-band (nm)**
1	**1-H**$^+$	-920	127	556
2	**1**	-1100	133	563
3	B_{12}	-900	124	551
4	(OH_2)CN-Cbi	-750	112[a]	530
5	$(CN)_2$-Cbi	-1170	139[a]	580

[a]values obtained from reference [37]

3.1.5. Model of the Charge Relay System: Partial Deprotonation with Benzoate

In the enzyme, the histidine residue undergoes partial deprotonation through H-bonding interactions with the charge relay system. Hence, this partial deprotonation is not associated with a change in the pH value of the binding pocket environment. Further studies were thus performed on the effect of partial deprotonation resulting from H-bonding rather than high pH. Therefore, the interaction between **1-H**$^+$ and a H-bonding acceptor were investigated, in order to imitate more closely the biological system. For this procedure, benzoic acid was chosen as H-bonding acceptor. The benzoic acid environment was rendered more aprotic by the use of H_2O/dioxane mixture as solvent. In those conditions, benzoate ions indeed constitute an interesting model of a buried carboxylate anion, as found in enzymes.[119] However, this study did not lead to any remarkable shift in the compound absorbance (Appendix I, Figure A 7). It was thus thought that the presence of water might be problematic for this experiment and the hydrophobic environment of a protein was of importance for efficient detectable H-bonding interaction. The solution came from immobilization of **1-H**$^+$ on $C18_{ec}$ silica material, which allows studying of proton release with diffuse reflectance spectroscopy (DRUV-vis), an approach recently introduced by our group.[81] Indeed, immobilized **1-H**$^+$ (**1-H**$^+_{\mathbf{SP}}$) remains in its base-on configuration upon immobilization, as indicated by its characteristic absorbance spectrum (α-band: 551 nm; β-band: 520 nm, Appendix I, Figure A 8). This behavior was however surprising, since B_{12} switches partly in its base-off form upon immobilization on $C18_{ec}$.[81] Comparison of the respective $pK_{base\text{-}off}$ values reveals that the base-on form of **1-H**$^+$ is roughly 100 times less favored than B_{12}, indicating that other parameters influence more strongly the configuration observed upon immobilization. The favored base-on configuration observed for **1-H**$^+_{\mathbf{SP}}$ is thus thought to result from the specific hydrophobicity of the imidazole ligand, which consequently yields to different interaction with the $C18_{ec}$ material.

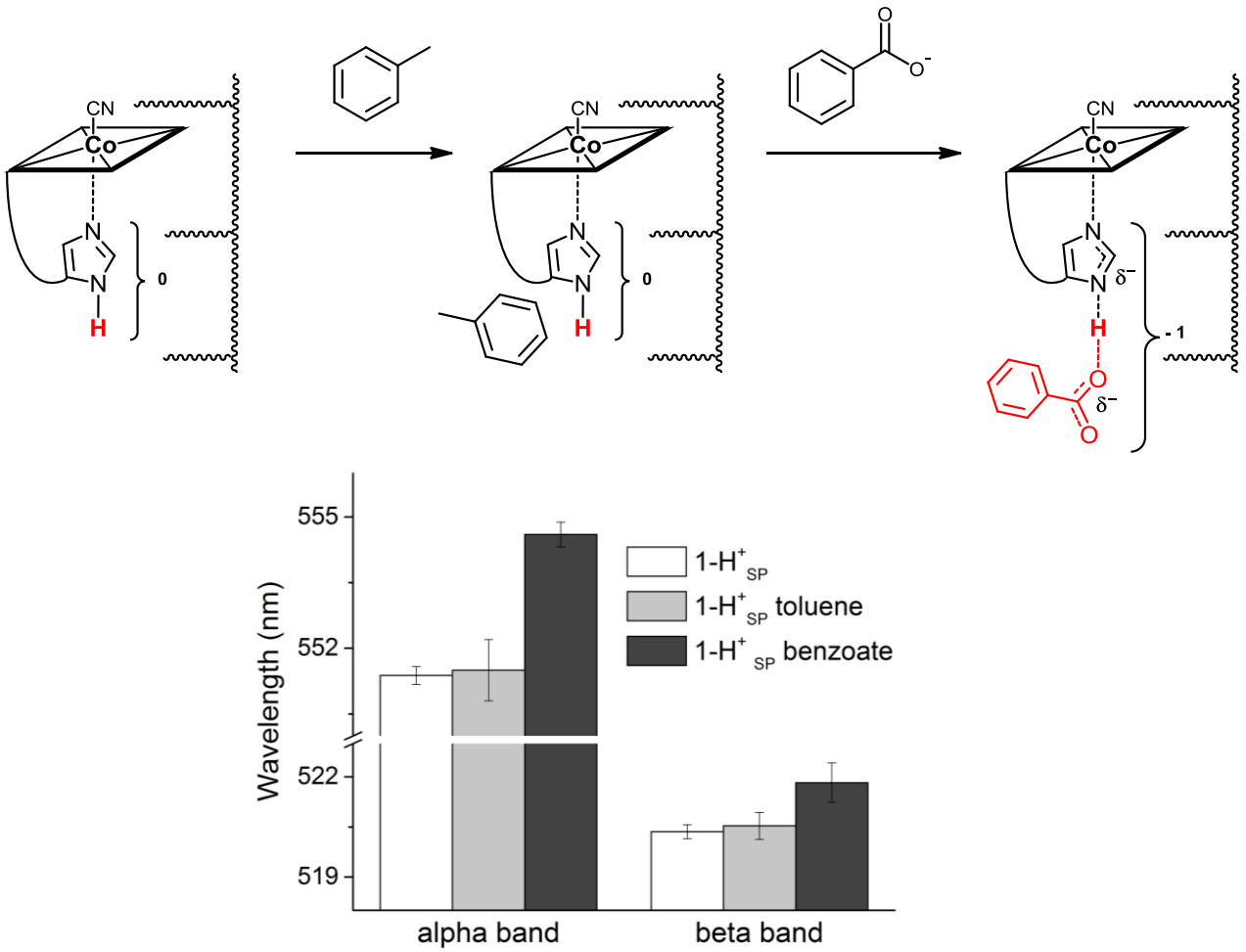

Figure 25 - Top: Proposed mechanism for the reaction of **1-H$^+$$_{SP}$** immobilized on C18$_{ec}$ (left) with toluene (middle) and with benzoate (tetrabutylammonium salt; right). Bottom: Absorbance for the α and β bands of immobilized **1-H$^+$$_{SP}$** (white), **1-H$^+$$_{SP}$** after the addition of toluene (grey) and **1-H$^+$$_{SP}$** after the addition of a solution of benzoate in toluene (black) (n=4) (charges are omitted).

Deprotonation of the immobilized imidazole base was first studied by adding a 1 M NaOH solution, which led to the expected bathochromic shift (6 nm for the alpha band), similar to the one observed under homogeneous conditions (Appendix I, Figure A 8). The study was then pursued by addition of toluene, which did not lead to any shift (Appendix I, Figure A 9). However, the addition of a tetrabutylammonium benzoate solution (saturated in toluene) exhibited a slight, but characteristic bathochromic shift of the α-band and β-band (4 nm and 2 nm respectively), (Figure 25, Appendix I, Figure A 10). Hydrogen bonding interactions between the benzoate species and the Nδ hydrogen of **1-H$^+$$_{SP}$** are suggested to be responsible for this spectral change.

The choice of benzoate as H-acceptor was impelled by the carboxylate ion presence, which closely imitates the aspartic acid residue found in the charge relay system. However, partial deprotonation of the imidazole moiety can be achieved with any H-acceptor, for example dioxane, and will lead to an identical shift of the α- and β-band. Indeed, performing the experiment with benzoic acid or dioxane alone led to the same bathochromic shift of 4 nm (α-band).

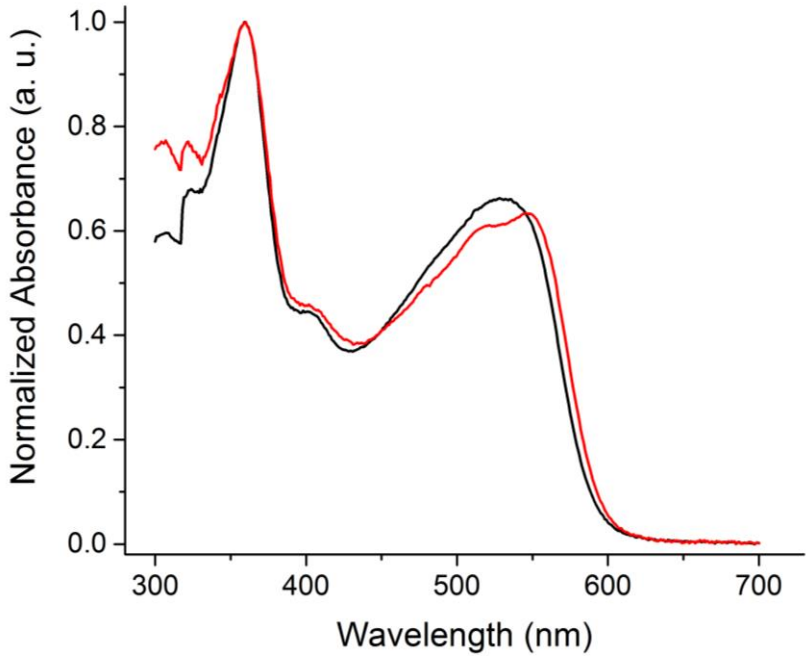

Figure 26 - DRUV-vis of B_{12} on $C18_{ec}$ before (black) and after addition of a saturated solution of benzoic acid in toluene (red).

Several experiments were performed to prove that the observed shift is indeed resulting from interaction with the imidazole moiety, and not another part of the molecule. These experiments were performed on several different blocked models, which were immobilized on $C18_{ec}$ and washed with a saturated solution of benzoic acid in toluene. However, this appeared to be a challenging study, due to coordination of benzoic acid to the cobalt center. B_{12} was the first model tested. As previously mentioned, the B_{12} undergoes partial decoordination upon immobilization on $C18_{ec}$, detected by the merging of the α- and β- bands, as well as a hypsochromic shift. Hence, addition of benzoic acid led to coordination, which resulted in the splitting of the α- and β- band (Figure 26). The same experiment was performed using $(CN)_2$-Cbi as model, however a hypsochromic shift was observed, resulting from replacement of one of the cyanide moiety by benzoic acid

(Appendix I, Figure A 11). A different peptide backbone B_{12}[c] was then tested, but this compound exhibited a similar behavior as B_{12} and shifted partially to base-off upon immobilization (Appendix I, Figure A 12). The last experiment was performed on the open-ring 14,15-dioxo B_{12} derivative,[d] which displays an extremely stable dicyano form. And indeed, for this compound addition of a saturated benzoic acid solution did not lead to any change in the absorbance spectrum (Figure 27). Discovery of this blocked model thus proved that the modulations observed for **1-H$^+_{sp}$** were indeed resulting for hydrogen bonding interaction with the imidazole group.

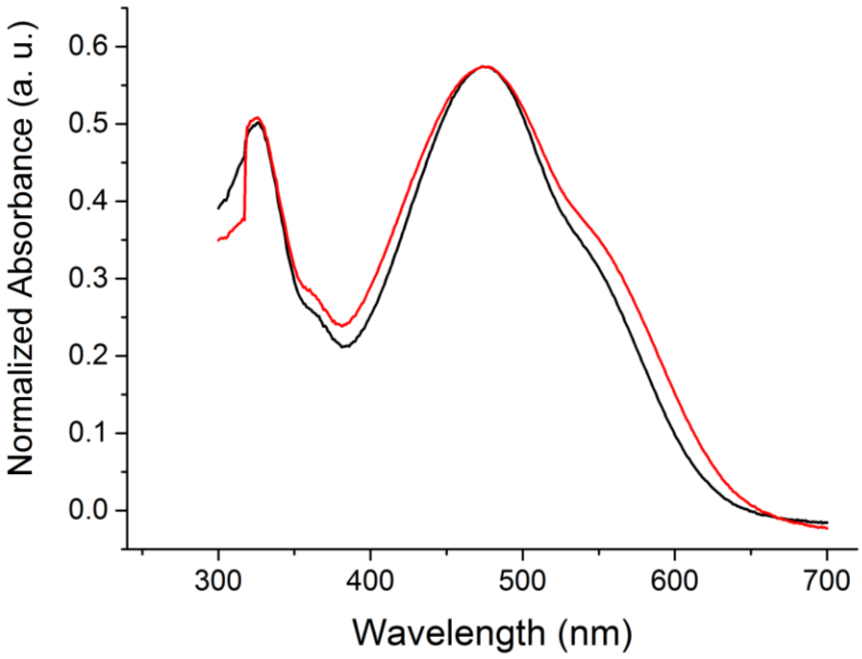

Figure 27 - DRUV-vis of the open-ring 14,15-dioxo B_{12} derivative $C18_{ec}$ before (black) and after addition of a saturated solution of benzoic acid in toluene (red).

[c] Peptide B_{12} was obtained from Dr. Kai Zhou.

[d] Generous gift from Lucas Prieto is aknowleged.

3.2. An Interesting Intermediate: Short Loop B_{12} Derivative as Antivitamin

This chapter is focused on the antivitamin B_{12} derivative, aimed at inhibiting the growth of *E. coli* bacteria. The antivitamin candidate **6** is depicted in Figure 28, together with the B_{12} derivative cobinamide (Cbi). In the first part of this chapter, the synthesis of **6** is presented. It is then followed by a detailed comparison between **6** and Cbi, achieved with UV-vis spectrometry, CV and NMR. The second part of this chapter reports of the biological studies performed on **6**.

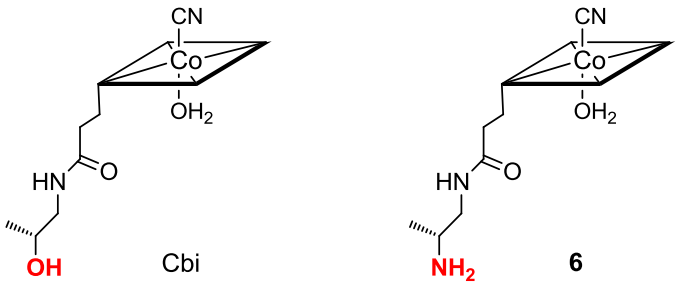

Figure 28 - Structure of cobinamide (Cbi) and of the incomplete B_{12} derivative **6** (charges are omitted).

3.2.1. Synthesis of 6 and Comparison with Cobinamide

The short loop B_{12} derivative **6** corresponds to an intermediate in the synthesis of **1-H**$^+$ (Chapter 2.1.1). It was synthesized by coupling Boc-ethylenediamine (**4**) to cobyric acid (**3**), using common coupling reagents, to obtain **5**. It was then followed by the deprotection of the amino group to give **6** (Scheme 12). The high resolution mass spectrum of **5** ($C_{54}H_{81}CoN_{13}O_9$) was found to be 1114.56100, which corresponds to $[M\text{-}H_2O]^+$ and fits tightly with the calculated mass of 1114.56067. Similar results were obtained with **6**, for which the measured high resolution mass spectrum is 1014.50900 ($C_{49}H_{73}CoN_{13}O_7$) for $[M\text{-}H_2O]^+$ (calculated: 1014.50824).

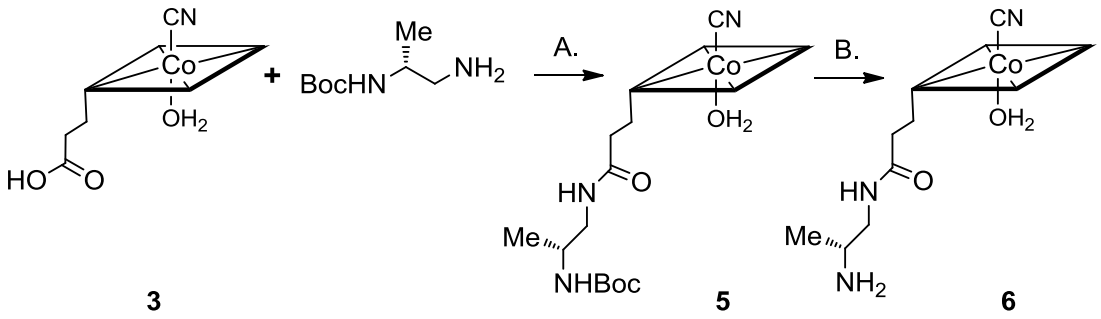

Scheme 12 - Synthesis of **6** (A. NEt_3, ethylchloroformate, DMF, 0°C. B. HCl 1 M.) (charges are omitted).

The structural difference between the B_{12} derivative cobinamide and **6** is minimal and stands in the end of the f-side chain, with a terminal hydroxyl for cobinamide while **6** is terminated with a primary amine (Figure 28). Due to their resemblance, these molecules share identical properties, as proven by the UV-vis (Figure 29), the cyclic voltammogram (Figure 30) and the NMR (Figure 31) presented in this chapter. The UV-vis of both compounds in their dicyano form indeed displays exactly identical maximum absorption wavelength as well as same extinction coefficient (ε). Both compounds thus exhibit an α-band at 579 nm (ε = 10089 $M^{-1}cm^{-1}$), a β-band at 541 nm (ε = 8735 $M^{-1}cm^{-1}$) and a γ-band at 368 nm (ε = 30508 $M^{-1}cm^{-1}$), as shown in Figure 29.

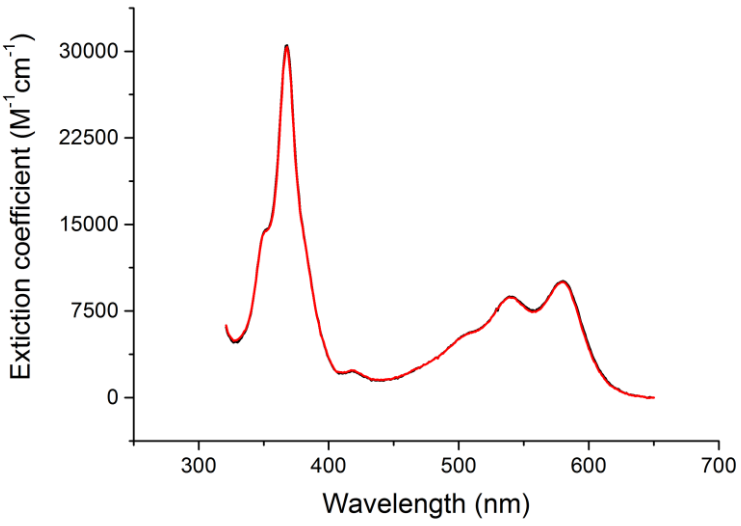

Figure 29 - Absorbance spectra of $(CN)_2$-Cbi (black) and **$(CN)_2$-6** (red).

Furthermore, the study of redox properties also revealed that both aquacyano Cbi and aquacyano **6** display identical cathodic and anodic potentials, with a reduction potential

at -741 mV and an oxidation potential at -674 mV (Figure 30). As expected, the slight difference existing between Cbi and **6** is not influencing the electrochemical properties of the Co-center.

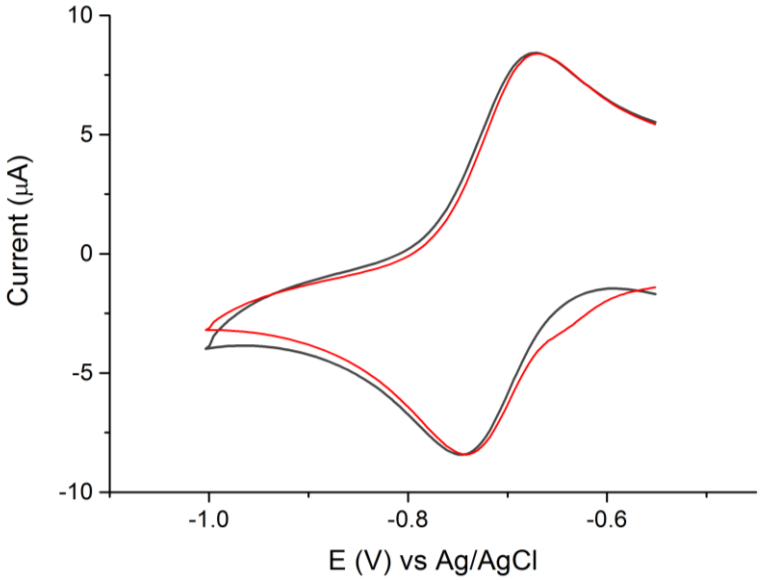

Figure 30 - Cyclic voltammogram of (OH_2)CN-Cbi (black) and **(OH_2)CN-6** (red).

However, comparison of both ^{1}H-NMR spectra of the dicyano forms revealed one major difference: the proton of C176 shifts from 3.37 to 3.96 when changing the terminal group from an amine to an alcohol, due to the increased deshielding effect of the hydroxyl moiety (Figure 31, red circles). However, all the signal originating from the corrin ring and the other side chains are identical, as for example the H10 NMR shift which is at 5.93 ppm for both compounds. Hence, cobinamide and the molecule **6** present a small structural difference, which can be detected only by ^{1}H-NMR. However, as expected, this modification does not alter the intrinsic properties, as indicated by the identical absorbance and redox properties.

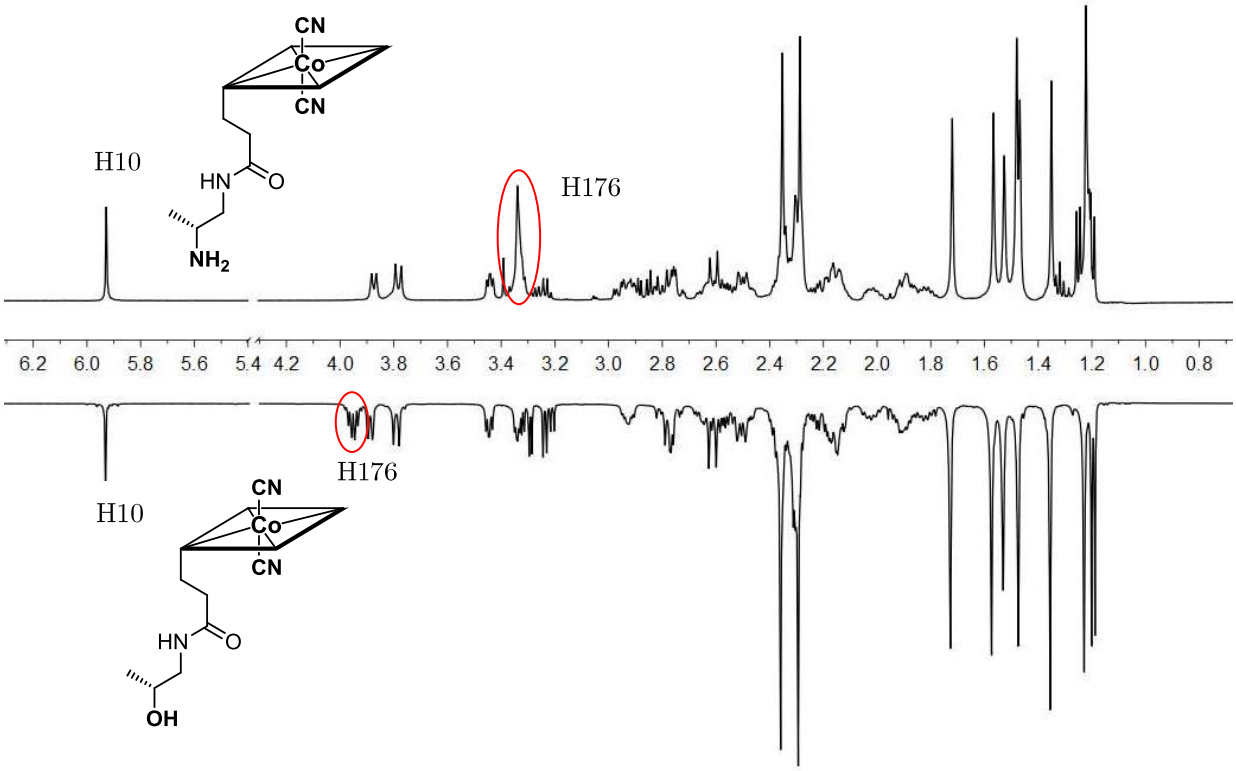

Figure 31 – ^{1}H-NMR of **$(CN)_2$-6** (top) and $(CN)_2$-Cbi (bottom) (charges are omitted).

Table 2– ^{1}H chemical shifts values of $(CN)_2$-6 and$(CN)_2$-Cbi.

	δ ^{1}H (ppm)	
	$(CN)_2$-6	**$(CN)_2$-Cbi**
C1A	1.53	1.54
C2A	1.57	1.58
C3	3.87	3.89
C7A	1.72	1.73
C8	3.44	3.45
C10	5.93	5.93
C12A	1.47	1.48
C12B	1.23	1.24
C13	3.33	3.34
C17B	1.35	1.36
C18	2.92	2.93
C19	3.78	3.80
C21	2.35/2.31	2.36/2.30
C31	2.00/2.32	2.01/2.33
C32	2.57/2.51	2.58/2.51
C51	2.29	2.30
C71	2.60/2.31	2.60/2.32
C81	2.15/1.82	2.15/1.83
C82	2.32	2.33
C131	2.19/1.82	1.20/1.82
C132	2.32/2.20	2.32/2.20
C151	2.36	2.36
C171	2.65/2.17	2.65/2.17
C172	2.49/1.80	2.50/1.81
C175	3.27/3.24	3.30/3.24
C176	**3.34**	**3.96**
C177	1.21	1.20
C181	2.76/1.89	2.78

3.2.2.Biological studies on E-Coli

As previously mentioned (Chapter 1.5), *E. coli* possesses as well a B_{12}-independent methionine synthase (MetE). The use of a mutated *E. coli* (NCIMB 8134) lacking this B_{12}-independent pathway was thus required for biological investigations, in order to obtain detailed insights about the antivitamin activity of our derivative.[98]

Replacement of the final –OH group in cobinamide is thought to impede the first phosphorylation step of the AdoCbl synthesis in *E. coli*. Bacteriologic tests are performed by our collaborator Pr. Helmut Brandl. Preliminary results of competition study (1 nM of cobinamide + 1-1000 nM of **6**) showed that **6** exhibited antibacterial activity already at 1 nM. However, this study is still in progress.

Additionally, biological tests were performed on healthy mammal cells.[e] According to previous studies, cobinamide binds extremely weakly to the human transport proteins IF and TCII (0.01 % and 0.5 % respectively, compared to 100 % for vitamin B_{12})[120] hence cellular internalization of cobinamide is improbable. [120-123] These tests were thus aimed at confirming the specificity of **6** for bacteria. **6** exhibited an $IC_{50} > 100$ µM, thus proving that it would target only bacterial cells, and that its uptake would not be a risk for human cell replication process.

It is however important to mention that the normal strain of *E. coli* is expected not to be reactive towards antivitamin B_{12}, due to the B_{12}-independent pathway. This study thus only represents a proof-of-concept.

[e] Studies performed by Dr. Loganathan Rangasamy from Pr. Dr. Gilles Gasser, University of Zurich

4. Conclusion and Outlook

4.1. Biomimetic Model

The aim of this project was the modeling of the His-on configuration found in the active site of B_{12}-dependent enzymes. More precisely, studies were performed to understand the effect of the histidine reversible deprotonation on the B_{12} cofactor. For this purpose, a biomimetic model was designed, synthetized and investigated. In this model, the natural backbone of B_{12} was replaced by a peptide loop terminated by an imidazole moiety, which can be deprotonated. Structural studies and calculations proved the resemblance between the biomimetic model and the structure of the B_{12}-histidine complex in methionine synthase, thus attesting of the good quality of the model.

The effect of the loop structure was as well investigated, and the study demonstrated that presence of a R-configured methyl group on the backbone influences the loop-coordination equilibrium. However, interestingly it does not modify the imidazole acidity.

The influence of imidazole deprotonation was thoroughly researched, using several different methods. Hence, an important shift of the reduction potential (200 mV) was discovered between B_{12} and the deprotonated model **1**. This interesting effect was furthermore related to a modification of the upper cyanide bond strength through trans influence. Studies of natural vitamin B_{12} showed that the same type of modulation of the redox potential is impossible for B_{12} alone. These results thus brought great insights into the role of histidine coordination to B_{12} cofactor in Nature. Indeed, histidine reversible protonation represents a way for B_{12}-dependent enzymes to control the cofactor's properties and reactivity by modulating its reduction properties.

Immobilization of the model on hydrophobic C18 silica allowed a closer imitation of the active site. It indeed made possible the partial deprotonation of the imidazole group through hydrogen bonding with an orthogonal carboxylate, thus emulating the charge relay system encountered in B_{12}-dependent enzymes.

These studies thus proved the importance of histidine coordination to the B_{12} cofactor, as well as the significant influence of partial deprotonation on the properties of cobalamins.

Hence, it is bringing great insights on the role of charge relay systems in B_{12}-dependent enzymes, which is thought to be the enzyme's mean to control the cofactor reactivity. Furthermore, a new system for mimicking complex biological architectures on hydrophobic surfaces was as well introduced. Such a method is expected to be of general interest as model of the local protein environment for investigating the triggering of cofactor's reactivity.

4.2. Antivitamin B_{12} as *E. Coli* Antibacterial

The considerable importance of vitamin B_{12} in cell replication processes is inspiring for the development of anticancer and antibacterial compounds. In this context, we proposed the design, synthesis and investigation of an incomplete B_{12} derivative as antivitamin B_{12} for antibacterial purpose. The design was based on the ability of *E. coli* to synthesize the AdoCbl cofactor from the short-loop cobinamide compound. Hence, it was expected that slightly modifying the short backbone of cobinamide from an hydroxyl to an amino group would prevent the backbone synthesis in *E. coli*, thus inhibiting bacterial growth.

The first part of this project consists of the comparison of the antivitamin derivative **6** and cobinamide. Performing UV-vis spectrometry, cyclic voltammetry and ^{1}H-NMR allowed to prove that the simple backbone modification results in a compound with identical properties as cobinamide. The only modest difference observed arose, as expected, in the ^{1}H-NMR were the resonances of the backbone were slightly shifted due to the presence of terminal amine.

Preliminary results of the bacteriological tests showed an important antibacterial effect, when performed on a mutant *E. coli* strain exclusively B_{12}-dependent. However, this investigation is still in process. In the future, supplementary biological studies are expected to be performed, starting by testing the normal *E. coli* strain.

5. Experimental Procedures

5.1. List of compounds – Structures

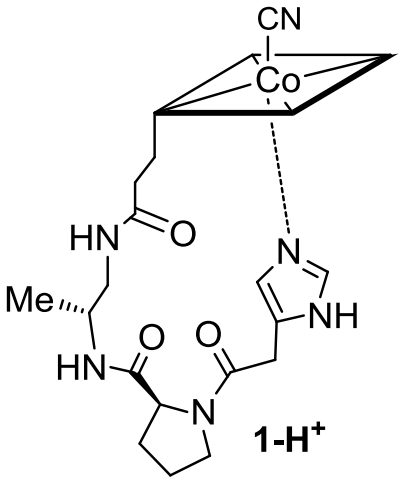

1-H$^+$

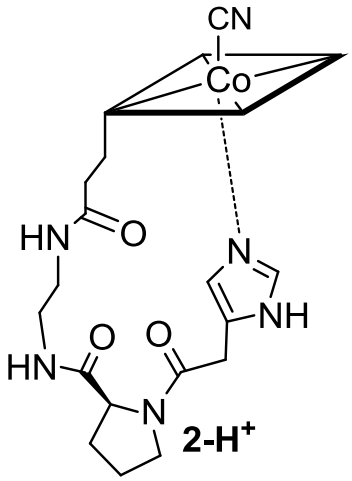

2-H$^+$

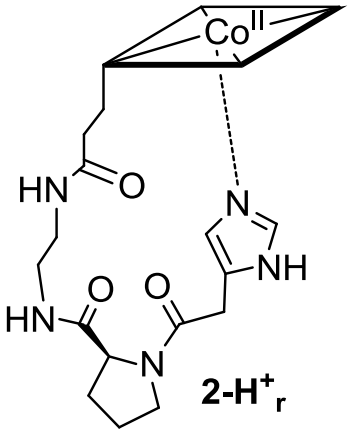

2-H^+_r

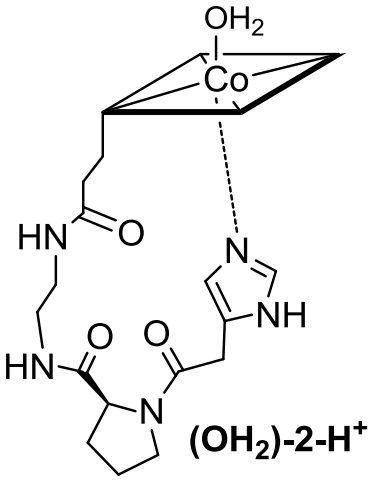

(OH$_2$)-2-H$^+$

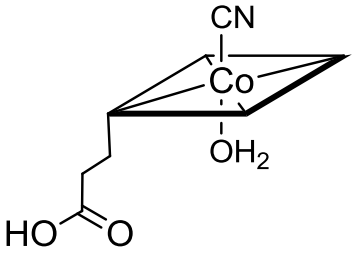

3

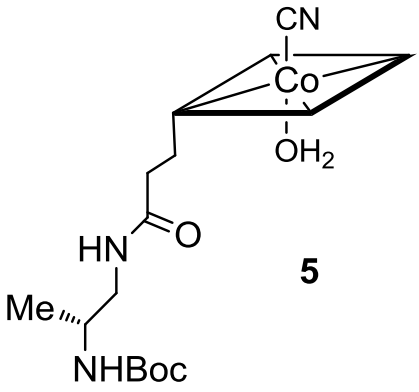

5

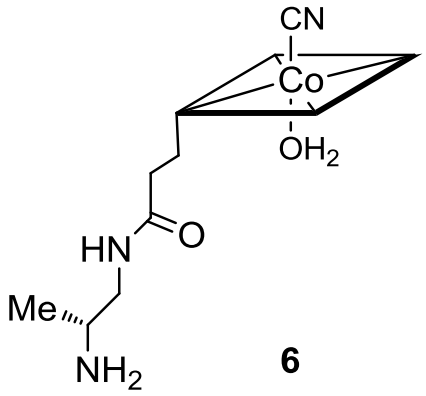
CN
Co
OH2
HN
O
Me
NH2

6

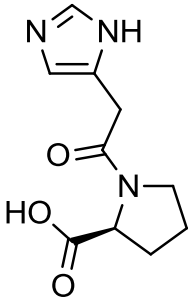
N
NH
O
N
HO
O

7

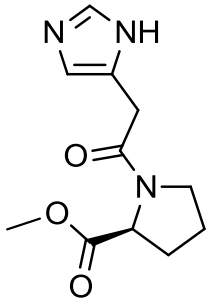
N
NH
O
N
O
O

10

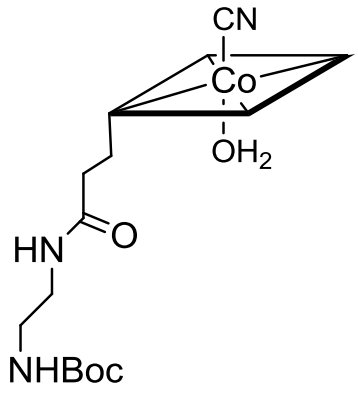
CN
Co
OH2
HN
O
NHBoc

12

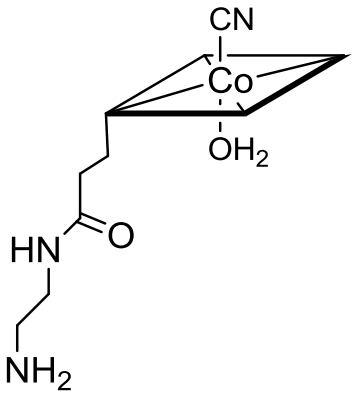
CN
Co
OH2
HN
O
NH2

13

5.2. Material and Methods

Chemicals - All chemicals were of reagent grade and used without further purification. Deuterated solvents were obtained from Armar Chemicals (Döttingen, Switzerland). Solvents for HPLC and UPLC were of the corresponding grade. Dicyanocobyric acid (**3**) was prepared from the method of Müller et al.[124]

HPLC - HPLC solvents were 0.1 % aqueous trifluoroacetic acid and methanol or acetonitrile. Analytical HPLC analyses were performed on a Merck-Hitachi L-7000 system equipped with a diode array UV-Vis spectrometer. Macherey Nagel Nucleosil $C18_{ec}$ RP columns (5 µm particle size, 100 Å pore size, 250 x 3 mm. Flow rate: 0.5 ml/min). Preparative HPLC separations were performed on a Varian Prostar system equipped with two Prostar 215 pumps, a Prostar 320 UV/Vis detector and Macherey Nagel Nucleosil $C18_{ec}$ RP columns (7 µm particle size, 100 Å pore size, 250 x 21 mm. Flow rate: 18 ml/min) was used as column.

Solid phase extraction (SPE) was conducted using Chromafix $C18_{ec}$ by Macherey-Nagel. The sample was dissolved in water and charged on the absorbent. After washing with water, the compound was eluted with MeOH.

UV-Vis spectra were recorded on a Cary 50 spectrometer using quartz cells with a path length of 1 cm.

pH values were measured using Metrohm 827 pH lab with a Metrohm glass electrode stored in 0.3 M KCl. The pH-meter was calibrated before each session of measurement.

pH titrations were performed in UV cuvettes, in 0.2 M KCl with concentrations of compound between 10 µM and 35 µM. Solutions of different concentrations of HCl (0.01 M to 6 M) or of NaOH (0.1 M to 5 M) were added, and the pH value was measured after each addition with the pH meter. The pK_a and $pK_{base\text{-}off}$ values were obtained from the analysis of a Boltzmann function: $y = A2 + (A1 - A2) / (1 + \exp((x - x_0) / dx))$ fitting.

NMR spectra were recorded on a Bruker AV-500 spectrometer (Karlsruhe, Germany). The chemical shifts are given in ppm relative to the signal from trimethylsilyl propanoic acid. Coupling constants J are given in Hz. The data processing was carried out with

MestreNova. Experiments at different pH were performed in 0.1 M phosphate buffer in D_2O (pH = 7.4) and pH 12.5 was obtained by adding ~1 µl of NaOD in 0.5 ml D_2O. The pH were controlled by pH meter after each addition of sample.

Mass spectra were recorded either in the positive or negative mode on an Esquire HCT from Bruker (Bremen, Germany). The injection rate was 3 µl/min. A nebulizer pressure of 10 psi, a dry gas flow rate of 5 l/min and a gas temperature of 350 °C were applied. All solvents were of LCMS grade.

High-resolution electrospray mass spectra were recorded on a Bruker maXis QTOF-MS instrument (Bruker Daltonics GmbH, Bremen, Germany). The samples were dissolved in MeOH and analyzed via continuous flow injection at 3 µL/min. The mass spectrometer was operated in positive ion mode with a capillary voltage of 4 kV, an endplate offset of -500 V, nebulizer pressure of 5.8 psig, and a drying gas flow rate of 4 L/min at 180 °C. The instrument was calibrated with a sodium formate solution (500 µl H_2O : 500 µl iPrOH : 20 ul HCOOH : 20 µl 0.1 M NaOH aq). The resolution was optimized at 30'000 FWHM in the active focus mode. The accuracy was better than 2 ppm in a mass range between m/z 118 and 1600. All solvent used were purchased in best LCMS qualities.

Cyclic voltammetry was conducted on a 757 VA computrace electrochemical analyzer (Ω,Metrohm). Ag/AgCl electrode was used as reference and glassy carbon as working electrode. The samples were dissolved in 0.1 M KCl (2 ml) in concentrations around 1.5 mM. Hexacyanoferrate (1 mM) was used as internal or external reference. Before each measurement, the glassy carbon electrode was polished for 1 minute and the sample was purged with nitrogen for 3 min.

UPLC solvents were 0.1 % aqueous formic acid and acetonitrile. UPLC measurements were performed on an Acquity™ Ultra performance LC and ACQUITY UPLC® BEH C18 column (1.7 µm 2.1×50 mm; flow rate: 0.3 ml/min).

DRUV/Vis spectra were recorded with a Lambda 650 S Perkin-Elmer UV/Vis spectrometer in the range 300–700 nm using a Quartz SUPRASIL precision cell (10 mm).

Immobilization on $C18_{ec}$ - The compound was dissolved in water and adsorbed to Chromafix $C18_{ec}$ (Macherey-Nagel). The C18 silica material was further rinsed with the desired solution (water, dioxane, toluene, saturated solution of benzoic acid or tetrabutylammonium benzoate in toluene or 1 M NaOH). The C18 silica cylinder was removed from the plastic holder by applying pressure from the other end with an empty syringe and an adapted connector. A slice of the C18 silica compound was then cut, let to dry and set between two quartz plates which were then tightly taped together.

2D-IR samples were prepared in buffered D_2O (10 µl), either 0.2 M acetic acid buffer (pH = 5.2), 0.1 M phosphate buffer (pH = 8.0) or 0.2 M potassium chloride/sodium hydroxide buffer (pH 12.5). The compound concentration was set between 15 and 25 mM, and controlled with UV-vis spectroscopy.

Cell culture [f] - Human breast adenocarcinoma cells (MCF 7) and human embryonic kidney cells (HEK293) were cultured in MEM (Gibco) and RPMI (Gibco) media respectively with 5 % fetal calf serum (FCS, Gibco), 100 U ml^{-1} penicillin and 100 mg ml^{-1} streptomycin at 37 °C and 5 % CO_2.

Cytotoxicity studies [f] - The cytotoxicity of the compounds towards human breast adenocarcinoma cells (MCF 7) and human embryonic kidney cells (HEK 293) was measured by a fluorometric cell viability assay. Resazurin (Promocell GmbH) has been used to establish the cytotoxicity of anticancer drug candidates against cancer cell line. Cells were plated in triplicates in 96-well plates at a density of ~5 x 103 cells/well in 100 µl 24h prior to treatment. Cells were then treated with increasing concentrations of compounds for 48h. After 48h in the incubator, the medium was replaced by 100 µl complete medium containing resazurin (0.2 mg/ml final concentration). After 4h of incubation at 37 °C, fluorescence of the highly red fluorescent resorufin product was quantified at 590 nm emission with 540 nm excitation wavelength in a SpectraMax M5 microplate Reader.

[f] Cell culture and cytotoxic studies were performed by Dr. Loganathan Rangasamy, from the group of Pr. Gilles Gasser (UZH).

QM/MM Calculations [g] **-** The geometry of the cobalamin molecule **1-H**$^+$ was optimized with a combined quantum mechanics/molecular mechanics (QM/MM) calculation using the Gaussian09's two-layer ONIOM method.[125-129] **1-H**$^+$ was partitioned into two regions as illustrated in Figure 32. The High Layer corresponds to the smallest part and was treated at the DFT level with the popular B3LYP (Becke, three-parameter, Lee-Yang-Paar) exchange-correlation functional [130-131] in conjunction with the LANL2DZ [132-135] basis set. In a two-layer model, the Low Layer consists of the entire molecule. The corresponding low layer atoms were treated with the UFF force field.[136] The geometry was then further optimized, using the 2D-ROESY results.

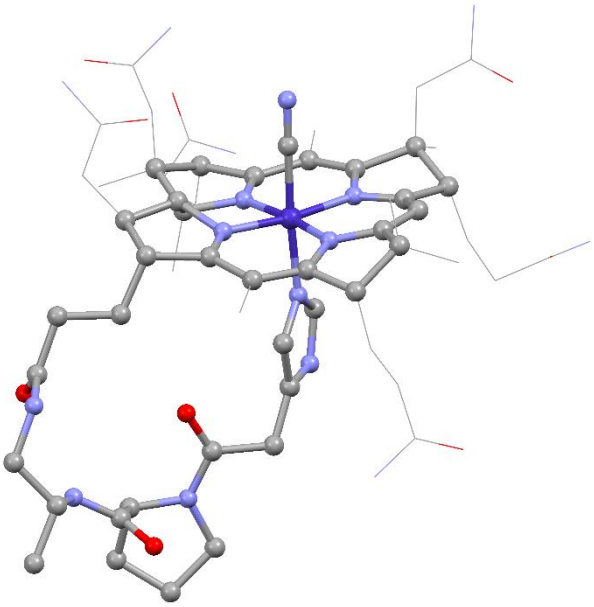

Figure 32 - ONIOM layer definition used for the QM/MM geometry optimization of **1-H**$^+$ (QM: balls and sticks, MM: wireframe).

[g] Calculations were performed by Dr. Olivier Blacque

Gradients:

Analytical 0.5 ml/min	Organic Solvent	Gradient (% corresponds to the percentage of organic solvent vs TFA-buffer)
Gradient 1	MeOH	0-5 min 5%. 5-30 min 5-100%
Gradient 2	MeOH	0-5 min 5%. 5-30 min 5-20%
Gradient 3	MeOH	0-5 min 25%. 5-30 min 25-100%.
Gradient 4	ACN	0-3 min 3%. 3-35 min 3-30%.
Gradient 5	ACN	0-3 min 25%. 3-35 min 25-50%.

Preparative 18 ml/min	Organic Solvent	Gradient (% corresponds to the percentage of organic solvent vs TFA-buffer)
Gradient 6	MeOH	0-3 min 25%. 3-30 min 25-100%.
Gradient 7	ACN	0-3 min 3%. 3-35 min 3-30%.
Gradient 8	ACN	0-3 min 10%. 3-35 min 10-40%.
Gradient 9	ACN	0-3 min 10%. 3-35 min 10-30%.
Gradient 10	MeOH	0-3 min 20%. 3-30 min 20-60%.

UPLC-MS 0.3 ml/min	Organic Solvent	Gradient (% corresponds to the percentage of organic solvent vs TFA-buffer)
Gradient 11	ACN	0-0.5 Min 5%. 0.5-2 min 5-30%. 2-4 min 30-100%

5.3. Reaction Schemes

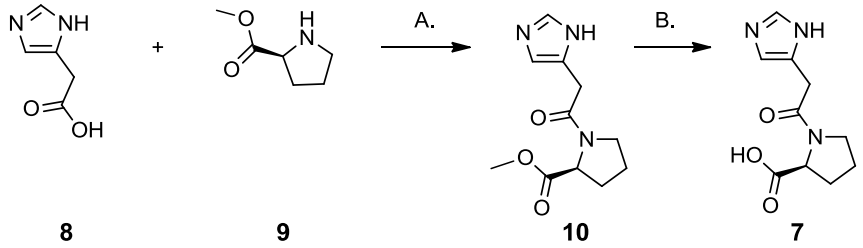

Scheme 13 - Synthesis of **7** (A: HOBt, EDC, DIPEA, DMF, 0°C. B: 0.5 M NaOH).

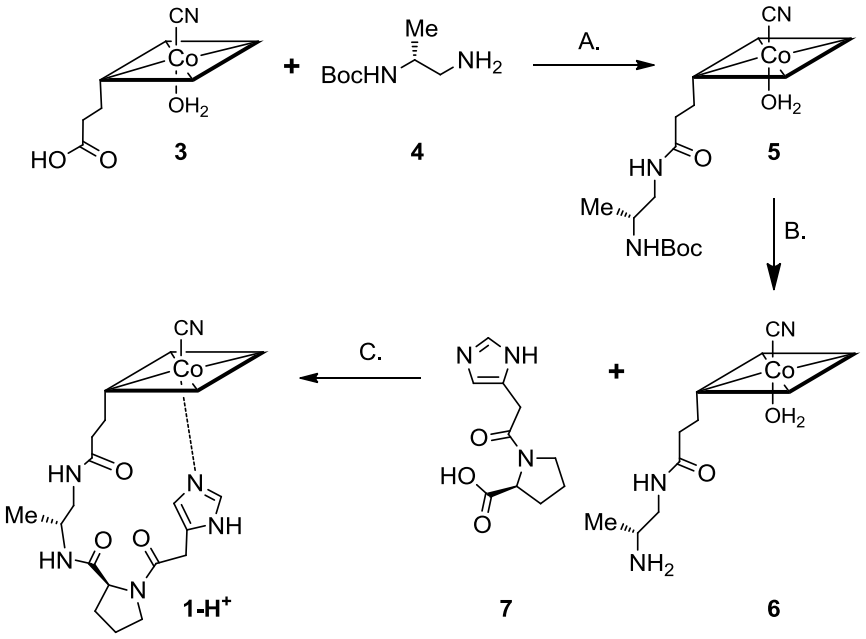

Scheme 14 - Synthesis of **1-H**$^+$ (A. NEt_3, ethylchloroformate, DMF, 0°C. B. HCl 1 M. C. DIPEA, HOBt, TBTU, DMF, 0°C) (charges are omitted).

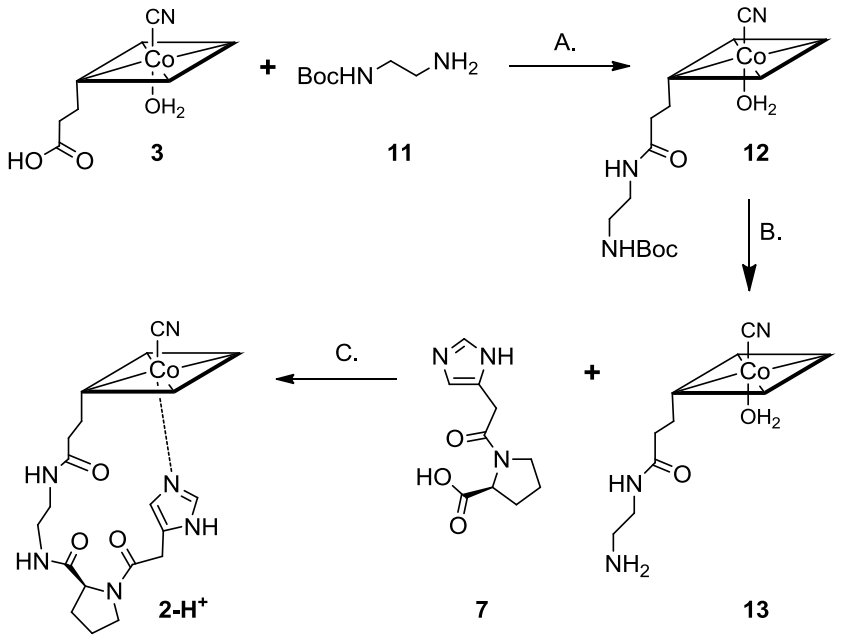

Scheme 15 - Synthesis of **2-H**$^+$ (A. NEt_3, ethylchloroformate, DMF, 0°C. B. HCl 1 M. C. DMAP, EDC, DMF, 0°C) (charges are omitted).

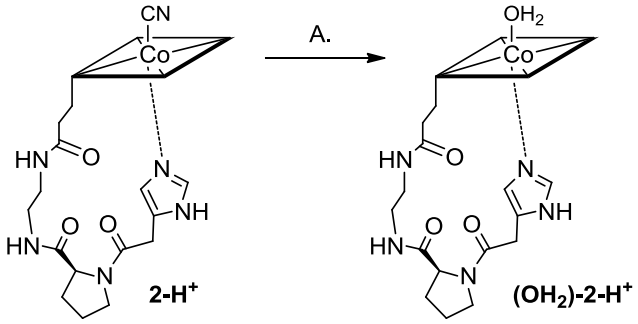

Scheme 16 – Synthesis of **(OH$_2$)-2-H**$^+$ (A: Zn pellets, 10% AcOH, RT) (charges are omitted).

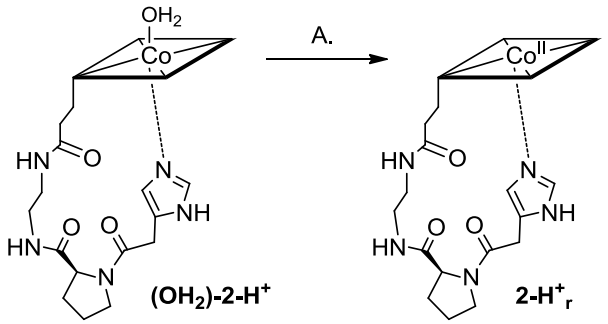

Scheme 17 –Synthesis of **2-H**^+_r (A: Formic acid, NEt_3, MeOH, RT) (charges are omitted).

5.4. Experimental Procedures

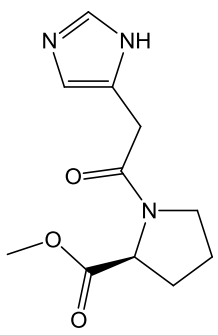

Compound **10**: Imidazole acetic acid (**8**) (200 mg, 1.23 mmol) was dissolved in dry DMF (8 ml) and cooled to 0°C. L-proline (**9**) (192 mg, 1.23 mmol) and HOBt (240 mg, 1.35 mmol) were then added. After 10 min, EDC (248 mg, 1.35 mmol) and DIPEA (214 µg, 1.26 mmol) were added, and the reaction mixture was let to stir overnight. The solution was added to 20 ml of a saturated $NaHCO_3$ water solution and extracted with 4 portions of 30 ml of dichloromethane (DCM). The organic phase was dried on $MgSO_4$. After filtration, the compound was purified by flash chromatography on silica gel (EA/DCM/MeOH/NH_3 16:24:10:1.5). The solvent was removed under reduced pressure, to obtain **10** as a transparent oil (213.7 mg, yield: 75 %).

TLC (Silicagel 60 F_{254}, EA/DCM/MeOH/NH_3 16:24:10:1.5): Rf = 0.51

HR-MS: $[M+H]^+$ calculated for $C_{11}H_{16}O_3N_3$: 238.11862, found 238.11821.

^{1}H-NMR: (D_2O, 500 MHz) δ /ppm = 7.97 (s, 1H), 7.13 (s, 1H), 4.50 (dd, J = 8.5, 4.0 Hz, 1H), 3.83 (d, J = 1.8 Hz, 2H), 3.77 (s, 3H), 3.76 - 3.51 (m, 2H), 2.43 - 2.27 (m, 1H), 2.11 - 1.99 (m, 3H). (a ratio of the syn / anti isomers of approximately 83:17 was calculated. Only the major isomer is reported).

^{13}C-NMR: (D_2O, 500 MHz) δ /ppm = 184.16, 177.73, 177.21, 174.47, 173.98, 167.80, 138.36, 132.54, 120.10, 63.13, 62.28, 56.05, 55.77, 50.80, 49.86, 35.42, 34.96, 34.23, 33.59, 31.84, 27.18, 24.83. (two isomers).

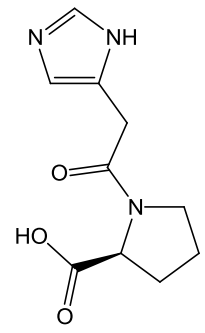

Compound **7**: **10** (100 mg, 0.42 mmol) was dissolved in 0.5 M NaOH, and let react for 2h. The pH was then set to 5 with a 1 M HCl solution, and the solvent was removed under reduced pressure. The salts were then removed by precipitation in 5 ml of MeOH and filtered off. After removal of the solvent under reduced pressure, 90.2 mg of a transparent oil was collected (90 mg, yield: 98 %).

HR-MS: $[M+H]^+$ calculated for $C_{10}H_{14}O_3N_3$: 224.10297, found 224.10325.

^{1}H-NMR : (D_2O, 400 MHz) δ / ppm = 8.75 (s, 1H), 7.47 (s, 1H), 4.37 (dd, J = 8.9, 4.0 Hz, 1H), 4.07 (s, 2H), 3.78 - 3.67 (m, 1H), 3.63 - 3.47 (m, 1H), 2.43 - 2.23 (m, 2H), 2.08 - 1.96 (m, 1H), 1.97 - 1.79 (m, 1H). (a ratio of the syn / anti isomers of approximately 60:40 was calculated. Only the major isomer is reported)

^{13}C-NMR : (D_2O, 500 MHz) δ / ppm = 181.69, 181.16, 172.08, 171.69, 136.37, 136.34, 129.64, 120.53, 65.39, 63.95, 51.84, 50.88, 50.29, 34.43, 33.05, 32.82, 32.47, 27.27, 25.47, 24.25. (two isomers).

HPLC: (gradient 2) 18.0 min

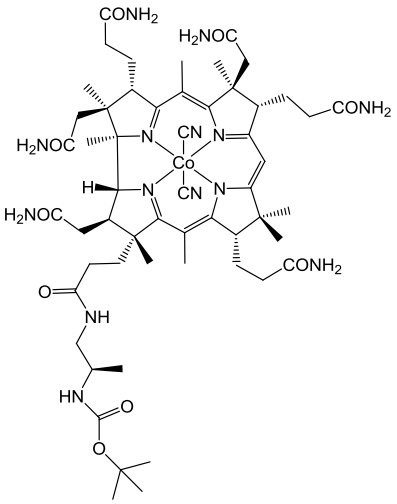

Compound **5**: Cobyric acid **3** (20 mg, 18.6 µmol) was dissolved in dry DMF (8 ml), then NEt_3 (18 µl, 133.3 µmol) and ethylchloroformate (10 µl, 105.0 µmol) were added. After 5 min, (R)-tert-Butyl (1-aminopropan-2-yl)carbamate **4** (20.7 mg, 111.6 µmol) was added. The reaction was quenched with water (15 ml) after 15 min, and washed with 3 portions of DCM (30 ml). The collected water phase was then purified by preparative HPLC (gradient 6) to afford **5** (12 mg, yield: 52 %).

HR-MS: $[M\text{-}CN]^+$ calculated for $C_{54}H_{81}CoN_{13}O_9$: 1114.56067, found 1114.56100.

UV-Vis: (H_2O) λmax / nm (log ε) = 579.9 (4.00); 539.0 (3.94); 368.0 (4.48); 311.9 (3.98); 277.0 (3.98).

^{1}H-NMR: (D_2O, 500 MHz) δ / ppm = 5.96 (s, 1H), 3.92 (d, J = 8.5 Hz, 1H), 3.82 (d, J = 10.5 Hz, 1H), 3.47 (dd, *J* = 7.0, 4.9 Hz, 1H), 3.37 (d, J = 5.8 Hz, 2H), 3.28 - 3.04 (m, 2H), 2.96 (s, 1H), 2.85 – 2.72 (m, 2H), 2.70 - 2.58 (m, 3H), 2.58 - 2.45 (m, 2H), 2.45 – 2.37 (m, 6H), 2.37 – 2.29 (m, 6H), 2.29 - 2.14 (m, 3H), 2.14 - 2.00 (m, 2H), 1.98 - 1.80 (m, 3H), 1.76 (s, 3H), 1.60 (s, 3H), 1.55 (s, 3H), 1.51 (s, 3H), 1.48 (s, 9H), 1.38 (s, 3H), 1.26 (s, 3H), 1.17 (d, J = 6.8 Hz, 3H).

^{13}C-NMR: (D_2O, 500 MHz) δ / ppm = 181.5, 181.4, 180.9, 180.4, 180.1, 179.5, 178.7, 178.6, 178.0, 177.9, 174.8, 166,2, 165.8, 122.6, 120.3, 118.0, 115.7, 107.9, 105.9, 93.8, 85.9,

83.5, 77.7, 73.9, 61.6, 59.0, 58.0, 56.0, 52.0, 49.6, 49.0, 49.1, 47.3, 46.6, 45.1, 41.6, 37.7, 35.6, 34.8, 34.7, 34.6, 34.3, 33.3, 30.5, 29.4, 28.1, 27.6, 24.5, 21.5, 21.3, 20.4, 20.1, 19.2, 17.9, 17.6.

UPLC-MS : (gradient 11) Rt = 2.2 min (α isomer), 2.3 min (β isomer) (m/z: 1114.6 = $[M\text{-}CN]^+$).

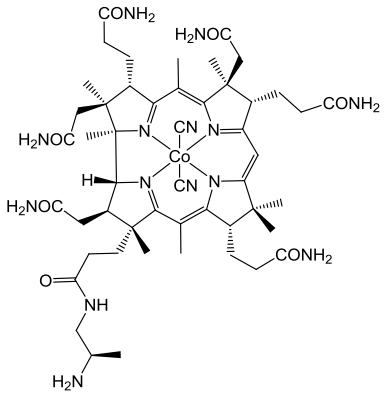

Compound **6**: **5** (20 mg, 16.1 µmol) was dissolved in 1 M HCl (6 ml) and let stirred for 1 hour. The reaction mixture was neutralized and the solvent was removed under reduced pressure. The mixture was purified by preparative HPLC (gradient 7) to afford **6** (15.6 mg, yield: 85 %).

HR-MS: $[M\text{-}CN]^+$ calculated for $C_{49}H_{73}CoN_{13}O_7$: 1014.50824, found 1014.50900.

UV-Vis: (H_2O) λmax / nm (log ε) = 579.0 (4.02), 538.9 (3.96), 417.0 (3.38), 366.9 (4.48), 307.0 (4.02), 275.9 (4.05).

^{1}H-NMR : (D_2O, 500 MHz) δ / ppm = 5.93 (s, 1H), 3.87 (d, J = 8.5 Hz, 1H), 3.78 (d, J = 10.4 Hz, 1H), 3.44 (dd, J = 7.0, 4.9 Hz, 1H), 3.33 (d, J = 14.0 Hz, 4H), 3.24 (s, 1H), 3.00 – 2.90 (m, 1H), 2.76 (dd, J = 10.7, 6.3 Hz, 2H), 2.68-2.54 (m, 3H), 2.54 – 2.45 (m, 2H), 2.39 – 2.33 (m, 6H), 2.33 – 2.26 (m, 6H), 2.26 – 2.09 (m, 4H), 2.09 - 1.97(m, 2H), 1.96 - 1.75 (m, 3H), 1.72 (s, 3H), 1.57 (s, 3H), 1.53 (s, 3H), 1.47 (s, 3H), 1.35 (s, 3H), 1.27 – 1.16 (m, 3H).

^{13}C-NMR : (D_2O, 500 MHz) δ / ppm = 181.6, 180.9, 180.4, 180.2, 179.7, 178.8, 178.1, 178.1, 174.9, 166.3, 166.0, 165.8, 165.7, 120.4, 118.0, 108.0, 105.9, 93.8, 85.9, 77.6, 61.6, 59.0, 58.0, 55.9, 52.0, 49.5, 49.1, 47.9, 47.4, 46.4, 41.7, 37.6, 35.2, 34.6, 33.6, 33.2, 33.1, 29.5, 28.5, 27.7, 24.5, 21.5, 21.3, 20.2, 20.1, 19.3, 17.9, 17.6, 17.5.

UPLC-MS : (gradient 11) Rt = 1.5 min (α isomer), 1.7 min (β isomer) (m/z: 1014.6 = $[M\text{-}CN]^+$).

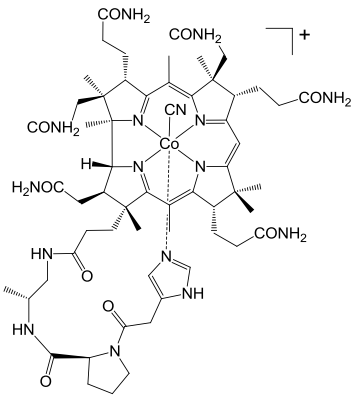

Compound **1-H**$^+$: **7** (12 mg, 53.3 µmol) was dissolved in dry DMF (4 ml) and cooled to 0°C. HOBt (6.6 mg, 48.8 µmol), TBTU (15.6 µl, 48.8 µmol) and DIPEA (68 µl, 399.9 µmol) were then added. After 5 minutes, the solution was added to a solution of **6** (20 mg, 17.5 µmol) dissolved in dry DMF (5 ml). The mixture was let to react for 18h. The reaction was then quenched with water (15 ml) and washed 3 times with DCM (20 ml). The water phase was further purified by preparative HPLC (gradient 6), which afforded a pink powder (10.47 mg, yield: 45 %). To obtain the base-on form of **1-H**$^+$, the solid was dissolved in water (6 ml) and KCN was added to obtain **(CN)$_2$-1**. The pH was then lowered to 3.8 with 1 M HCl, and the flask was let open to react for 24h. To obtain the ^{13}CN-**1-H**$^+$derivative, the same procedure was applied, using K^{13}CN as salt.

HR-MS: $[M+H]^{2+}$ calculated for $C_{59}H_{85}CoN_{16}O_9$: 610.30032, found 610.30054.

UV-Vis : (0.2 M KCl) λmax / nm (log ε) = 555 (3.85); 521 (3.81); 411 (3.40); 320 (3.76); 305 (3.86); 277 (3.97).

^{1}H-NMR **(CN)$_2$-1**: (D_2O, 500 MHz) δ / ppm = 7.75 (s, 1H), 7.06 (s, 0.6H), 7.04 (s, 0.4H), 5.93 (s, 1H), 4.64 (d, J = 8.3 Hz, 0.4H), 4.40 (dd, J = 8.8, 4.0 Hz, 0.6H), 4.05 (dd, J = 12.9, 6.4 Hz, 1H), 3.87 (d, J = 8.7 Hz, 1H), 3.80 (s, 2H), 3.78 – 3.68 (m, 3H), 3.47 – 3.42 (m, 1H), 3.32 (d, J = 6.2 Hz, 3H), 2.96 - 2.88 (m, 1H), 2.82 – 2.67 (m, 2H), 2.64 - 2.40 (m, 5H), 2.39 – 2.23 (m, 15H), 2.22 – 2.06 (m, 4H), 2.07 – 1.96 (m, 3H), 1.94 – 1.78 (m, 4H), 1.72 (s, 3H), 1.55 (s, 3H), 1.49 (s, 3H), 1.33 (s, 3H), 1.22 (s, 3H), 1.14 (dd, J = 14.0, 6.7 Hz, 5H).

^{13}C-NMR **(CN)$_2$-1**: (D_2O, 500 MHz) δ / ppm = 181.5, 180.9, 180.4, 180.1, 179.7, 178.8, 178.1, 176.8, 175.2. 174.9, 166.3, 166.0, 139.0, 134.2, 122.7, 121.6, 120.37, 119.8, 108.0, 105.9, 93.9, 85.9, 77.9, 63.8, 61.6, 59.2, 59.1, 56.0, 52.0, 51.1, 49.5, 49.1, 49.0, 48.4, 46.5, 46.4, 45.0, 41.7, 37.7, 35.6, 35.5, 35.2, 34.7, 34.5, 33.2, 32.7, 29.4, 28.4, 27.7, 27.1, 24.6, 24.5, 21.5, 21.3, 20.2, 19.7, 19.3, 18.0, 17.6.

UPLC-MS : (gradient 11) Rt = 1.8 min (α isomer), 2.0 min (β isomer) (m/z: 1219.3 $[M]^+$; 610.4 $[M+H]^{2+}$).

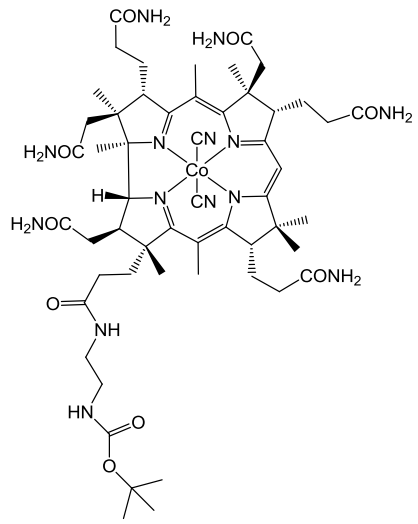

Compound **12**: Cobyric acid (**3**) (20 mg, 18.6 µmol) was dissolved in dry DMF (8 ml), then NEt_3 (20 µl, 148.1 µmol) and ethylchloroformate (10 µl, 105.0 µmol) were added. After 5 min, Boc-ethylenediamine (**11**) (20 µl, 126.3 µmol) was added. After 15 min, the reaction was quenched with water, and washed with 3 portions of DCM. The reaction mixture was purified with preparative HPLC chromatography (gradient 6), to afford **12** (10.2 mg, yield: 45 %).

HR-MS: $[M\text{-}CN]^+$ calculated for $C_{53}H_{79}CoN_{13}O_9$: 1100.54502, found 1100.54612.

UV-Vis : H_2O λ max / nm (log ε) = 580 (4.00); 539 (3.95); 368 (4.48); 313 (4.03); 276 (4.02)

^{1}H-NMR : (D_2O, 500 MHz) δ / ppm = 5.91 (s, 1H), 3.85 (d, J = 8.6 Hz, 1H), 3.76 (d, J = 10.5 Hz, 1H), 3.42 (dd, *J* = 6.9, 5.0 Hz, 1H), 3.31 (s, 3H), 3.22 (d, J = 4.6 Hz, 2H), 2.90 (s, 1H), 2.81-2.67 (m, 1H), 2.66 - 2.52 (m, 3H), 2.52 - 2.38 (m, 2H), 2.38 - 2.30 (m, 6H), 2.30 - 2.23 (m, 8H), 2.23 - 2.05 (m, 3H), 2.05 – 1.94 (m, 2H), 2.94 - 1.84 (m, 2H), 1.84 - 1.73 (m, 1H), 1.70 (s, 3H), 1.54 (s, 3H), 1.50 (s, 3H), 1.45 (s, 3H), 1.43 (s, 9H), 1.32 (s, 3H), 1.20 (s, 3H).

^{13}C-NMR : (D_2O, 500 MHz) δ / ppm = 181.4, 181.3, 180.8, 180.4, 180.2, 179.6, 178.7, 178.6, 178.0, 174.9, 166.2, 165.7, 161.0, 122.6, 120.3, 118.0, 108.0, 105.8, 93.8, 85.9, 83.6, 78.0, 61.6, 59.1, 58.1, 56.1, 56.0, 52.0, 49.5, 46.5, 45.0, 42.1, 41.8, 41.7, 37.7, 35.3, 35.2, 34.7, 34.6, 34.5, 33.3, 32.7, 30.6, 29.4, 28.7, 27.7, 27.6, 24.5, 21.6, 21.3, 20.1, 19.4, 18.0, 17.8.

HPLC: (gradient 3): Rt: 17.5 (α-isomer); 18.3 (β-isomer)

UPLC-MS: (gradient 11) m/z (1100.7) = Rt: 3.2 min (alpha isomer) 3.4 min (beta isomer)

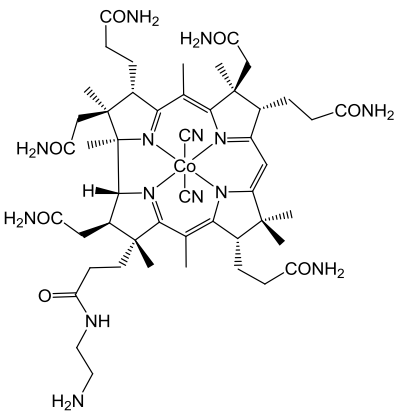

Compound **13**: **12** (20.0 mg, 16.2 µmol) was dissolved in 1 M HCl and let react for an hour. After neutralization, the solvent was removed under reduced pressure. The mixture was purified by preparative HPLC (gradient 7), to afford **13** (14 Mg, yield: 91%).

HR-MS: $[M\text{-}CN+H]^{2+}$ calculated for $C_{48}H_{72}CoN_{13}O_7$: 500.74993, found 500.75005

UV-Vis : H_2O λ max / nm (log ε) = DiCN: 580 (3.99); 539 (3.95); 414 (3.45); 368 (4.48); 312 (4.04); 276 (4.08).

^{1}H-NMR : (D_2O, 500 MHz) δ / ppm = 5.92 (s, 1H), 3.87 (d, J = 8.2 Hz, 1H), 3.78 (d, J = 10.2 Hz, 1H), 3.44 (s, 1H), 3.34 (s, 2H), 2.91 (s, 1H), 2.85 (s, 4H), 2.82 – 2.73 (m, 2H), 2.68 -2.42 (m, 5H), 2.42 - 2.32 (m, 5H), 2.32 - 2.25 (m, 7H), 2.25 - 2.07 (m, 4H), 2.07 - 1.97 (m, 1H), 1.97 - 176 (m, 3H), 1.72 (s, 3H), 1.56 (s, 3H), 1.52 (s, 3H), 1.46 (s, 3H), 1.35 (s, 3H), 1.22 (s, 3H).

^{13}C-NMR : (D_2O, 500 MHz) δ / ppm = 181.6, 181.4, 180.9, 180.4, 180.2, 179.7, 178.7, 178.1, 174.9, 165.9, 165.7, 122.7, 120.3, 118.0, 115.7, 108.0, 106.0, 93.8, 85.9, 77.8, 61.6, 59.1, 57.9, 56.0, 51.7, 49.6, 49.1, 46.5, 45.1, 44.5, 42.6, 37.7, 35.3, 35.2, 34.7, 34.6, 34.6, 34.4, 33.2, 29.4, 28.5, 27.8, 24.5, 21.5, 21.3, 20.2, 19.3, 17.9, 17.6.

UPLC: (gradient 8): m/z: 1000.6 $[M\text{-}CN]^+$ Rt: 1.4 min (a-isomer); 1.6 min (b-isomer).

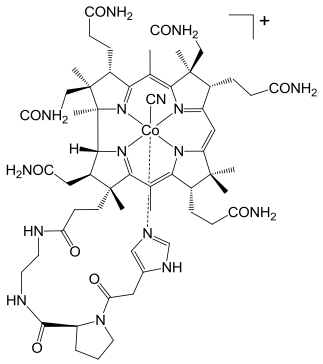

Compound **2-H$^+$**: **7** (19.7 mg, 88.0 µmol) was dissolved in DMF (5 ml) and cooled down to 0°C. DMAP (10.7 mg, 88.0 µmol) was then added. After 10 min, the solution was added to a solution of **13** (20 mg, 17.6 µmol) in dry DMF (8 ml). After 30 min, EDC (13.7 mg, 88.0 µmol) was added. The mixture was let to react for 18h. The reaction mixture was quenched with water and washed with 3 portions of DCM. Purification of the crude mixture was performed with preparative HPLC (gradient 6) to afford **2-H$^+$** (6.7 mg, yield: 29 %). To obtain the base-on form of **2-H$^+$**, the solid was dissolved in 6 ml of water and KCN was added to obtain the **(CN)$_2$-2** derivative. The pH was then lowered to 3.8, and the flask was let open to react for 24h. UV-vis was used to verify the completion of the reaction.

HR-MS: $[M+H]^{2+}$ calculated for $C_{58}H_{83}CoN_{16}O_9$: 603.29250, found 603.29267

UV-Vis : (0.2 M KCl) lmax / nm (log e) = 555 (3.95); 523 (3.92); 411 (3.56); 362 (4.46); 321 (3.93); 306 (4.00); 278 (4.09)

^{1}H-NMR of **$(CN)_2$-2**: (500 MHz, D2O) δ / ppm = 7.73 (s, 1H), 7.05 (s, 1H), 5.92 (s, 1H), 4.43 (dd, J = 8.7, 4.1 Hz, 1H), 3.86 (d, J = 8.6 Hz, 1H), 3.79 (s, 2H), 3.78-3.64 (m, 3H), 3.43 (dd, J = 7.1, 4.9 Hz, 1H), 3.41 – 3.26 (m, 5H), 2.90 (s, 1H) , 2.78 - 2.69 (m, 2H), 2.65 - 2.39 (m, 5H), 2.29 - 2.31 (m, 4H), 2.31 - 2.23 (m, 9H), 2.23 – 2.05 (m, 4H), 2.05 - 1.92 (m, 5H), 1.91 - 1.74 (m, 3H), 1.71 (s, 3H), 1.55 (s, 3H), 1.49 (s, 3H), 1.46 (s, 3H), 1.33 (s, 3H), 1.21 (s, 3H).

^{13}C-NMR of **$(CN)_2$-2**: (500 MHz, D2O) δ / ppm = 181.6, 181.5, 181.1, 180.0, 180.5, 180.0, 179.6, 178.8, 175.3, 175.2, 166.5, 166.1, 165.9, 165.8, 139.0, 134.6, 121.9, 119.9, 118.2, 115.9, 110.8, 108.1, 94.8, 86.1, 77.8, 63.6, 61.2, 59.1, 57.8, 56.0, 51.1, 51.0, 49.8, 49.3, 46.5, 45.0, 41.7, 41.6, 41.4, 37.6, 35.8, 35.4, 35.2, 34.7, 34.6, 34.4, 33.0, 32.6, 29.4, 28.4, 27.6, 27.3, 23.4, 21.5, 20.1, 19.2, 17.7, 17.4.

UPLC-MS : (gradient 11) m/z = 1205.7 $[M]^+$ 603.8 $[M+H]^{2+}$, Rt = 1.9 min.

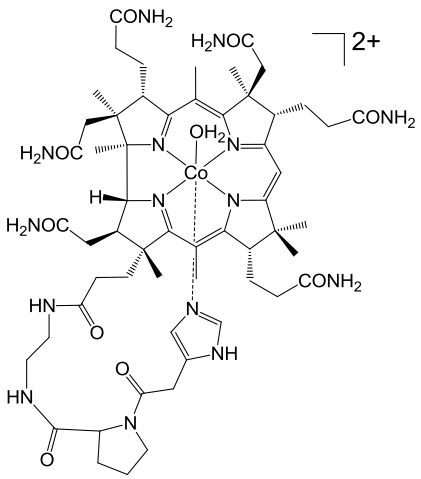

Compound **(OH_2)-2-H^+** : **1-H^+** (6.5 mg, 4.8 µmol) was dissolved in 10 % acetic acid (6 ml), which was degassed with argon during 1h. Zn pellets (800 mg) were then activated with HCl (6 M) and washed with water after 30s, before addition to the solution. After 15 min, the reaction mixture changed color from pink to brown. Mixture was let to react for 2h30 before filtering, and the solution was oxygenated with a stream of air. Removing of the salts was achieved by phenol extraction: the compound was extracted from the water phase using a phenol/DCM mixture (1:1 vw), and then extracted in the water phase by addition of 1 volume equivalent of isobutanol and 3 volume equivalents of DCM. The water phase was then washed with DCM and the solvent was removed under pressure. To obtain the base-on configuration, the pH was set to 7 with NH_3 solution. The Compound was used for cyclic voltammetry measurements without further purification.

UV-vis **$(OH_2)_2$-2-H^+** (base-off)**:** (H_2O) λmax / nm = 522, 494, 410, 351, 272.

UV-vis **(OH_2)-2-H^+** (Base-on)**:** (H_2O) λmax / nm = 539, 509, 357, 319, 274.

UPLC-MS : (gradient 11) Rt = 1.5 min, (m/z: 589.9 = $[M]^{2+}$).

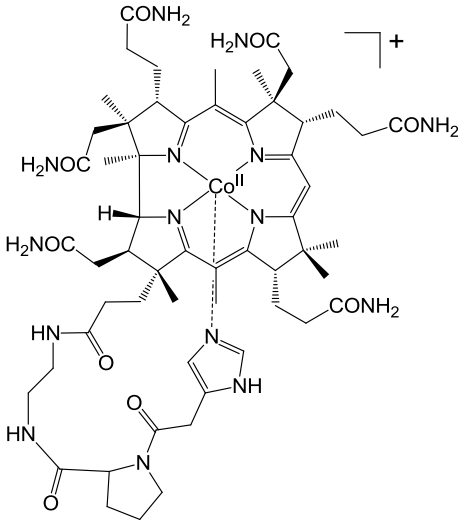

Compound **2-H^+_r**: **(OH_2)-2-H^+** (5 mg, 3.8 μmol) was dissolved in MeOH (2 ml), the solution was deoxygenated with a stream of argon (10 min). Formic acid (50 μl) and trimethylamine (187 μl) were added. Color change from red to brown was observed after 30 min. The reaction mixture was then used without further purification for cyclic voltammetry measurements. Compound is sensitive to air. UV-Vis : (H_2O) λmax / nm = 472, 405, 312.

5.5. NMR Table and numbering

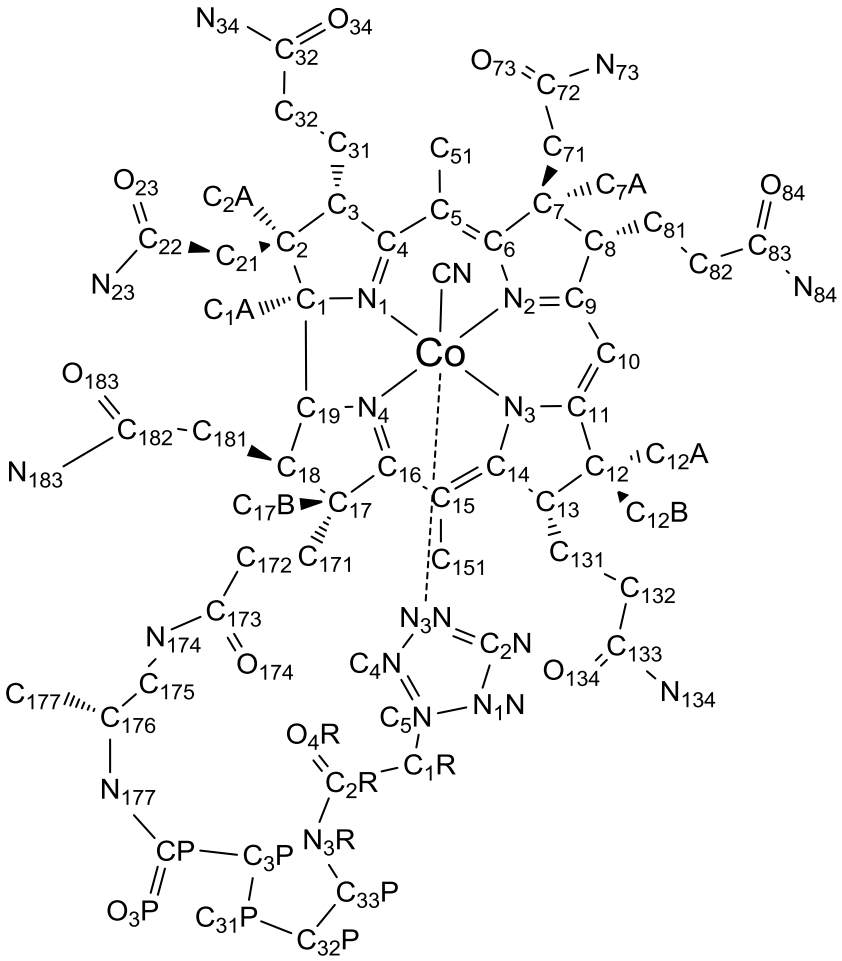

	δ (ppm)					
	$(CN)_2$-5		$(CN)_2$-6		$(CN)_2$-1	
	^{1}H	^{13}C	^{1}H	^{13}C	^{1}H	^{13}C
C1		85.9				85.9
C1A	1.55	24.5	1.53	24.5	1.49	24.5
C2		49.1				49.1
C2A	1.60	19.2	1.57	19.3	1.55	19.3
C3	3.92	59.0	3.87	59.0	3.87	59.2
C4		179.5				179.7
C5		107.9				108
C6		165.8				166
C7		52.0				49.0
C7A	1.76	21.5	1.72	21.5	1.72	21.5
C8	3.47	58.0	3.44	58.0	3.41	59.1
C9		174.8				174.9
C10	5.96	93.8	5.93	93.8	5.93	93.9
C11		181.4				180.4
C12		49.6				49.5
C12A	1.51	21.3	1.47	21.3	1.46	21.3
C12B	1.26	33.3	1.22	33.2	1.22	33.2
C13	3.37	56.0	3.33	55.9	3.32	56
C14		166.2				166.3
C15		105.9				105.9
C16		178.7				180.1
C17		61.6				61.6
C17B	1.38	20.1	1.35	20.1	1.33	20.2
C18	2.96	41.6	2.92	41.7	2.89	41.7
C19	3.82	77.7	3.78	77.6	3.74	77.9
C21	2.40/2.34	45.1	2.35/2.31	44.9	2.32/2.26	45
C31	2.35/2.04	27.6	2.0/2.32	27.7	2.24/1.98	27.7
C32	2.60/2.56	37.7	2.57/2.51	37.6	2.55/2.46	37.7
C51	2.32	17.9	2.29	17.9	2.25	18
C71	2.65/2.33	46.6	2.60/2.31	47.4	2.58/2.27	46.5
C81	2.20/1.86	29.4	2.15/1.82	29.4	2.12/1.79	29.4
C82	2.25	34.3	2.32	33.6	2.26/1.93	32.7
C131	2.22/1.94	28.1	1.82/2.19	28.5	2.08/1.86	28.4
C132	2.35/2.26	34.7	2.32/2.20	34.6	2.16/2.09	24.6
C151	2.4	17.6	2.36	17.5	2.27	17.6

	$(CN)_2$-5		$(CN)_2$-6		$(CN)_2$-1	
	^1H	^{13}C	^1H	^{13}C	^1H	^{13}C
C172	2.48/1.94	35.6	2.49/1.80	33.1	2.44/1.85	35.5
C175	3.82/3.21	47.3	3.33/3.25	47.9	3.32	46.4
C176	3.37	49.0	3.34	49.5	4.05	48.4
C177	1.17	20.4	1.21	20.1	1.12	19.7
C181	2.8	34.6	2.76	35.2	2.73	35.2
C179 (Boc)	1.48	30.5				
C3P					4.64/4.40	63.8
C31P					2.28	34.7
C32P					1.97	27.1
C33P					3.76 / 3.70	51.1
C1R					3.80	35.6
C2R						175.2
C2N					7.75	139
C4N					7.06/7.04	119.8
C5N						134.2

δ (ppm)

	$(CN)_2$-12		$(CN)_2$-13		$(CN)_2$-2	
	^1H	^{13}C	^1H	^{13}C	^1H	^{13}C
C1				85.9		86.1
C1A	1.50	24.5	1.52	24.5	1.49	23.4
C2				49.1		49.3
C2A	1.54	19.4	1.56	19.3	1.55	19.2
C3	3.85	59.1	3.87	59.1	3.86	59.1
C4				179.7		179.6
C5				108.0		108.1
C6				165.9		166.1
C7				51.7		51.0
C7A	1.70	21.6	1.72	21.5	1.71	21.5
C8	3.42	56.0	3.44	57.9	3.43	57.8
C9				174.9		175.2
C10	5.91	93.8	5.92	93.8	5.92	93.8
C11				180.4		180.5
C12A	1.45	21.3	1.46	21.3	1.46	21.5

	$(CN)_2$-12		**$(CN)_2$-13**		**$(CN)_2$-2**	
	^{1}H	^{13}C	^{1}H	^{13}C	^{1}H	^{13}C
C12B	1.20	33.3	1.22	33.2	1.21	33.0
C13	3.31	56.1	3.34	56.0	3.32	56.0
C14				170.1		165.9
C15				106.0		108.1
C16				180.2		180.0
C17				61.6		61.2
C17B	1.32	20.1	1.35	20.2	1.32	20.1
C18	2.90	41.7	2.92	41.8	2.9	41.7
C19	3.76	78.0	3.78	77.8	3.75	77.8
C21	2.32/2.26	45.0	2.32/2.27	45.1	2.32/2.28	45.0
C31	2.30/1.99	27.7	2.32/2.01	27.8	2.29/1.99	27.6
C32	2.48	37.7	2.53	37.7	2.57/2.49	37.6
C51	2.27	18.0	2.28	17.9	2.28	17.7
C71	2.61/2.30	46.5	2.62/2.26	46.5	2.60/2.29	46.5
C81	2.14/1.80	29.4	2.16/1.81	29.4	2.13/1.83	29.4
C82	2.30	34.7	2.22	34.5	2.28/1.95	32.6
C131	2.15/1.88	28.7	2.18/1.89	28.5	2.13/1.88	28.4
C132	2.29/2.19	34.6	2.33	34.6	2.30/2.20	34.6
C151	2.34	17.8	2.35	17.6	2.33	17.4
C171	2.54/2.06	34.5	2.61	34.7	2.56/2.07	34.4
C172	2.43/1.84	35.3	2.49	35.3	2.44/1.87	35.4
C175	3.42	41.8	3.34	44.5	3.36	41.4
C176	3.22	42.1	2.85	42.6	3.36	41.6
C177						
C181	2.74	35.2	2.78	35.2	2.74	35.2
C179 (Boc)	1.43	30.6				
C3P					4.65/4.41	63.6
C31P					2.39/2.30	34.7
C32P					2.00	27.6
C33P					3.71	51.1
C1R					3.79	35.8
C2R						175.3
C2N					7.74/7.73	139.9
C4N					7.05/7.02	119.9
C5N						134.6

Acknowledgments

I would like to start this chapter by thanking PD. Felix Zelder for his supervision. His motivation, his availability and our constructive discussions were an important support during my Ph.D. I appreciated as well his will to share my happiness towards good results as well as his support when these results were not as expected.

I wish to thank Prof. Dr. Roger Alberto for following my work as head of doctoral committee and for the interesting ideas he brought to the projects. I enjoyed as well being part of the Alberto Group Retreats.

I am thankful to Prof. Dr. Roland Sigel for his support, as committee member as well as via the CMSZH. The graduate school retreats were always a pleasure.

I wish to thank the SNF, CMSZH and SCNAT/SCS for the different financial supports throughout my thesis.

I want to thank Dr. Thomas Fox, for his great help with the NMR measurements, and Dr. Olivier Blacque for the calculations. I thank as well Dr. Philip Johnson and Klemens Koziol for the 2D-IR measurements and the insights they brought me concerning this technique. I would like to express my gratitude to our collaborator Prof. Dr. Helmut Brandl, for his help with biological tests as well as all the work he accomplished for the antibacterial experiments. I thank Dr. Loganathan Rangasamy for the cell studies.

During these four years, I had the chance to work with many lab mates. I would like to thank all of them for the discussions and nice working environment in the lab. In particular, I wish to thank Dr. Kai Zhou, for introducing me to the B_{12} world and for sharing his tricks. I would like to thank Dr. Christine Männel-Croisé for her great support in my beginnings. Philipp Pfingstag and Balz Aebli were the best master student one could hope for, and I am thankful for all the great time we had together, inside and outside the University. I wish to thank Dr. René Oetterli for all he did and is still doing for me, for being a great support and a crazy friend, and for translating my abstract. I thank Namita Kumari for the nice group dinner she organized and the great Indian food. Finally, I want to thank Lucas Prieto for being an amazing lab mate, always available for help and questions, and for being such a great friend.

I wish to thank the entire former ACI as well as my colleagues of the UPLC-MS service for the great working atmosphere.

I am very thankful for all the friends I met in Zurich, especially Dr. Cristina Mari and Angelo Frei for spicing up my life during these four years. I want to thank my family the most, for the great and constant support in every steps of my life. A special thank you goes to Alexander Szentkuti, for his support and tolerance.

Curriculum Vitae

Personal Information:

Name:	Marjorie Cendrine Sonnay
Date of Birth:	30.09 1986
Nationality:	Swiss

Education

2012 - 2015	Ph.D. Chemistry, University of Zurich, Switzerland
2009 - 2011	Master of Sciences in Molecular and Biological Sciences, Swiss Institute of Technology (EPFL), Switzerland
	Sep-Dec 2011 Master project, University of Edinburgh, United Kingdom
2006 – 2009	Bachelor of Science in Chemistry and Chemical Engineering, Swiss Institute of Technology (EPFL)

Publications

Sonnay, M., Fox, T., Blacque, O., Zelder, F, "Modulating the Cobalt Redox Potential through Imidazole Hydrogen Bonding Interactions in a Supramolecular Biomimetic Protein-Cofactor Model", submitted.

Zelder, F; Sonnay, M; Prieto, L., "Antivitamins for medicinal applications.", ChemBioChem, 2015, 16, 1264-1278.

Zelder F; Zhou, K; Sonnay, M., "Peptide B12: emerging trends at the interface of inorganic chemistry, chemical biology and medicine", Dalton Trans., 2013, 42, 854-862.

Conference Contributions

2015	Poster presentation at CEMM, Hawaii
	Oral presentation at CanBIC-5, Canada
2014	Oral presentation at ISBOMC 2014, Austria
2013	Poster presentation at the Koordinationschemie treffen 2013, Germany
2013 – 2015	Poster presentations at the Swiss Chemical Society Meetings, Switzerland

Awards

2015	CMSZH Travel Award from the Graduate School of Chemical and Molecular Sciences Zurich
	SCNAT/SCS Chemistry Travel Award from the Swiss Academy of Sciences

Appendix I – Supplementary Spectra

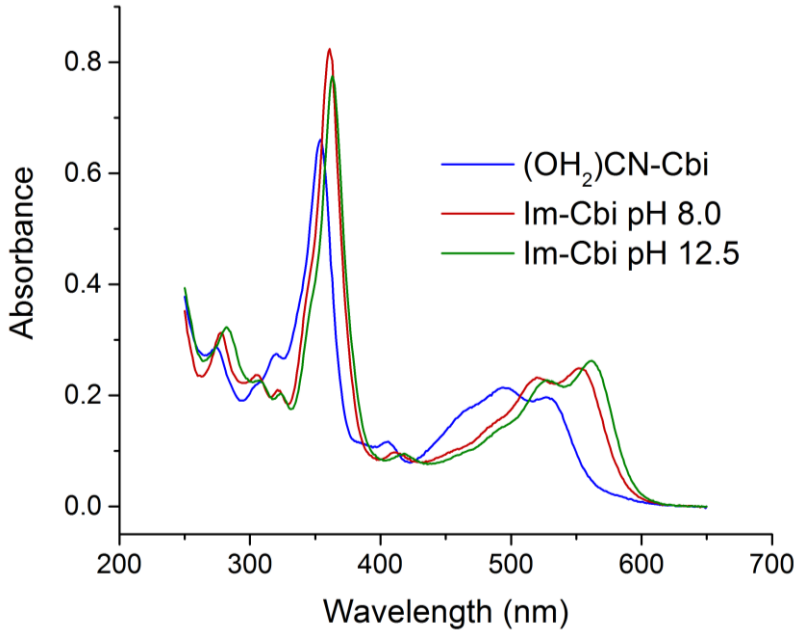

Figure A 1 - Absorbance spectra of (OH_2)CN-Cbi (blue) and imidazole-bound cobinamide (Im-Cbi) at pH 8.0 (red) and pH 12.5 (green) in H_2O .

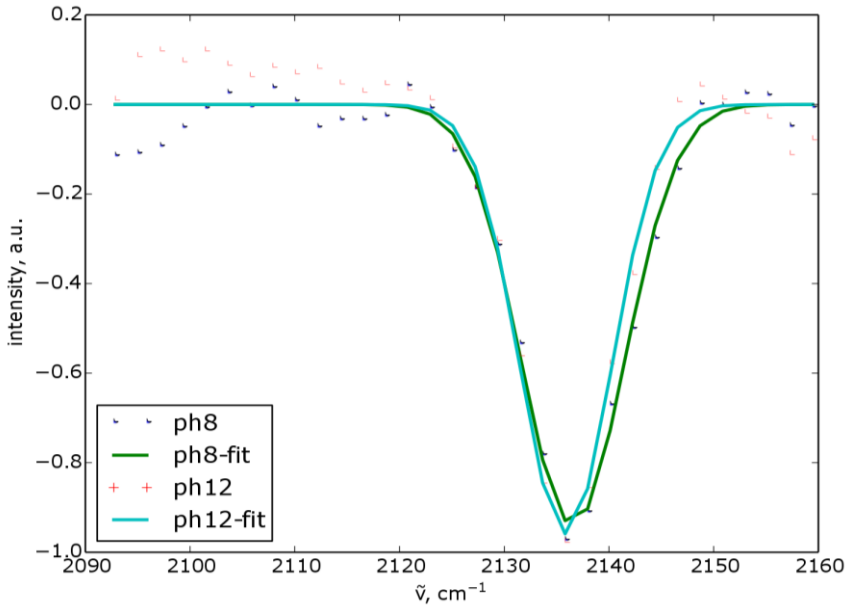

Figure A 2 - 2D IR diagonal cut and corresponding fitting of Im-Cbi at pH 8.0 (green) and pH 12.5 (blue) in the corresponding buffer.

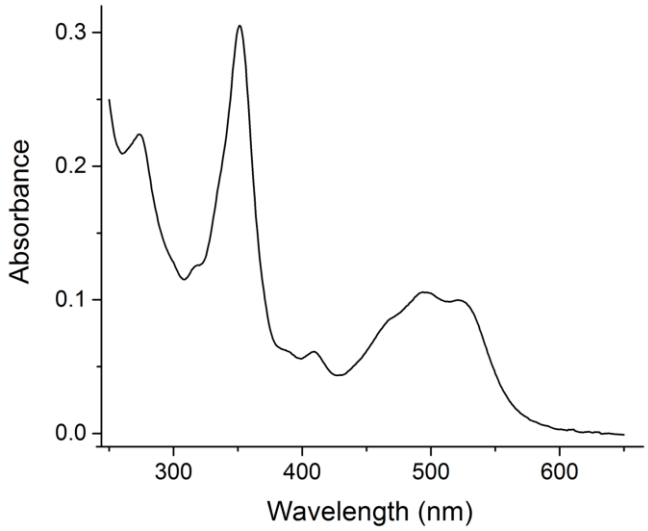

Figure A 3 - Absorbance spectra of **(OH_2)-2-H^+** in H_2O.

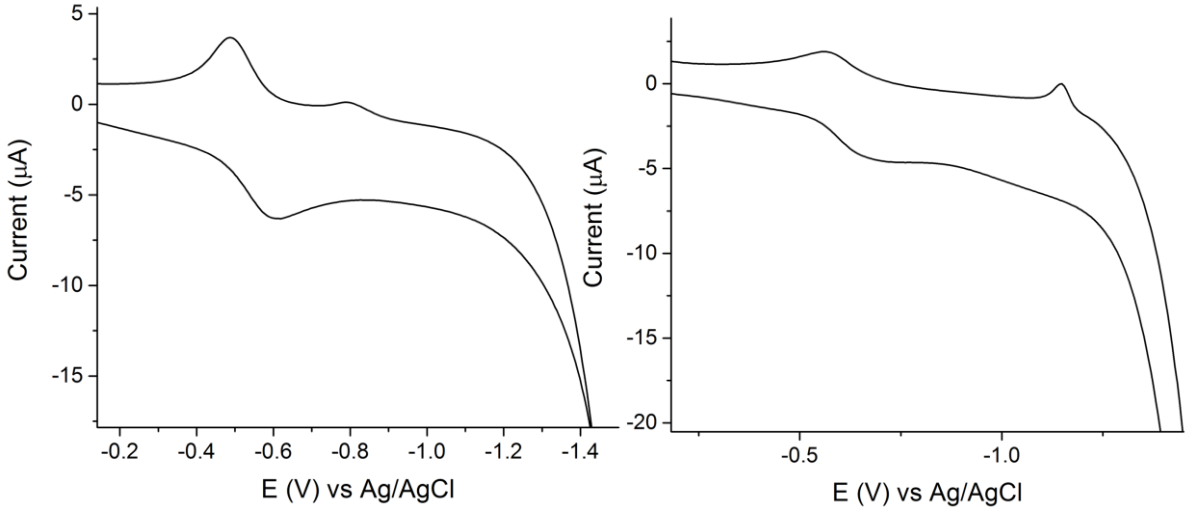

Figure A 4 - Cyclic voltammogram of **(OH_2)-2-H^+** at pH 7.5 (left) and pH 11.5 (right) in 0.1 M KCl.

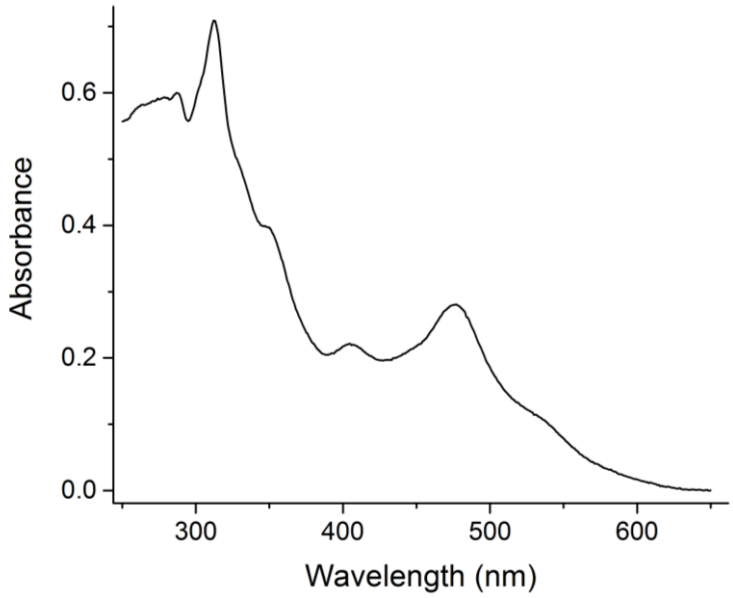

Figure A 5 - Absorbance spectra of **2-H**$^{+}_{r}$ in H_2O.

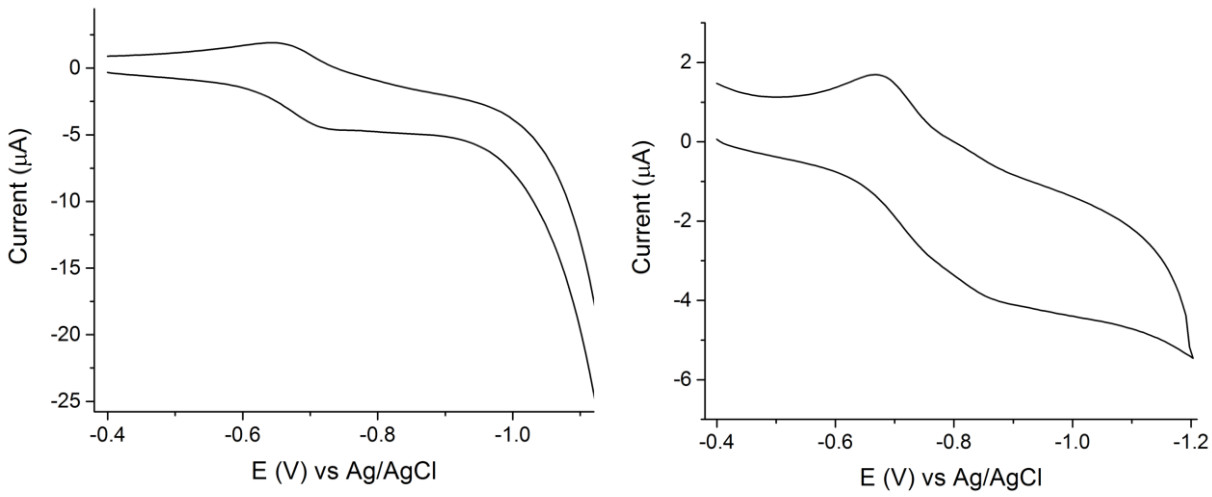

Figure A 6 - Cyclic voltammogram of **2-H**$^{+}_{r}$ at pH 5 (left) and pH 12 (right) in 0.1 M KCl.

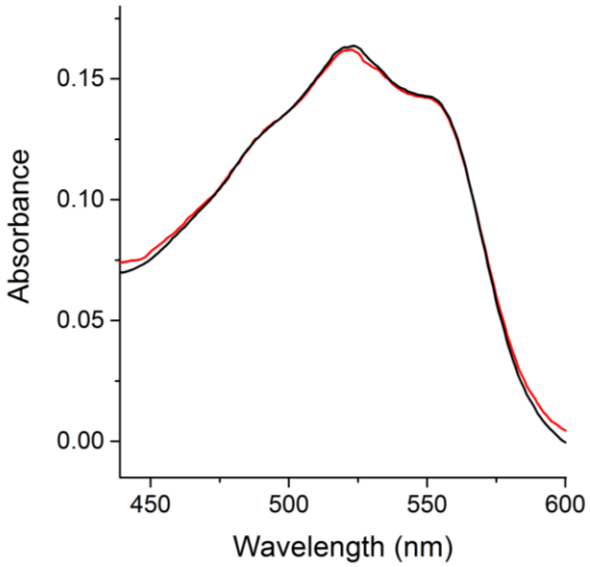

Figure A 7 - Absorbance spectra of **1-H**$^+$ in dioxane/H_2O (black) and after addition of 0.1 M benzoic acid (red), dioxane mole fraction: 0.17.

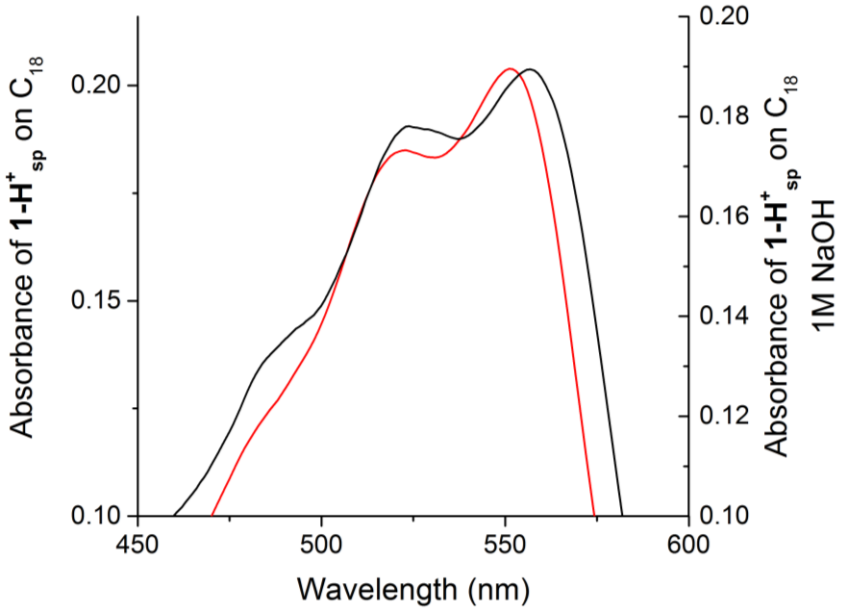

Figure A 8 - DRUV-vis of **1-H**$^+_{sp}$ (red) and **1-H**$^+_{sp}$ after addition of 1 M NaOH solution (black).

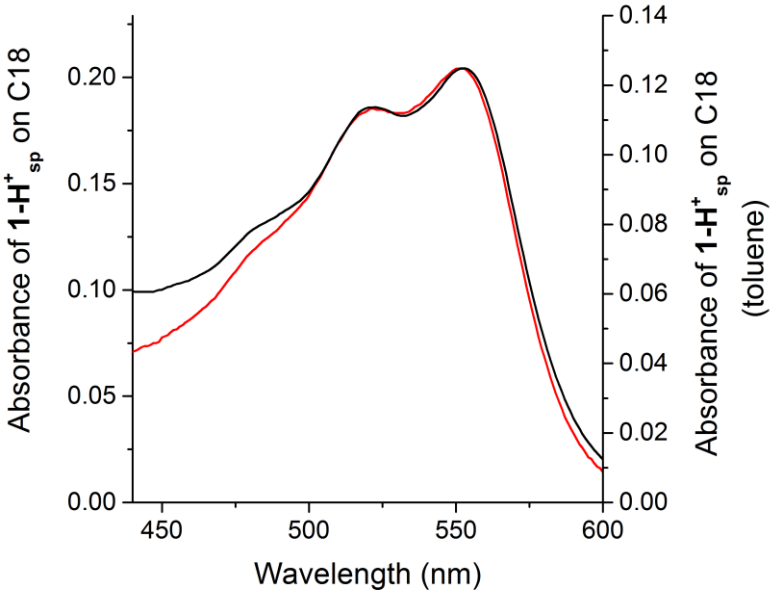

Figure A 9 - DRUV-vis of **1-H**$^{+}_{sp}$ (red) and **1-H**$^{+}_{sp}$ after addition of toluene (black).

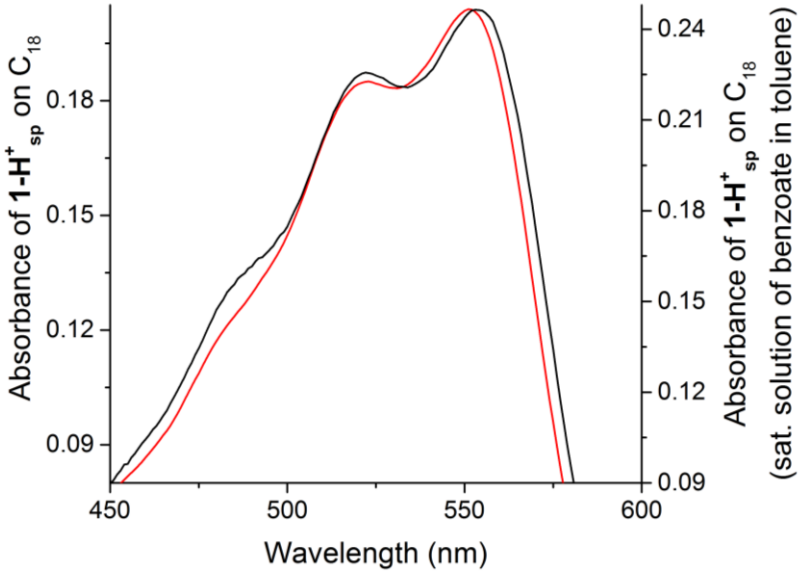

Figure A 10 - DRUV-vis of **1-H**$^{+}_{sp}$ (red) and **1-H**$^{+}_{sp}$ after addition of a saturated tetrabutylammonium benzoate solution in toluene (black).

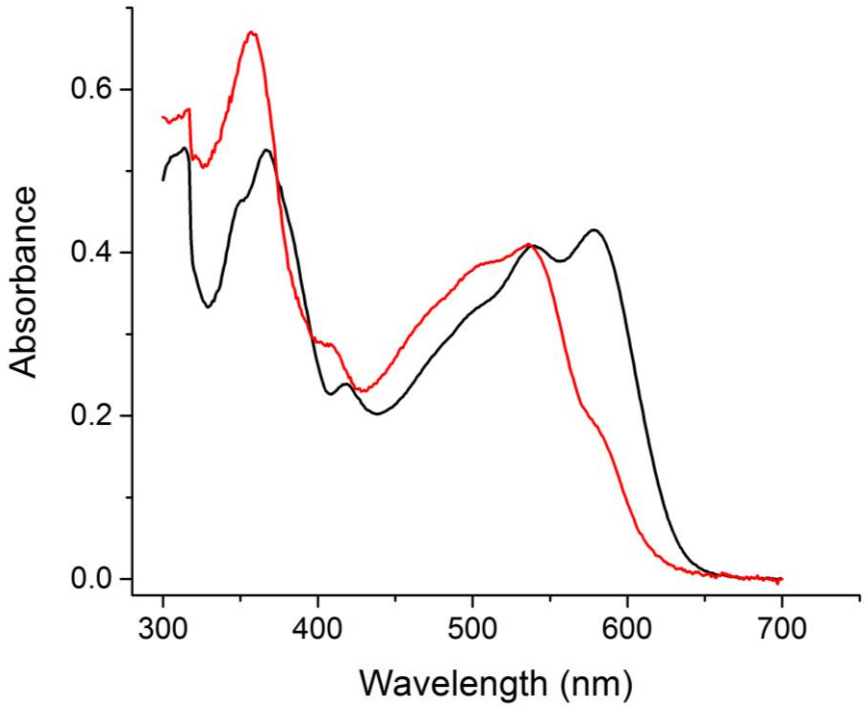

Figure A 11 - DRUV-vis of $(CN)_2$-Cbi on $C18_{ec}$ before (black) and after addition of a saturated solution of benzoic acid in toluene (red).

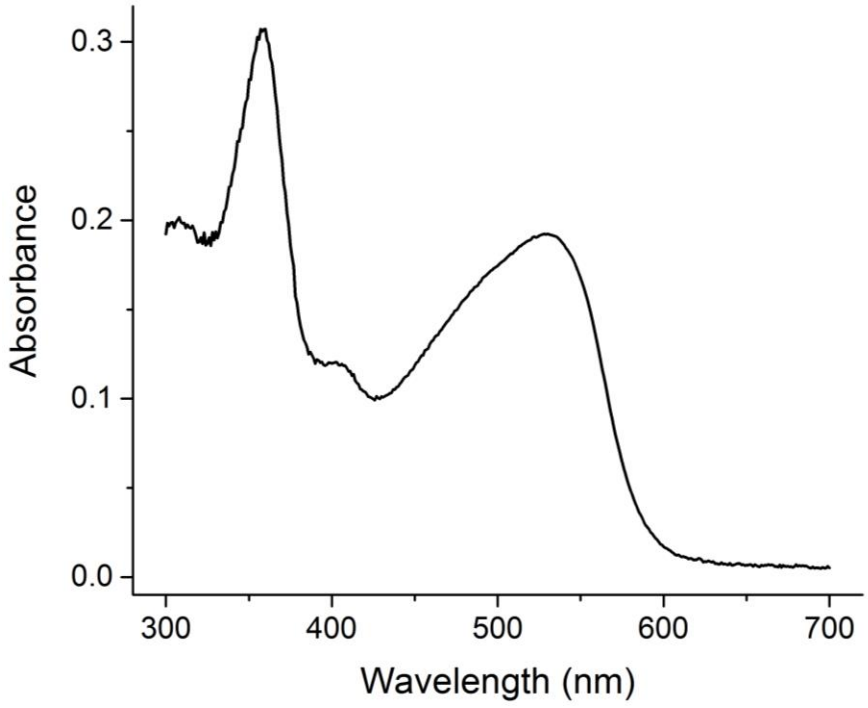

Figure A 12 - DRUV-vis of pB_{12} on $C18_{ec}$.

6. References

[1] E. L. Smith, *Nature* **1948**, *161*, 638-638.

[2] E. L. Rickes, N. G. Brink, F. R. Koniuszy, T. R. Wood, K. Folkers, *Science* **1948**, *107*, 396-397.

[3] D. C. Hodgkin, J. Pickworth, J. H. Robertson, *Nature* **1955**, *176*, 325-328.

[4] P. G. Lenhert, D. C. Hodgkin, *Nature* **1961**, *192*, 937-938.

[5] R. B. Woodward, *Pure Appl. Chem.* **1973**, *33*, 145-178.

[6] R. Banerjee, Chemistry and Biochemistry of B12, Vol. 1st Ed., Wiley-Interscience, New York, **1999**.

[7] G. C. Hayward, H. A. O. Hill, J. M. Pratt, N. J. Vanston, R. J. P. Williams, *J. Chem. Soc.* **1965**, 6485-6493.

[8] K. L. Brown, *Chem. Rev.* **2005**, *105*, 2075-2149.

[9] F. Zelder, K. Zhou, M. Sonnay, *Dalt. Trans.* **2013**, *42*, 854-862.

[10] P. Butler, M. O. Ebert, A. Lyskowski, K. Gruber, C. Kratky, B. Kräutler, *Angew. Chem. Int. Edit.* **2006**, *45*, 989-993.

[11] A. Eschenmoser, *Angew. Chem. Int. Ed.* **1988**, *27*, 5-39.

[12] F. Kreppelt, PhD thesis, ETHZ (Switzerland), **1991**.

[13] T. Toraya, A. Ishida, *J. Biol. Chem.* **1991**, *266*, 5430-5437.

[14] M. Fukuoka, S. Yamada, S. Miyoshi, K. Yamashita, M. Yamanishi, X. Zou, K. L. Brown, T. Toraya, *J. Biochem.* **2002**, *132*, 935-943.

[15] K. Zhou, F. Zelder, *Angew. Chem. Int. Edit.* **2010**, *49*, 5178-5180.

[16] B. Kräutler, S. Ostermann, in The Porphyrin Handbook, Vol. 11 (Eds.: K. M. Kadish, Kevin M. Smith, R. Guilard), Elsevier Science, San Diego, **2003**, pp. 229-276.

[17] B. Kräutler, in Chemistry and Biochemistry of B12, Vol. 1st Ed. (Ed.: R. Banerjee), Wiley-Interscience, New York, **1999**, pp. 315-342.

[18] R. A. Firth, H. A. O. Hill, J. M. Pratt, R. J. P. Williams, W. R. Jackson, *Biochemistry* **1967**, *6*, 2178-2189.

[19] T. A. Stich, A. J. Brooks, N. R. Buan, T. C. Brunold, *J. Am. Chem. Soc.* **2003**, *125*, 5897-5914.

[20] R. A. Firth, H. A. O. Hill, J. M. Pratt, R. G. Thorp, R. J. P. Williams, *J. Chem. Soc. A* **1969**, 381-386.

[21] J. M. Pratt, in Inorganic Chemistry of Vitamin B12 (Ed.: J. M. Pratt), Academic Press, New York, **1972**, p. 44.

[22] R. H. Abeles, D. Dolphin, *Acc. Chem. Res.* **1976**, *9*, 114-120.

[23] R. Banerjee, C. Gherasim, D. Padovani, *Curr. Opin. Chem. Biol.* **2009**, *13*, 484-491.

[24] A. K. Petrus, T. J. Fairchild, R. P. Doyle, *Angew. Chem. Int. Ed.* **2009**, *48*, 1022-1028.

[25] K. Gruber, B. Puffer, B. Kräutler, *Chem. Soc. Rev.* **2011**, *40*, 4346-4363.

[26] A. Marchaj, D. W. Jacobsen, S. R. Savon, K. L. Brown, *J. Am. Chem. Soc.* **1995**, *117*, 11640-11646.

[27] J. F. Kolhouse, R. H. Allen, *J. Clin. Invest.* **1977**, *60*, 1381.

[28] M. J. Nielsen, M. R. Rasmussen, C. B. F. Andersen, E. Nexø, S. K. Moestrup, *Nature Reviews Gastroenterology and Hepatology* **2012**, *9*, 345-354.

[29] W. Buckel, B. T. Golding, *Chem. Soc. Rev.* **1996**, *25*, 329-337.

[30] T. Toraya, *Chem. Rec.* **2002**, *2*, 352-366.

[31] S. Chowdhury, R. Banerjee, *Biochemistry* **2000**, *39*, 7998-8006.

[32] F. Mancia, G. A. Smith, P. R. Evans, *Biochemistry* **1999**, *38*, 7999-8005.

[33] J. Masuda, N. Shibata, Y. Morimoto, T. Toraya, N. Yasuoka, *Structure* **2000**, *8*, 775-788.

[34] R. Banerjee, *Biochemistry* **2001**, *40*, 6191-6198.

[35] T. Takahashi-Iñiguez, E. García-Hernandez, R. Arreguín-Espinosa, M. E. Flores, *J. Zhejiang Univ. Sci. B* **2012**, *13*, 423-437.

[36] R. Banerjee, S. Chowdhury, Vol. 1st Ed. (Ed.: R. Banerjee), Wiley-Interscience, New York, **1999**, pp. 707-730.

[37] K. L. Brown, in Chemistry and Biochemistry of B12, Vol. 1st Ed. (Ed.: R. Banerjee), Wiley-Interscience, New York, **1999**, pp. 197-238.

[38] M. L. Ludwig and, R. G. Matthews, *Annu. Rev. Biochem* **1997**, *66*, 269-313.

[39] R. Padmakumar, S. Taoka, R. Padmakumar, R. Banerjee, *J. Am. Chem. Soc.* **1995**, *117*, 7033-7034.

[40] T. Toraya, *Cell. Mol. Life Sci.* **2000**, *57*, 106-127.

[41] C. L. Drennan, S. Huang, J. T. Drummond, R. G. Matthews, M. L. Ludwig, *Science* **1994**, *266*, 1669-1674.

[42] R. G. Matthews, M. Koutmos, S. Datta, *Curr. Opin. Struct. Bio.l* **2008**, *18*, 658-666.

[43] R. G. Matthews, *Acc. Chem. Res.* **2001**, *34*, 681-689.

[44] R. V. Banerjee, R. G. Matthews, *FASEB J.* **1990**, *4*, 1450-1459.

[45] R. V. Banerjee, V. Frasca, D. P. Ballou, R. G. Matthews, *Biochemistry* **1990**, *29*, 11101-11109.

[46] K. P. Jensen, U. Ryde, *J. Am. Chem. Soc.* **2003**, *125*, 13970-13971.

[47] H. P. C. Hogenkamp, G. T. Bratt, S. Z. Sun, *Biochemistry* **1985**, *24*, 6428-6432.

[48] F. Zelder, M. Sonnay, L. Prieto, *ChemBioChem* **2015**, *16*, 1264-1278. Copyright Wiley-VCH Verlag GmbH & Co. KGaA. Reproduced with permission.

[49] R. G. Matthews, in Chemistry and Biochemistry of B12, Vol. 1st Ed. (Ed.: R. Banerjee), Wiley-Interscience, New York, **1999**, pp. 681-706.

[50] L. Stryer, in Biochemistry, 3 ed., W. H. Freeman and Company, New York, **1988**, pp. 614-616.

[51] G. R. McLean, P. M. Pathare, D. S. Wilbur, A. C. Morgan, C. S. Woodhouse, J. W. Schrader, H. J. Ziltener, *Cancer Res.* **1997**, *57*, 4015-4022.

[52] S. Cortellino, J. Xu, M. Sannai, R. Moore, E. Caretti, A. Cigliano, M. Le Coz, K. Devarajan, A. Wessels, D. Soprano, *Cell* **2011**, *146*, 67-79.

[53] J. T. Jarrett, M. Amaratunga, C. L. Drennan, J. D. Scholten, R. H. Sands, M. L. Ludwig, R. G. Matthews, *Biochemistry* **1996**, *35*, 2464-2475.

[54] K. S. Conrad, C. D. Jordan, K. L. Brown, T. C. Brunold, *Inorg. Chem.* **2015**, *54*, 3736-3747.

[55] J. T. Jarrett, C. Y. Choi, R. G. Matthews, *Biochemistry* **1997**, *36*, 15739-15748.

[56] D. M. Blow, J. J. Birktoft, B. S. Hartley, *Nature* **1969**, *221*, 337-340.

[57] W. Appel, *Clin. Biochem.* **1986**, *19*, 317-322.

[58] D. M. Blow, *Trends Biochem. Sci* **1997**, *22*, 405-408.

[59] P. Carter, J. A. Wells, *Nature* **1988**, *332*, 564-568.

[60] G. Dodson, A. Wlodawer, *Trends Biochem. Sci* **1998**, *23*, 347-352.

[61] C. J. Reedy, B. R. Gibney, *Chem. Rev.* **2004**, *104*, 617-650.

[62] M. Nakatani, *J. Biochem. Tokyo* **1960**, *48*, 633-639.

[63] R. G. Douglas, D. L. Rousseau, *J. Struct. Biol.* **1992**, *109*, 13-17.

[64] D. B. Goodin, D. E. McRee, *Biochemistry* **1993**, *32*, 3313-3324.

[65] L. Banci, A. Rosato, P. Turano, *J. Biol. Inorg. Chem.* **1996**, *1*, 364-367.

[66] G. F. da Silva, V. P. Shinkarev, Y. A. Kamensky, G. Palmer, *Biochemistry* **2012**, *51*, 8730-8742.

[67] V. P. Chacko, G. N. La Mar, *J. Am. Chem. Soc.* **1982**, *104*, 7002-7007.

[68] T. G. Spiro, G. Smulevich, C. Su, *Biochemistry* **1990**, *29*, 4497-4508.

[69] G. N. L. Mar, F. A. Walker, in The Porphyrins, Vol. IV (Ed.: D. Dolphin), Academic Press, New York, **1978**, pp. 67-157.

[70] K. S. Reddy, T. Yonetani, A. Tsuneshige, B. Chance, B. Kushkuley, S. S. Stavrov, J. M. Vanderkooi, *Biochemistry* **1996**, *35*, 5562-5570.

[71] L. Marboutin, A. Desbois, C. Berthomieu, *J. Phys. Chem. B* **2009**, *113*, 4492-4499.

[72] H. Fujii, *J. Am. Chem. Soc.* **2002**, *124*, 5936-5937.

[73] H. Fujii, T. Yoshida, *Inorg. Chem.* **2006**, *45*, 6816-6827.

[74] D. Nonaka, H. Wariishi, K. G. Welinder, H. Fujii, *Biochemistry* **2010**, *49*, 49-57.

[75] S. E. Bowman, K. L. Bren, *Inorg. Chem.* **2010**, *49*, 7890-7897.

[76] M. Fasching, W. Schmidt, B. Kräutler, E. Stupperich, A. Schmidt, C. Kratky, *Helv. Chim. Acta* **2000**, *83*, 2295-2316.

[77] R. A. Firth, H. A. O. Hill, J. M. Pratt, R. G. Thorp, R. J. P. Williams, *J. Chem. Soc. A* **1968**, 2428.

[78] J. M. Puckett, M. B. Mitchell, S. Hirota, L. G. Marzilli, *Inorg. Chem.* **1996**, *35*, 4656-4662.

[79] A. J. Brooks, M. Vlasie, R. Banerjee, T. C. Brunold, *J. Am. Chem. Soc.* **2004**, *126*, 8167-8180.

[80] A. J. Reig, K. S. Conrad, T. C. Brunold, *Inorg. Chem.* **2012**, *51*, 2867-2879.

[81] C. Männel-Croisé, F. Zelder, *Chem. Commun.* **2011**, *47*, 11249-11251.

[82] M. S. Hamza, X. Zou, R. Banka, K. L. Brown, R. van Eldik, *Dalt. Trans.* **2005**, 782-787.

[83] F. Zelder, M. Sonnay, L. Prieto, *ChemBioChem* **2015**, *16*, 1264-1278.

[84] J. C. Somogyi, K. Trautner, in Vitamine, Vol. 3 (Eds.: R. Ammon, W. Dirscherl), Georg Thieme, Stuttgart, **1974**, pp. 10-138.

[85] G. Domagk, *Angew. Chem.* **1935**, *48*, 657-667.

[86] G. Domagk, *Deutsch. Med. Wochenschr.* **1935**, *61*, 829-832.

[87] J. Drews, *Science* **2000**, *287*, 1960-1964.

[88] P. Griminger, *J. Nutr.* **1987**, *117*, 1325-1329.

[89] A. Ko, in Cancer Management in Man: Chemotherapy, Biological Therapy, Hyperthermia and Supporting Measures, Vol. 13 (Ed.: Boris R. Minev), Springer Netherlands, **2011**, pp. 125-143.

[90] W. Friedrich, in Vitamin B12 und verwandte Corrinoide (Ed.: W. Friedrich), Georg Thieme Verlag, Stuttgart, **1975**, pp. 81-87.

[91] F. Zelder, R. Alberto, in The Porphyrin Handbook, Vol. 25 (Eds.: K. M. Kadish, Kevin M. Smith, R. Guilard), Elsevier Science, San Diego, **2012**, pp. 83-130.

[92] J. C. Escalante-Semerena, *J. Bacteriol.* **2007**, *189*, 4555-4560.

[93] J. G. Lawrence, J. R. Roth, *J. Bacteriol.* **1995**, *177*, 6371-6380.

[94] E. Raux, H. L. Schubert, M. J. Warren, *Cell. Mol. Life Sci.* **2000**, *57*, 1880-1893.

[95] L. A. Maggio-Hall, K. R. Claas, J. C. Escalante-Semerena, *Microbiology* **2004**, *150*, 1385-1395.

[96] K. E. Helliwell, G. L. Wheeler, K. C. Leptos, R. E. Goldstein, A. G. Smith, *Mol. Biol. Evol.* **2011**, msr124.

[97] J. C. Gonzalez, R. V. Banerjee, S. Huang, J. S. Sumner, R. G. Matthews, *Biochemistry* **1992**, *31*, 6045-6056.

[98] B. D. Davis, E. S. Mingioli, *J. Bacteriol.* **1950**, *60*, 17.

[99] P. E. Nielsen, M. Egholm, R. H. Berg, O. Buchardt, *Science* **1991**, *254*, 1497-1500.

[100] P. E. Nielsen, *Accounts Chem. Res.* **1999**, *32*, 624-630.

[101] U. Diederichsen, H. W. Schmitt, *Angew. Chem. Int. Edit.* **1998**, *37*, 302-305.

[102] A. Eschenmoser, C. E. Wintner, *Science* **1977**, *196*, 1410-1426.

[103] S. M. Chemaly, *Dalt. Trans.* **2008**, 5766-5773.

[104] T. Eicher, S. Hauptmann, The Chemistry of Heterocycles: Structures, Reactions, Synthesis, and Applications 2nd, John Wiley & Sons, **2003**.

[105] M. Rossi, J. P. Glusker, L. Randaccio, M. F. Summers, P. J. Toscano, L. G. Marzilli, *J. Am. Chem. Soc.* **1985**, *107*, 1729-1738.

[106] A. M. Calafat, L. G. Marzilli, *J. Am. Chem. Soc.* **1993**, *115*, 9182-9190.

[107] P. L. Gaus, A. L. Crumbliss, *Inorg. Chem.* **1976**, *15*, 739-741.

[108] T. E. Needham, N. A. Matwiyoff, T. E. Walker, H. P. C. Hogenkamp, *J. Am. Chem. Soc.* **1973**, *95*, 5019-5024.

[109] L. H. Jones, *Inorg. Chem.* **1963**, *2*, 777-780.

[110] F. A. Miller, C. H. Wilkins, *Anal. Chem.* **1952**, *24*, 1253-1294.

[111] S. Yoshikawa, D. H. O'Keeffe, W. S. Caughey, *J. Biol. Chem.* **1985**, *260*, 3518-3528.

[112] B. M. M. Salih, S. Satyanarayana, *Afr. J. Pure Appl. Chem.* **2009**, *3*, 170-176.

[113] G. Davidson, in Spectrosc. Prop. Inorg. Organomet. Compd., Vol. 35, RSC, Cambridge, UK, **2002**, pp. 282-338.

[114] M. T. Zanni, P. Hamm, Cambridge University Press New York, **2011**.

[115] K. L. Brown, *Dalt. Trans.* **2006**, 1123-1133.

[116] T. Andruniow, P. M. Kozlowski, M. Z. Zgierski, *J. Chem. Phys.* **2001**, *115*, 7522-7533.

[117] D. Lexa, J. M. Saveant, J. Zickler, *J. Am. Chem. Soc.* **1980**, *102*, 2654-2663.

[118] M. Ruetz, R. Salchner, K. Wurst, S. Fedosov, B. Kräutler, *Angew. Chem. Int. Ed.* **2013**, *52*, 11406-11409.

[119] M. Komiyama, M. L. Bender, M. Utaka, A. Takeda, *Proc. Natl. Acad. Sci.* **1977**, *74*, 2634-2638.

[120] E. Stupperich, E. NexØ, *Eur. J. Biochem.* **1991**, *199*, 299-303.

[121] J. Wuerges, G. Garau, S. Geremia, S. N. Fedosov, T. E. Petersen, L. Randaccio, *Proc. Natl. Acad. Sci.* **2006**, *103*, 4386-4391.

[122] E. V. Quadros, Y. Nakayama, J. M. Sequeira, *Biochem. Biophys. Res. Commun.* **2005**, *327*, 1006-1010.

[123] S. N. Fedosov, L. Berglund, N. U. Fedosova, E. Nexø, T. E. Petersen, *J. Biol. Chem.* **2002**, *277*, 9989-9996.

[124] O. M. G. Müller, *Naturforsch.* **1966**, 1159.

[125] M. J. Frisch, G. W. Trucks, H. B. Schlegel, G. E. Scuseria, M. A. Robb, J. R. Cheeseman, G. Scalmani, V. Barone, B. Mennucci, G. A. Petersson, *Gaussian Inc., Wallingford, CT* **2010**.

[126] S. Dapprich, I. Komáromi, K. S. Byun, K. Morokuma, M. J. Frisch, *J. Mol. Struct.: THEOCHEM* **1999**, *461*, 1-21.

[127] T. Vreven, K. Morokuma, Ö. Farkas, H. B. Schlegel, M. J. Frisch, *J. Comput. Chem.* **2003**, *24*, 760-769.

[128] T. Vreven, K. S. Byun, I. Komáromi, S. Dapprich, J. A. Montgomery, K. Morokuma, M. J. Frisch, *J. Chem. Theory Comput.* **2006**, *2*, 815-826.

[129] T. V. F. Clemente, M. J. Frisch, in Quantum Biochemistry, C. Matta Wiley VCH, Weinheim, **2010**, pp. 61-84.

[130] A. D. Becke, *J. Chem. Phys.* **1993**, *98*, 5648-5652.

[131] C. Lee, W. Yang, R. G. Parr, *Phys. Rev. B* **1988**, *37*, 785.

[132] P. J. H. T. H. Dunning, in Modern Theorectical Chemistry, Vol. 3 (Ed.: H. F. Schaefer III), Plenum, New York, **1977**, pp. 1-28.

[133] P. J. Hay, W. R. Wadt, *J. Chem. Phys.* **1985**, *82*, 270-283.

[134] P. J. Hay, W. R. Wadt, *J. Chem. Phys.* **1985**, *82*, 299-310.

[135] W. R. Wadt, P. J. Hay, *J. Chem. Phys.* **1985**, *82*, 284-298.

[136] A. K. Rappé, C. J. Casewit, K. S. Colwell, W. A. Goddard Iii, W. M. Skiff, *J. Am. Chem. Soc.* **1992**, *114*, 10024-10035.

[137] K. L. Brown, D. R. Evans, *Inorg. Chem.* **1990**, *29*, 2559-2561.

[138] K. L. Brown, X. Zou, L. Salmon, *Inorg. Chem.* **1991**, *30*, 1949-1953.

[139] K. L. Brown, X. Zou, *J. Am. Chem. Soc.* **1992**, *114*, 9643-9651.

[140] K. L. Brown, X. Zou, *Inorg. Chem.* **1992**, *31*, 2541-2547.

[141] K. L. Brown, L. Salmon, J. A. Kirby, *Organometallics* **1992**, *11*, 422-432.

[142] P. Pfingstag, Master thesis, University of Zurich (Zürich), **2013**.

[143] K. L. Brown, S. Peck-Siler, *Inorg. Chem.* **1988**, *27*, 3548-3555.

[144] M. D. Waddington, R. G. Finke, *J. Am. Chem. Soc.* **1993**, *115*, 4629-4640.

[145] J. Halpern, *Science* **1985**, *227*, 869-875.

[146] M. Ruetz, R. Salchner, K. Wurst, S. Fedosov, B. Kräutler, *Angew. Chem. Int. Ed.* **2013**, *52*, 11406-11409.

[147] D. Dolphin, A. W. Johnson, R. Rodrigo, *J. Chem. Soc.* **1964**, 3186-3193.

[148] O. T. Magnusson, P. A. Frey, *J. Am. Chem. Soc.* **2000**, *122*, 8807-8813.

[149] N. E. Brasch, A. G. Cregan, M. E. Vanselow, *J. Chem. Soc., Dalton Trans.* **2002**, 1287-1294.

[150] N. E. Brasch, R. J. Haupt, *Inorg. Chem.* **2000**, *39*, 5469-5474.

[151] J. I. Toohey, D. Perlman, H. A. Barker, *J. Biol. Chem.* **1961**, *236*, 2119-2127.

[152] H. Weissbach, J. N. Ladd, B. E. Volcani, R. D. Smyth, H. A. Barker, *J. Biol. Chem.* **1960**, *235*, 1462-1473.

[153] S. J. Brodie, A. G. Cregan, R. van Eldik, N. E. Brasch, *Inorg. Chim. Acta* **2003**, *348*, 221-224.

[154] A. W. Johnson, N. Shaw, *J. Chem. Soc.* **1962**, 4608-4614.

[155] A. Ishida, T. Toraya, *Biochemistry* **1993**, *32*, 1535-1540.

[156] H. Mosimann, B. Kräutler, *Angew. Chem. Int. Edit.* **2000**, *39*, 393-395.

[157] B. Kräutler, *Chem. Eur. J.* **2015**, *21*, 11280-11287.